EXPERIMENTAL OPTIMIZATION OF DRILLING, ROCK STRENGTH AND BACKFILLING FOR MINING BY DRILLING APPLICATIONS

by

Weizhou Quan

A thesis submitted to the School of Graduate Studies in partial fulfillment of the requirements for the degree of

Master of Engineering

Faculty of Engineering and Applied Science

Memorial University of Newfoundland

October 2021

St. John’s, Newfoundland and Labrador, Canada

Abstract

A comprehensive study has been conducted to study rock characterizations, drilling performance through drill-off-test (DOT), optimization of cemented tailings backfill (CTB), and investigation of anti-washout property for CTB. The mechanical strengths and ultrasonic velocity of granite, representing high strength of natural isotropic rock, and rock like material (RLM), representing high strength synthetic isotropic rock, were determined in the laboratory. Empirical equations have been developed between these parameters. A novel strength testing method named mono UCS-PLI test was proposed to reduce limitations and strictness of the conventional standard strength tests. Then, the drilling rate of penetration (ROP) as main function of drilling performance was evaluated through two different drill bit types, including roller cone (RC) bit and polycrystalline diamond compact (PDC) bit. Sandstone was used as the testing rock, representing a tight and low permeability isotropic formation. A fully instrumented laboratory scale drilling simulator was used for drilling experiments. Weight on bit (WOB), rotary speed (rpm) and water flow rate (FR) were monitored and recorded. The drilling performance was evaluated based on drilling parameters and drill bit type. Besides, investigations of the use of lower binder proportions and optimization of backfill strength development were conducted because of the relatively high cost of Portland cement. The optimization work studied the effects of lower binder proportions (2 wt.% and 4 wt.% by solids mass) and internal vibration on the designed CTB density and mechanical strength development. An extra 10.9% tailings can be placed into extracted wellbore when the CTB is fully vibrated. This behaviour allows more tailings to be securely placed underground and further reduces the surface tailings impoundment requirements and the costs of tailings disposal for the mining industry. The first design of cemented tailings backfill preparation system is a batch system based on many technical experiences from those successful operations. Finally, an anti-washout admixture was found to achieve the anti-washout property of the designed CTB, which can prevent the CTB from being affected by the water during placement.

Acknowledgements

As time goes on, the two-year life of my master's study at Memorial University of Newfoundland is about to end. Recall that in the past two years, there have been too many stories, and I am glad that I was a participant or witness of these stories. Without knowledgeable teachers' and energetic colleagues' help, I would not be able to spend my graduate study life so smoothly. Now I want to express my heartfelt gratitude to them.

First of all, I would like to deeply thank my supervisor, Dr. Stephen Butt, whose guidance and encouragement have given me much insight into my studies. It is my honor to benefit from his suggestions and supervision. I also express my thanks to my co-supervisor Dr. Yahui Zhang for his support and help.

In addition, I also want to thank all the DTL group members, especially Zijian Li and Dr. Abdelsalam Abugharara, for their kind assistance and explanations that helped me through the whole process of my study. It is a great experience for me to spend this time in such a positive and enthusiastic group.

Finally, my heartful thanks also go to my parents and friends for their unconditional love, support, patience, and company.

Table of Contents

List of Figures

List of Tables

List of Symbols and Abbreviations

D_e = Equivalent core diameter

V_p = P-wave velocity

V_s = S-wave velocity

σ_t = Tensile strength

A = Cross-section area

E = Young's modulus

F = Correction factor

k = Drillability constant

L = Pulse propagation distance

P = Failure load

μ = Poisson's ratio

AWA = Anti-washout admixture

BTS = Brazilian tensile strength

CTB = Cemented tailings backfill

DOC = depth of cut

FA = Fly ash

HRWR = High range water reducer

ITS = Indirect tensile strength

LDS = Large drilling simulator

PC = Portland cement

PLI = Point load index

RLM = Rock like material

ROP = Rate of penetration

rpm = rotary speed

SEM = Scanning electron microscope

UCS = Unconfined compressive strength

WOB = Weight on bit

XRD = X-ray diffraction

Chapter 1. Introduction

1.1 Background

Drilling Technology Laboratory (DTL) group at Memorial University of Newfoundland is currently collaborating with Anaconda Mining for the development of Sustainable Mining by Drilling (SMD) project to mine several of narrow-vein deposits currently held by the company (Lopez-Pacheco, 2019). The SMD project is developed based on the concept of mining by drilling, where the full ore vein will be excavated through a sequence of primary and secondary holes. All the ore is recovered as drill cuttings, which eliminates the need to use explosives to fragment the ore and the need to crush the ore as a first stage of mineral processing. The need for underground ventilation is eliminated since the ore is recovered using surface operations. After the vein has been mined, the hole is refilled with backfill, barely leaving an environmental footprint. Therefore, the investigation and optimization of each operation require the scope of research activities in the SMD project.

1.2 Research Motivation and Objectives

In mining, geotechnical, and petroleum engineering, having a good knowledge of physico-mechanical properties of studied rocks provides the requisite basis for the project development stage. Construction projects such as water conservancy and hydropower, transportation, mining, industrial and civil buildings, all involve rock analysis works (Armaghani et al., 2015). For an instance, rock strength that taken into consideration for the drill bit selection and optimizing drilling parameters, is an important affecting factor of the drilling efficiency. In addition, accurate characterization of rock properties is the prerequisite for the evaluation of the wellbore stability to ensure the safety for personnel and machinery. Investigation of the correlations between unconfined compressive strength (UCS), indirect tensile strength (ITS), and point load index (PLI), and ultrasonic velocities can provide a simple and quick method on site or in laboratory to calculate various parameters for rock properties, instead of time-consuming and complex tests of each parameter. Furthermore, conventional testing methods of mechanical properties of rocks require strict sampling conditions, which make the work expensive and time-consuming, and hard to achieve on site. Therefore, investigation of novel strength testing methods and new correlating methods have dawn attention from lots of researchers (Yoshikawa et al., 1981; Sheshde & Cheshomi, 2015; Haftani et al., 2013). This work is to study the empirical relationships between physico-mechanical properties and ultrasonic velocities. Also, a new approach for strength evaluation and prediction is proposed for isotropic rocks. The results can be used in the drill-off-test and analysis of wellbore stability.

Optimization of drilling process or exploring optimal rate of penetration (ROP) in mining and petroleum engineering has always been the research focus to improve drilling efficiency and reduce costs. This field is also one of the main research streams at the Drilling Technology Laboratory at Memorial University of Newfoundland. In SMD project, drilling rigs are used to surgically remove the ore through directional drilling. The holes will be drilled in the sequence of primary and secondary. Therefore, it is essential to investigate the relations and difference between drilling parameters, including weight on bit (WOB), rotary speed (rpm), drill bit type and bit hydraulics, to maximize the drilling process for optimal drilling performance and minimize the costs. Additionally, numerous researches have been conducted to study the performance of roller cone (RC) and polycrystalline diamond compact (PDC) bits and establish ROP prediction models (Maurer, 1962; Offenbacher, 1983; Ahmed et al., 2020). However, the relation between ROP of PDC bit and RC bit for specific rocks has not been studied thoroughly. Mensa-Wilmot et al. (2002) stated that PDC bits usually drill twice as fast as RC bits in shale. But as for sandstone, there is rare information indicating the ROP relations between PDC bit and RC bit. This work is to conduct a comparative study on drilling performance based on various drilling parameters and drill bit type. Also, the relation between ROP of PDC bit and RC bit for sandstone will be investigated to provide a new correlation for sandstone.

In SMD project, one of the significant objectives is to reduce the environment impact and barely leave an environment footprint (Lopez-Pacheco, 2019). Backfilling is the most important work of the post-mining procedure, which utilized the waste tailings to enhance underground stability and for waste tailings disposal (Lopez-Pacheco, 2019). Waste residue, fly ash, gangue and tailings are common solid wastes in mining industries. According to Jones et al. (2012), 14 billion tonnes of tailings are produced annually worldwide. Cemented tailings backfill (cemented paste backfill) has been put forwarded since 1970's and has been utilized in mining industries after decades' development. The technology of cemented tailings backfill can utilize the storage of up to 60% of the tailings which can reduce the requirement of surface tailings pond to reduce the environmental issues. DTL group has adopted the cemented tailings backfill technique and developed the primary recipe of cemented tailings backfill for the SMD project (Someehneshin et al., 2020). The recommended constituents of backfill for SMD project consist of waste tailings, Portland cement, fly ash and water. The fly ash, as a solid waste, not only can be utilized in the backfill, but also can enhance the strength development of backfill due to its pozzolanic property. In this work, the optimization study, including investigations of the use of lower binder proportions and optimization of backfill strength development will be conducted to further increase the usage of waste tailings and reduce the backfill cost.

Considering the practical operation, the designed cemented tailings backfill (CTB) will be placed into the wellbore filled with water. To reduce the influence of the water on CTB behaviour, underwater concrete method is a potential solution to be applied on the CTB to achieve this target. Underwater concrete is a concrete that has high flowability which can place down to the borehole by its self-weight and the good compaction can be achieved without vibration. The anti-washout admixture (AWA) is the indispensable thing to achieve the benefits for underwater concrete method. AWA is added into the concrete to improve or enhance the stability of fresh cementitious mixtures. However, the application of CTB underwater placing is more difficult to achieve due to the low cementitious materials contained in backfill mixture. This work is to explore anti-washout admixtures in our designed CTB to achieve anti-washout property and the to optimize the flowability of CTB.

1.3 Thesis Outline

This thesis consists of total seven chapters. **Chapter 1** gives the background information of SMD project, clarifies the research motivation and objectives, and outlines the contents of this thesis. This thesis contains three papers, which are accepted for publications in American Rock Mechanics Association (ARMA) 55th US Rock Mechanics/ Geomechanics Symposium and in Canadian Geotechnical Society 74th Canadian

Geotechnical Conference. Additionally, the works related to design of first field backfill preparation system and investigation of anti-washout property for CTB are included in this thesis.

Chapter 2 is the comprehensive **Literature Review** part that covers main four sub-sections, including characterization of rocks, factors affecting drilling performance, general information of CTB technique, and application of anti-washout admixture on backfill.

Chapter 3 is the **Evaluations of Mechanical Property and Ultrasonic Velocity for Isotropic Rocks**, which determines the mechanical strengths of rocks and develops the empirical equations for the strength predictions between strengths and ultrasonic velocities. The mineral components and micro-structure of rocks are analyzed by XRD and SEM, respectively. Determination of mechanical strengths provide the basis for the drilling experiments work in Chapter 4. In addition, a novel strength testing method named mono UCS-PLI test, which may avoid the necessity for time consuming and tedious laboratory testing, is proposed to reduce limitations and strictness of the conventional standard strength tests.

Chapter 4 is **the Investigation of Drilling Performance using PDC and RC Drill Bits**. In this part, sandstone specimens are tested through rotary drilling in the laboratory by a fully instrumented laboratory scale drilling simulator using two drill bits. Different sets of weight on bit and rotary speed under the same condition of water flow rate are adopted. The applied load on bits and operational rpm were recorded, rate of penetration and depth of cut are calculated in all tests. A comparative study is conducted, and drilling performance is evaluated based on drilling parameters and drill bit type.

Chapter 5 is the **Optimization of Cemented Tailings Backfill (CTB) and First Field Backfill System Design**. In this optimization work, the effects of lower binder proportions (2 wt.% and 4 wt.% by solids mass) and internal vibration on the designed CTB density, unconfined compressive strength (UCS), tensile strength, and the amount of tailings usage are evaluated. For the internal vibration analysis, four different vibrating conditions are adopted using an electronic vibrator to give contrast analysis. The first design of cemented tailings backfill preparation system is a batch system based on many technical experiences from those successful operations.

Chapter 6 is the **Qualitative Analysis of Cemented Tailings Backfill (CTB) with Anti-washout Admixture**. Liquid and powdered anti-washout admixtures are investigated to achieve the anti-washout property for designed CTB based on different dosages and backfill preparation recipe. The flowability of CTB is improved by water reducing mixture and the mini slump cone test is conducted to assess the early stiffening of CTB mixture.

Last, **Chapter 7** presents the **Conclusions and Recommendations**. The main findings are summarized and can provide the reference for the future work.

Chapter 2. Literature Review

2.1 Testing Methods of Rock Physico-mechanical Properties

2.1.1 Unconfined compressive strength (UCS)

With the rapid development of engineering construction, many test methods for estimating the strength of rocks have begun to be used. The compressive strength of a rock refers to the maximum pressure that it can withstand in the unconfined state (Avar & Zcan, 2021). In other words, it refers to the stress required to fracture the rock. The most important strength test is the compressive strength test. The measurement of the maximum compressive strength of the rock is usually carried out in a fixed laboratory, and a special hydraulic press with a capacity of ten to one hundred tons or more is used to crush the test sample (Shea & Kronenberg, 1993). In order to test the compressive strength of the rock, the sample needs to be made into the shape of a cube or a cylinder, and its size also depends on the rock.

Many factors can affect the unconfined compressive strength (UCS) of rocks and the most important are the following three factors, namely, the structure, the nature of the bond, and the direction of the pressure (Chau & Wong, 1996). The compressive strength of rock is also determined by the direction of applied compressive stress. For sedimentary rocks, they have bedding. If the direction of stress is perpendicular to the bedding, the compressive strength of the rock is the greatest. In addition, some rocks often have structures such as cracks, veins or schisms. If their direction is the same as the direction of the fracture surface (plane of failure), it will naturally have a great impact on the compressive strength of the rock.

The UCS of rock is one of the basic mechanical properties of rock. For a long time, the uniaxial compressive strength of rocks has been widely used as the basis of rock classification and used to evaluate rock engineering geological characteristics and rock mass quality (Sepahi et al, 2014). However, the use of conventional test methods to determine the compressive strength of rocks is often limited by funding, time, sampling, and sample preparation, especially for weathered rocks and weak rocks. In the engineering survey, due to the lack of rock test data and the difficulty of obtaining it, the classification and evaluation of on-site rocks have caused great difficulties. Therefore, since the 1970s, a new method that can quickly determine the strength of rocks on site - point load test has been widely used in various projects (Nazir et al, 2013). One reason is that the point load strength of the rock can be measured directly and quickly on site. On the other hand, the point load strength of the rock has a very good correlation with the compressive strength (Yasin et al, 2018). The compressive strength of the rock can be calculated by measuring the point load strength. This not only saves time and effort, but also has higher economic value.

2.1.2 Point load index (PLI)

According to the point load index (PLI) of the rock, one can calculate and determine the uniaxial compressive strength and tensile strength of the rock, determine the anisotropy of the rock, determine the weathering zone, estimate the drilling speed, and classify the rock (Hahri et al, 2021). The point load test is to place a rock specimen between two spherical cone-shaped pressure plates and apply a concentrated load to the specimen until it fails. When having a huge sampling area, the point load strength value is used to estimate the uniaxial compressive strength value, which can fully grasp the rock mechanical properties of the entire area, has economic advantages, and the test is convenient and fast (Teymen, 2021). Many researchers have used mathematical statistics and calculus derivation, numerical simulation, and other methods to give empirical formulas and the conversion factor depends on different rock types to predict PLI (Shcherban et al, 2021). Point load test is a test method that uses portable instruments to quickly determine the uniaxial compressive strength of rocks. Irregular tests on the spot can be used. For testing of rock samples or core specimens, the rock point load test does not require processing of rock samples, and the equipment is portable. It can be used for indoor and on-site tests and is especially suitable for on-site rapid strength tests of broken, low-strength and easily weathered rock samples (Hsieh, 2021). A comparison of the test results of the point load strength and the uniaxial compressive strength of the traditional standard specimens through examples proves the basic consistency of the results, which shows that the rapid field test of the rock strength is basically accurate and feasible.

Most rocks have the characteristics of anisotropic specificity. The point load test to determine the strength anisotropy of the rock is superior to other conventional experiments. The point load test is widely used in the test of irregular rock samples with its unique advantages, as long as the vertical and the maximum and minimum strength of the rock can be obtained by testing the bedding of parallel rocks or various weak surfaces (Mardoukhi et al, 2021). When the number of specimens is sufficient, the test results are closer to the saturated uniaxial compressive strength values of the regular specimens. Therefore, point load strength can also be used as a basis for rock classification. By analyzing the relationship between the point load strength and the uniaxial compressive strength, an empirical formula for determining the uniaxial compressive strength by the point load strength can be obtained.

2.1.3 Indirect tensile strength (ITS)

The rock sample reaches the ultimate stress value when it fails under tensile force. The indirect tensile strength (ITS) of rock is one of the physical and mechanical properties of rock. The tensile strength of rock is much smaller than the compressive strength. Therefore, tensile failure has become an important phenomenon worthy of study in rock drilling and blasting. Rock tensile strength test methods can be divided into two types: direct method and indirect method (Habibi et al, 2021). There are many types of this method, and the commonly used methods include disk and cylindrical radial fracturing. The disk radial fracturing method is the famous "Brazilian test", that is, a solid disk is used to damage it by radial compression to obtain the tensile strength (Shaunik & Singh, 2021). The cylindrical radial fracturing method usually uses two contact points to pressurize the cylinder to obtain the tensile strength. In engineering practice, due to the cracks in the rock mass, the tensile strength is generally not considered. The way of cushion strips directly affects the degree of contact between the load and the contact surface of the test piece, thereby affecting the testing accuracy of the rock tensile strength. Therefore, in the rock tensile strength measurement experiment, it is very important to adopt a reasonable bedding strip method and bedding strip size to reduce the error of the measurement results.

2.1.4 Acoustic elastic property (P-wave velocity)

Seismic techniques have been widely used in geotechnical engineering, mining engineering and petroleum engineering for many years due to its simplicity. As a non-destructive method, the measurement of P-wave velocity, depending on the density and elastic properties, is utilized to determine the dynamic properties of rocks. Many factors (Kahraman, 2001) have influence on the P-wave velocity, including lithology, rock density, porosity, anisotropy, grain size and shape, pore water, confining pressure, temperature, etc. The P-wave, also referred to primary wave or pressure wave, is the fastest wave can travel in rocks. This feature allows it to be commonly used to characterize rock properties in lab and field for drilling purpose. Also, the P wave velocity will drastically drop in gas media can be an indicator to estimate porosity.

The relations between P-wave velocity and rock properties have been approved by many researchers (Smorodinov et al., 1970; Inoue and Ohomi, 1981; Boadu, 2000; Ozkahraman et al., 2004; Yasar and Erdogan, 2004; Sharma and Singh, 2007; Khandelwal and Singh, 2009). Sharma and Singh (2007) found that impact strength index, slake durability index and UCS can be estimated using P-wave velocity with the given empirical equations for similar types of rock mass, which can shorten testing time and avoid tedious testing operations. Inoue and Ohomi (1981) stated that the P-wave velocity has poor correlation with the UCS of soft rocks. Khandelwal and Ranjith (2010) found that the P-wave velocity is closely related with different rock properties and correlated the various index properties of various rock types with P-wave velocity with obtained empirical equations with very high coefficient of determination. Yasar and Erdogan (2004) established linear relationships among carbonate rock density, Young's modulus, UCS and P-wave velocity.

2.2 Drilling Performance

In oil and gas drilling, it is essential to maximize the drilling process for optimal drilling performance and minimize costs. The drilling rate of penetration (ROP) can be evaluated as main function of drilling performance. In the field of oil and gas exploration and development, achieving optimal ROP to produce safer and more efficient drilling performance is a key requirement (Pak et al., 2017; Zhang et al., 2013; Omar et al., 2017; Jain et al., 2017). The rate of penetration achieved with the bit has a direct and obvious effect on the cost per foot drilled. There are some variables, which affect the rate of penetration. Lots of experimental work (Galle et al., 1963; Mechem et al., 1965; Alum et al., 2011) has been done to study the effect of these variables on drilling rate. The cost per foot drilled is directly proportional to ROP obtained by the bit. The ROP is influenced by a number of factors. These factors that affect the rate of penetration are: drill bit type, weight on bit (WOB), rotary speed (rpm), drilling fluid properties, bit hydraulics and rock formation properties (Bilgesu et al., 1997). The sonic log of the offset wells is used to select the bit type in the bit design process. Optimal mud weight and hydraulics parameters are also calculated using data from a nearby well. Each formation's attributes might be considered as constant. As a result, we may change WOB and rpm in the experiments to obtain the optimal ROP (Paes et al., 2005).

One of the main research objectives in drilling engineering is the establishment of ROP model. In order to investigate the suitable ROP model, it is necessary to figure out the influence of various factors on ROP, which is a significant way to effectively predict and improve ROP under given conditions. There are two main factors that affect the ROP: one is the objective factors, including geological conditions and strata characteristics; the other is subjective factors, including bit structure, weigh on bit (WOB), rotating speed (rpm) and hydraulic parameters.

2.2.1 Drill bit type

2.2.1.1 Roller cone (RC) bit

In the oil and gas industry, roller cone (RC) bits are commonly used and their performance has a direct impact on drilling quality and cost (Winters et al., 1987). When drilling into the formation, the RC bit not only has the function of impacting and crushing, but also has the function of shearing and breaking on rocks. Therefore, when drilling into various formations, including soft, medium, and hard formations, the roller bit can be adapted to them (Zhou et al., 1994). Significant improvement of bit performance can directly reduce the drilling cost. The rate of penetration model of RC bit is used to reflect the influence of various factors on drilling speed. At present, it is necessary to improve the penetration rate and quality of drilling to reduce the cost. And it is also important to optimize the drilling parameters.

Mechanism

In the process of drilling, the roller cone (RC) bit revolves around its own axis while it rotates in the wellbore, and sometimes slides when it rolls at the bottom of the well. Therefore, the composite movements of the RC bit will cause the rock breaking, mainly including impact crushing and shear crushing. The WOB applied on the bit transfers the energy to the bit teeth, thus crushing the formations in large volume (as shown in Figure 2.1). The teeth on the steel bit are mainly wedge-shaped, which crushes into the formations to break the rocks. For the carbide teeth, the teeth are mainly spherical and conical. During rotary drilling, the single and double teeth contact the bottom hole alternately, and the vertical vibration of the cone forms the impact effect, which attributes to the rock breaking with the static load. When the teeth of a cone bit break rocks, it depends not only on the static WOB, but also on the impact load produced when the teeth rush to the rock at the maximum speed due to the longitudinal vibration of the bit. In order to achieve the great crushing during drilling, the teeth are required to crush and impact the rocks. Meanwhile, there must be shear effect which is mainly manifested as the roller at the bottom of the well and the sliding of the teeth on the rocks.

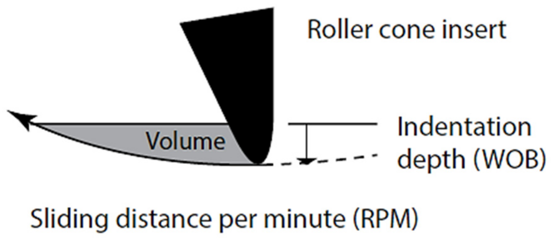

Figure 2.1 Mechanism of RC bit (IADC, 2014)

2.2.1.2 Polycrystalline diamond compact (PDC) bit

The advent of polycrystalline diamond compact (PDC) bit is an outstanding achievement of oil and gas industry in 1980s. Up to now, PDC bit still plays a vital role in the drilling industry and is widely used in the field. The actual drilling situation shows that the selection of PDC bit parameters directly affects the drilling performance, and then affects the drilling rate, drilling quality and drilling cost. Different formation properties and PDC bit structures will give the different drilling performance.

PDC bit is a kind of shearing bit, which has the characteristics of low WOB, low pump pressure and high speed. Shear fracture is an effective way to break rock in drilling since the shear strength of rock is approximately 10% of the compressive strength. The main method of rock breaking for PDC bit is shear fracture. Moreover, the wear resistance of PDC bit with very thin and hard polycrystalline diamond layer is more than 100 times higher than that of tungsten carbide substrate. Therefore, PDC bit can keep sharpening in the process of cutting rock and can make full use of the weakness of low shear strength of rock, shearing rock in soft to medium hard homogeneous formations. PDC bit needs less energy to break the formation by shearing than by rolling, and can maintain self sharpening, thus it has higher footage and rate of penetration (ROP) than roller cone (RC) bit (Offenbacher et al., 1983; Glowka et al., 1984).

Mechanism

A large number of studies show that the compressive strength of rock is the highest strength, followed by the shear strength, and the tensile strength is the lowest. The compressive strength is often several to ten times higher than the shear strength. Therefore, the shearing cutting method is relatively feasible and effective. The composite cutting structure of the bit makes use of the mechanical properties of rock and adopts efficient shearing method to break rock, so as to achieve the purpose of efficient drilling. When the bit is drilling into the soft to medium hardness formation, the cutting teeth overcome the formation stress and slide forward under the action of WOB and torque. The rock is broken along its shear direction and produces plastic flow under the action of the cutting teeth, as shown in Figure .2. The cutting process is very similar to that of cutting metal. The cuttings are then carried away to the annulus between the bit and the wellbore by the nozzle.

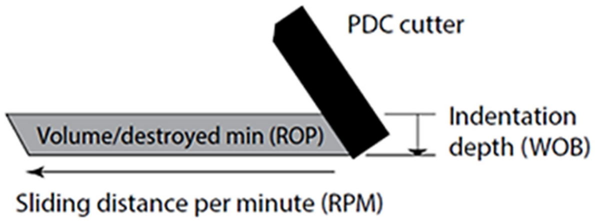

Figure 2.2 Mechanism of PDC bit (IADC, 2014)

2.2.2 Effect of weight on bit (WOB)

During drilling, bit teeth drill into formation under applied WOB, and WOB becomes one of the most important factors affecting bit penetration rate because it affects bit penetration depth. Laboratory experiment and field tests have showed that the ROP is very sensitive to WOB, and the relationship between WOB and ROP is almost linear on the premise of full bottom hole purification (Figure), but the change rate of ROP with WOB is different with different rock strength. In fact, with the gradual increase of WOB, the cuttings will be accumulated and the ROP will decrease correspondingly.

2.2.3 Effect of rotary speed (rpm)

Rotary speed (rpm) is a term that describes how fast a drill bit rotates. The effect of rpm on the rate of penetration (ROP) varies with the type of drill bit. Many researchers have investigated the relationships between two parameters. Generally, when WOB is low, ROP increases with the increase of rpm, but when WOB is high, ROP increases slowly with the increase of rotational speed, which is mainly caused by the untimely removal of cuttings. If the increase of ROP is not proportionate to changes in rpm, the poor response is referred to as founder point as shown in Figure . The relationship can be expressed as Eq. 1 (Ye, 2004):

$$R \propto n^{\lambda} \quad [1]$$

where n is rotary speed and λ is the rpm exponent.

According to Ransey (2019), the rpm exponent is usually less than one. A value of 0.7–0.8 seems to fit the majority of situations for both insert and milled-tooth bits. From some laboratory research, the exponent may also be functionally dependent on the pressure differential across the bottom of the hole. This effect may be accounted for by performing drill-off tests at the rig site.

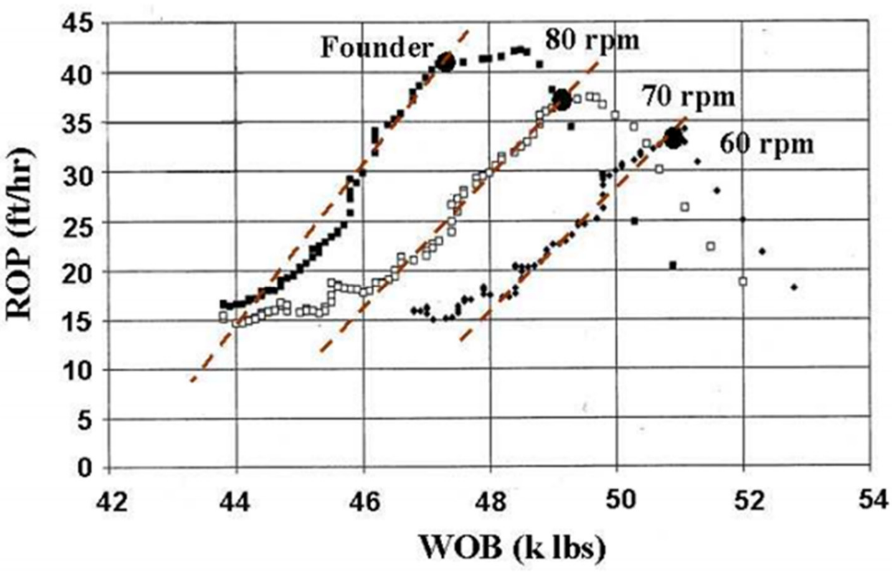

Figure 2.3 Drill off test data showing non-linear response (Dupriest & Koederitz, 2005)

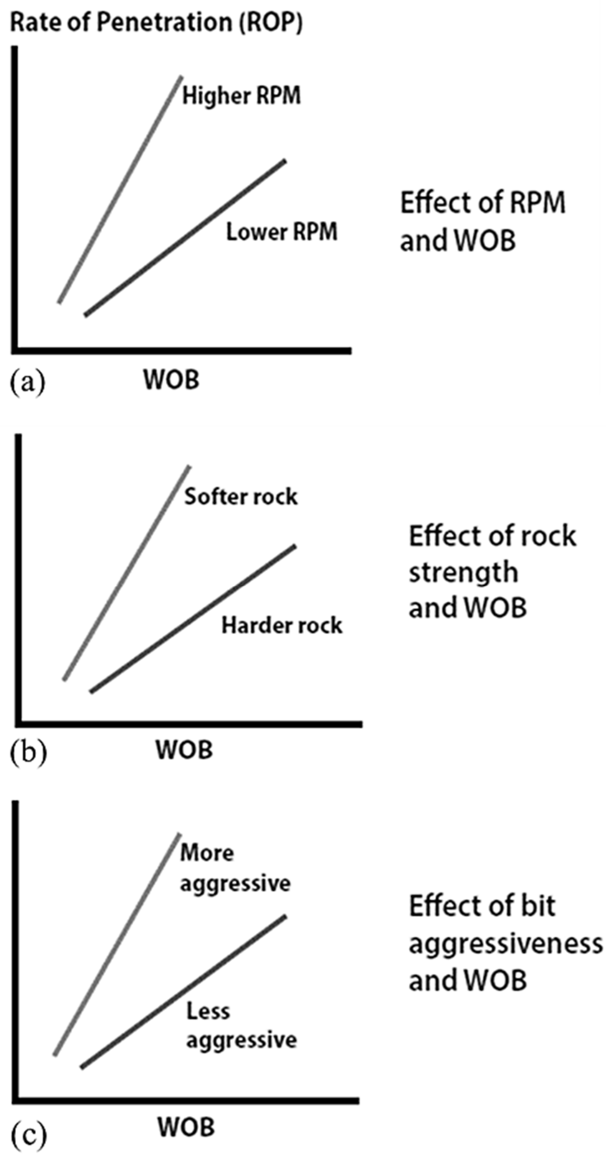

Figure 2.4 Effect of (a) WOB and rpm; (b) rock strength; (c) bit aggressiveness on ROP (IADC, 2014)

2.2.4 Effect of formation strength

Although the same bit type and drilling parameters are adopted, it will give different ROPs when the bit drills into formations with different strengths. This situation is mainly caused by different formation characteristics, which can be described by drillability coefficient. Drillability coefficient is a comprehensive coefficient, which includes many factors other than those considered in ROP equation. Its value can be obtained from ROP equation and field drilling data. It can be seen from Figure 2.4 that with the increase of WOB, the corresponding increase amplitude of ROP is different due to different formation hardness. Kolapo (2021) conducted the analysis of effects of mechanical strengths of rocks on ROP and found that the increase in rock strength will cause a reduction in ROP, which means the higher strength of formation gives lower ROP.

In softer formation, WOB has an obvious effect on ROP. When WOB is extremely high, the ROP will decrease sharply due to bit balling. However, the ROP increases with the increase of rpm, the drilling mode of low WOB with high rpm should be adopted.

In harder formation, the influence of WOB on ROP decreases. In addition, the hardness and abrasiveness of harder formation are higher than that of soft formation. And the wear of bit teeth will be intensified, and the service life of bit will be reduced. Therefore, while maintaining the optimal ROP, the rpm should be controlled at a lower speed, and the drilling mode of medium WOB with medium rpm should be adopted. When the bit teeth are worn, the WOB should be increased to obtain high ROP.

2.2.5 Effect of drilling fluid flow rate (FR)

The drilling fluid flow rate (FR) is one of the essential parameters that should be optimized to achieve the optimal drilling efficiency. The drilling fluid in the drill hole serves as many purposes, including removal of cuttings, cooling and lubrication of drill bit, prevention of collapse, etc.

The main problems to be considered in selecting drilling fluid types are to ensure wellbore stability and reduce bit balling. There are two commonly used types of drilling fluids, including water-based drilling fluid and oil-based drilling fluid. Low price and simple preparation procedure are the main benefits of water-based drilling fluid, but the cuttings are more likely to hydrate, resulting in bit balling. Furthermore, the oil-based drilling fluid can effectively inhibit the hydration and has a good lubrication performance which can alleviate the wear of bit cutters, but the price is more expensive.

The viscosity of drilling fluid affects bit ROP indirectly by influencing circulating pressure loss, bit cleaning and bottom hole cleaning. Under the certain horsepower, with the increase of drilling fluid viscosity, the pressure drop in the drill string and annulus will increase, the pressure drop at the nozzle will decrease, the flushing and cooling performance on the drill bit will be weakened correspondingly. The cleaning of bottom hole cuttings will slow down, thus increasing the possibility of bit balling and reducing the ROP.

2.3 Background of Cemented Tailings Backfill (CTB)

2.3.1 Industrial solid wastes

Construction, mining, and other related engineering industries are the fundamental fields in the development of human society, playing an important role in the economies of many countries around the world. However, solid wastes, as produced by mining and other engineering industries, have the characteristics of dispersion, harmfulness, and dislocation (Gou et al., 2019). Since a large amount of solid waste has become one of the important factors that result in environmental problems, solid wastes are transformed into new materials through technical treatment to improve the utilization efficiency of resources and reduce the impact on the environment (Cao et al., 2008).

The mining solid waste has its particularity, which belongs to the "complex resources" including natural waste and artificial waste. It is often characterized by high metal content or special trace elements. Waste residue, fly ash, gangue and tailings are common solid wastes in mining industries. According to Jones et al. (2012), 14 billion tonnes of tailings are produced annually worldwide. Some of the tailings in the form of slurry contain metals, sulfide mineralization, and processing chemicals, which affect groundwater and surface water by seepage (Sako et al., 2018). When dry tailings are stacked together, they occupy a lot of land area and may affect the air quality by the wind. Based on the local geomorphology, rainfall, and wind strength, the mining waste, rich in heavy metals, can be transferred from waste rock dumps and tailings storage facilities into the adjacent soils and streams through runoff and atmospheric deposition (Ghorbel et al., 2010). Furthermore, mining leachates, derived from mine waste, can migrate into the groundwater system either in particulate or soluble forms. As a result, topsoil and surface waters around mines may reflect the impact of lateral contamination, whilst the groundwater system is generally exposed to vertical contamination (Davis et al., 2010). Therefore, the greening of the mineral production process is one of the important mining environmental problems to be solved urgently. A large number of previous scholars have begun to verify the feasibility of utilization of tailings as aggregates, supplementary cementitious material, and for cement clinker production by a series of experiments (Gou et al., 2019).

Tailings are just a general term, and the types of tailings include but are not limited to metal tailings from iron, copper, gold, lead, zinc processing, and nonmetal tailings from oil sand, quartz, phosphate, forsterite processing according to their ore deposit. The types of tailings can be also classified depending on the refining methods of minerals, known as gravity tailings, flotation tailings, magnetic tailings, and chemical tailings in the extractive industry (Gou et al., 2019). However, the chemical compositions of tailings are highly variable according to their types of tailings. As a result, if tailings are only classified according to their ore bodies or their refining methods, it is not sufficient for material researchers to understand the nature of tailings and to reuse tailings. The physical properties of tailings are less different among all kinds of tailings compared to the chemical compositions and mineral phases of tailings (Cao et al., 2008). The size fractions of tailings are classified as sand, silt, and clay based on a variety of methods and standards in many mining operators. With the progress of grinding technology, there are more and more silt and clay in the tailings, and even if tailings are used as aggregate, the maximum size of tailings is less than 1 mm in some literature (Filho et al., 2017). In general, the tailings have a highly rough and irregular surface (Zhao et al., 2014), since the grindability of various mineral phases in the tailings is different. Due to the mineral phases, the tailings have a varied density and water absorption (Cao et al., 2008). The technology of cemented paste backfill (CPB) can utilize the storage of up to 60% of the tailings, but the other 40% of the tailings will remain and thus the overall utilization of reduced storage number of tailings has become the focus of research as construction materials, for instance in brick, autoclaved aerated concrete, ceramics, glass, and geopolymers/alkali-activated materials, etc.

Fly ash or ground granulated blast furnace slag are common solid wastes in industrial production. The amount of coal waste (fly ash), released by factories and thermal power plants has been increasing throughout the world, and the disposal of a large amount of fly ash has become a serious environmental problem. The present-day utilization of ash on a worldwide basis varied widely from a minimum of 3% to a maximum of 57%, yet the world average only amounts to 16% of the total ash (Joshi et al., 1997). Fly ash particles are considered to be highly contaminating, due to their enrichment in potentially toxic trace elements which condense from the flue gas. Research on the potential applications of these wastes has environmental relevance, in addition to industrial interest. Considerable research is being conducted worldwide on the use of waste materials to avert an increasing toxic threat to the environment or to streamline present waste disposal techniques by making them more affordable. It follows that an economically viable solution to this problem should include the utilization of waste materials for new products rather than land disposal (Ahmaruzzaman et al., 2010).

Fly ash is generally grey, abrasive, mostly alkaline, and refractory. The geotechnical properties of fly ash (e.g., specific gravity, permeability, internal angular friction, and consolidation characteristics) make it suitable for use in the construction of roads and embankments, structural fill, etc. The pozzolanic properties of the ash, including its lime binding capacity, make it useful for the manufacture of cement, building materials concrete, and concrete-admixed products. The chemical composition of fly ash like a high percentage of silica (60–65%), alumina (25–30%), magnetite, Fe_2O_3 (6–15%) enables its use for the synthesis of zeolite, alum, and precipitated silica. The other important physicochemical characteristics of fly ash, such as bulk density, particle size, porosity, water holding capacity, and surface area make it suitable for use as an adsorbent (Ahmaruzzaman et al., 2010).

2.3.2 Backfill types

Backfill material is categorized as hydraulic backfill, paste backfill, and rock backfill. In order to increase the strength of the backfill material, a small amount of binder (Portland cement and fly ash) is added to the mixture. Paste backfill not only supports the ground for the pillars and walls, but also helps stop caving, roof collapse, and improves pillar recovery (Coates 1981). The paste backfills can obtain a similar strength of rock backfills by using less cement than hydraulic backfills. It utilizes different size distribution of tailings and consists of high solid contents, resulting in the reduction of surface tailings impoundment requirements. While, rock and hydraulic backfills prefer less solid content or larger size distribution of tailings. Furthermore, the decant water from paste backfills can be virtually eliminated, which gives the lower costs and reduces associated problems with barricade set-up. The existing borehole delivery systems of slurry fills can also be applied to the paste backfills delivery. In the SMD project, the selected type of backfill system is paste backfill system (cemented tailings backfill). Paste backfill system is less complex than rock backfill and hydraulic backfill system in the design work of preparation and distribution.

2.3.3 Design of cemented tailings backfill (CTB)

The technology of cemented paste (tailings) backfill (CTB) is implemented in many modern mines around the world, especially in Canada (Grice, 1998). The standard components of a cemented tailings backfill mixture, including the tailings, binder and water, must be mixed thoroughly to produce a homogeneous mixture. However, there is no definition referring to the standard backfill. The properties of CTB highly depend on the properties of tailings and binders. Tailings size distribution plays a significant role in the porosity and the strength of the backfill. In particular, the proportion of fines (less than 20 μm) in the tailings has a strong influence on the strength gain of the cemented paste backfill. CTB made of fine tailings usually generates lower strength. Besides, in most cases, the CTB must contain at least 15% by weight of particles less than 20 μm in diameter. As for our mining tailings, there are only 10% tailings of less than 130 μm. Portland cement has a finer size distribution than the mine tailings. Therefore, the Portland cement was added to paste backfill to improve the pumpability and strength of the mixture significantly. In our backfill design, fly ash was also used as a binder. Unlike Portland cement, fly ash possesses some hydraulic properties, and particles are typically spherical, ranging in diameter from less than 1 up to 150 μm, the majority being less than 45 μm. In most applications, fly ash is used to achieve the benefits, such as reducing the cement content to reduce costs, improving the workability and rheological properties, and achieving required levels of strength in backfill beyond 90 days of curing (long-term curing).

2.4 Underwater Concrete Method and its Application on Backfill

Underwater concrete method has been a method for the construction with high water levels and almost all off- and on-shore structures. Underwater concrete is one special type of high-performance concrete, mixed with the indispensable anti-washout admixture, which has high flowability and can place down to the borehole by its self-weight. Underwater anti-washout concrete focuses on the improvement of the performance of concrete itself, that is, by adding underwater non-dispersing agents and flocculants (thickeners) to increase the viscosity of the concrete itself, so as to realize the direct drop and pouring of concrete in the water. When it meets with water, the binders will not be lost, the concrete will not segregate, and it can self-level and self-compact. For an instance, the addition of 5% silica fume and 0.05% triethanolamine early strength agent can significantly improve the early strength of underwater non-dispersible concrete (Imam, 2004). The underwater anti-washout concrete mixed with this formula can fully meet the specification requirements.

Anti-washout admixture (AWA) is added into the concrete to improve or enhance the stability of fresh cementitious mixtures. AWA is composed of water-soluble cellulose ethers or water-soluble acrylic polymers and its main function is to increase the viscosity of the cemented mixture. AWA has strong anti-dispersion and fluidity, which make it possible to realize the self-leveling and self-compacting of underwater concrete, effectively inhibit the water dispersion of cemented mixture during placement and pollution of the construction water area (Hama et al., 1997).

Most of the currently used underwater anti-washout admixtures are of compound type. In addition to the main thickening agent, water reducer and other main agents are usually used to ensure the overall performance of concrete such as washing resistance and fluidity. In 1978, Japan introduced this technology from Germany and carried out research based on the actual situation of the country, and successively developed special admixtures for the preparation of underwater concrete. The research on underwater anti-washout concrete mainly focuses on the improvement of anti-dispersing agent, the application technology of underwater anti-washout concrete, and the actual construction operation. Compared with ordinary concrete, underwater anti-washout concrete is very beneficial for protecting sea-retaining projects, seaside concrete structures, marine concrete structures, and preventing seawater corrosion (Sikandar et al., 2020). In the development of anti-washout property for cemented mixture, a significant point is the choice of raw materials, especially the choice of the AWA. There are many kinds of AWAs that can be used as the anti-dispersing agent, and their respective performance characteristics are different. Therefore, which AWA is chosen as the main anti-washout agent requires a series of judgment analysis and comparison from laboratory tests (Yahia et al., 2001).

Regarding the construction of underwater concrete, because its purpose and construction method are different, the concrete mix ratio should not be the same. It is advisable to mix underwater non-dispersing agent and prepare underwater anti-washout concrete for the construction of underwater concrete for repairing parts of buildings with a relatively large number of pouring warehouses. For cast-in-place piles and underground continuous walls, it is not necessary to construct underwater non-dispersed concrete, and the mix ratio selection test can be carried out in accordance with relevant regulations (Heniegal, 2016a).

Other defects of underwater concrete are mainly manifested in fluidity deviation and rapid fluidity loss (Heniegal et al., 2016b). To prepare underwater anti-washout concrete and maintain its certain fluidity, it is also necessary to add water reducer into the cemented mixture working with AWA. Both the underwater non-dispersing agent and the water reducer have retarding effect. When the two admixtures are used in combination, the prepared underwater anti-washout concrete has a longer retardation time and lower initial strength of the concrete, which should be paid attention to. In addition, underwater non-dispersing agent is an important part of preparing underwater non-dispersing concrete (Niroshan et al., 2018). Although relevant national ministries and commissions have issued relevant test procedures, the performance and unit price of various products on the market vary greatly (Nakhla et al., 2005). The most important thing is that considering the total amount of underwater anti-washout on the market from the dosage to the unit price, a higher cost per cubic meter of concrete needs to be added. The increase in the cost of concrete is difficult for many construction units to accept, and this will directly restrict the promotion and application of underwater anti-washout admixture in the future.

At present, cemented tailings backfill is an important part of green mining technology. It is an ideal way to solve the collapse of underground goafs, and it is the need to solve the problem of large-scale underground mining. CTB has attracted increasing attention and has been used more and more in actual mining projects. However, due to the small amount of cementitious materials contained in CTB, the backfill materials will be easily affected when the placement condition is full of water. Although the research about the application of AWAs on backfilling technique is rare, it is necessary to investigate the underwater placement of backfill which can eliminate many restrictions.

Chapter 3. Evaluations of Physico-mechanical Properties for Isotropic Rocks

3.1 Introduction

In mining, geotechnical, and civil engineering, physico-mechanical properties of rocks play an indispensable role in the design and construction procedures. In the process of analyzing rock mechanical properties, it is of great importance to get a good knowledge of relationships among unconfined compressive strength (UCS), indirect tensile strength (ITS), and point load index (PLI). Construction projects such as water conservancy and hydropower, transportation, mining, industrial and civil buildings, all involve rock works (Armaghani et al., 2015). Correct analysis of the rock physico-mechanical properties is a prerequisite for rock excavation, reinforcement, and support to ensure construction safety, engineering economy, and building safety. Measurement of ultrasonic velocities is often utilized on site or in laboratory to characterize the dynamic properties of rocks. Since it is a non-destructive method with simple procedures, it has been increasingly used in mining, petroleum and geotechnical engineering (Khandelwal et al., 2010). Many studies have been conducted to investigate the relationships between ultrasonic velocities and physico-mechanical properties (Saito et al. 1974; Youash 1970; Gaviglio 1989). The aim of this work is to investigate the relationships between physico-mechanical properties and ultrasonic velocities. Also, a new approach for strength evaluation and prediction is proposed for specific isotropic rocks.

3.2 X-ray Diffraction (XRD) Analysis

X-ray diffractometer was used to analyze the crystal structure distribution of the materials in the whole experiment (Kralik & Biffis, 2001). X-ray diffraction is an effective method for crystal structure analysis in laboratory. The crystal structure of each material is different and the crystal structure includes parameters such as lattice type and spacing between crystal planes. After irradiating the measured sample with X-ray of certain energy, substances in the sample will be stimulated to produce secondary fluorescence X-rays, so the qualitative analysis of compounds can be carried out by measuring the position of the diffraction angle. Quantitative analysis can be carried out to accurately measure the peak strength of the line and the relationship between the line strength and the angle can determine the size and shape of the grain.

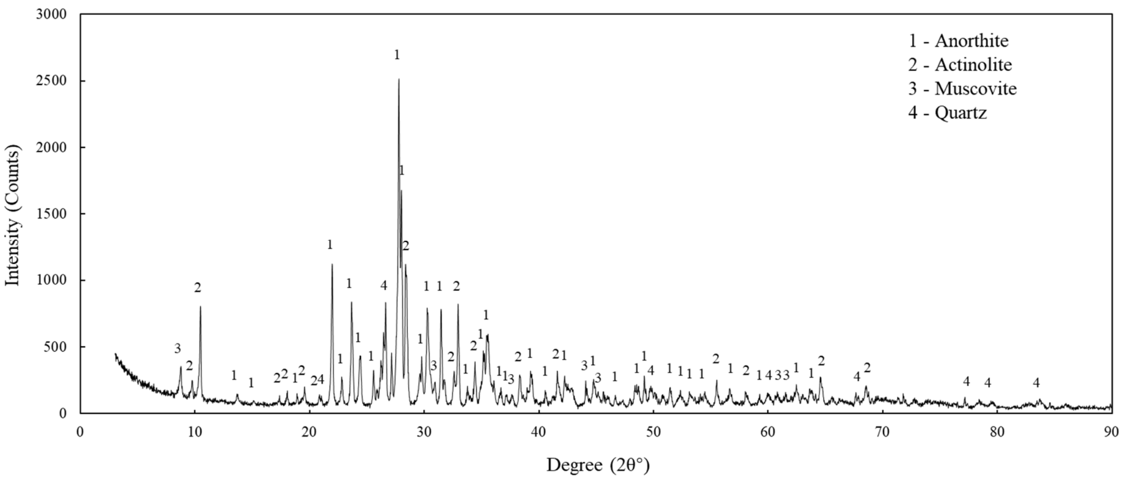

Figure 3.1 XRD pattern of granite

Figure 3.1 and Figure 4.1 reveal the XRD curve graphs of granite and sandstone. The mineral compositions are calculated by semi-quantitative analysis. The granite mainly consists of anorthite (61.4%), actinolite (22.4%), muscovite (13%) and quartz (3.2%). The sandstone mainly consists of quartz (81%), albite (14.3), clinochlore (3%) and kaolinite (0.6%).

3.3 Scanning Electron Microscope (SEM) Analysis

Scanning electron microscope (SEM) is used for the observation and analysis of morphology, structure, and composition of samples (Yu & Lu, 2019). SEM is a kind of grating scanning on the surface of the sample after focusing the electron beam emitted by the electron gun. The composition, morphology and structure of the sample surface are observed and analyzed by detecting the signal generated by the interaction between the electron and the sample. The interactions between the incident electron and the sample will stimulate secondary electron, backscattered electron, absorbed electron, Auger electron, cathode fluorescence and characteristic X-rays. SEM mainly uses secondary electron, backscattered electron, and characteristic X-ray signals to analyze the surface characteristics of samples and is widely used in materials, physics, chemistry, biology, geology, archaeology, microelectronics industry, etc.

The form and texture of the granite and sandstone particles were detected by the analysis of images captured through SEM. Figure 3.2 and Figure 3.3 display the micrographs of the granite and sandstone. It is observed that both of two rocks have non-spherical form of particles and show heterogeneous microstructure. The particles are agglomerated and dense dispersed with different sizes and irregular shapes.

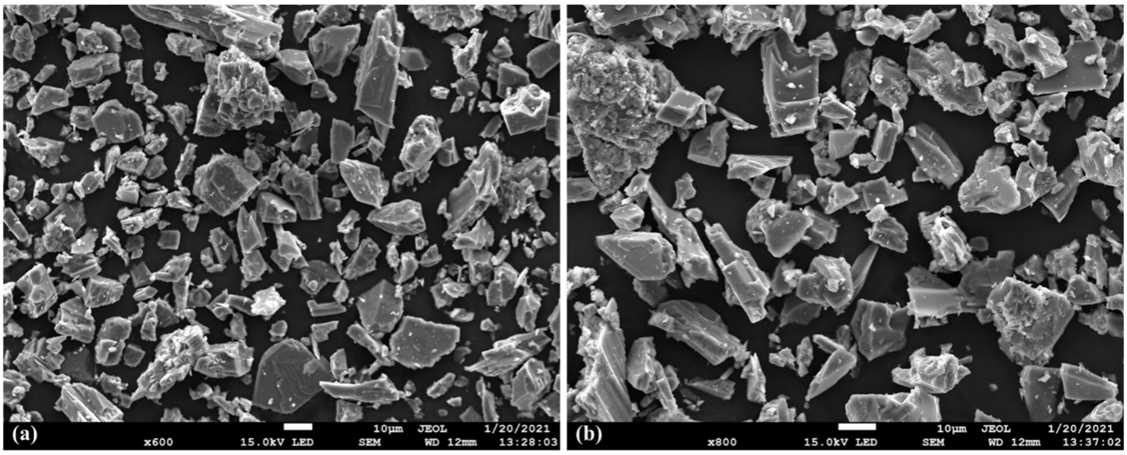

Figure 3.2 SEM micrographs of the granite: magnifications of (a) 600 and (b) 800 times

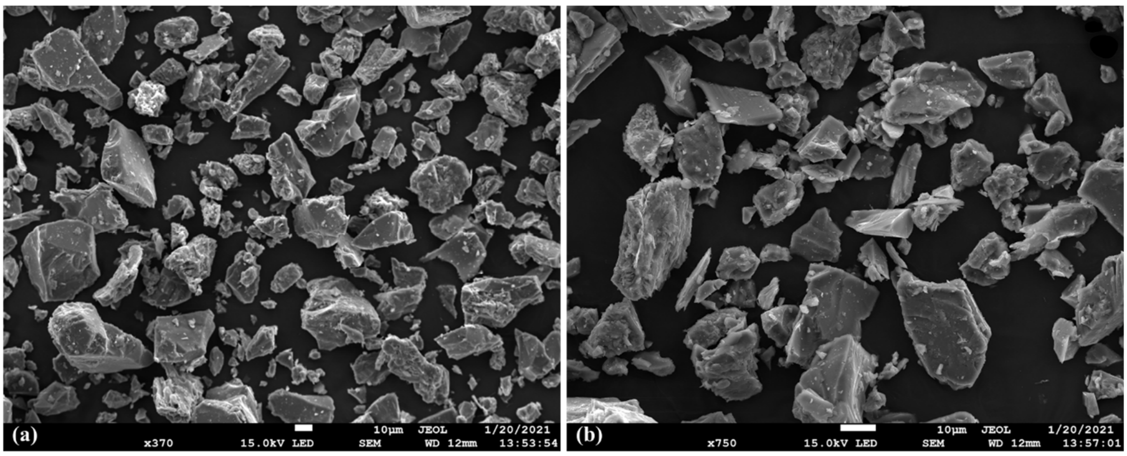

Figure 3.3 SEM micrographs of the sandstone: magnifications of (a) 370 and (b) 750 times

3.4 Empirical Correlations and A New Approach for Strength Evaluation of Isotropic Rocks (Paper #1)

Weizhou Quan[1], Golam Rasul[1], Abdelsalam Abugharara[1], Mohammad Azizur Rahman[2], Yahui Zhang[1] & Stephen Butt[1]

[1]Department of Process Engineering – University of Newfoundland, St. John's, NL, Canada

[2]Department of Petroleum Engineering – Texas A&M University at Qatar, Doha, Qatar

This section is a paper accepted in the 74th Canadian Geotechnical Conference and authored by Weizhou Quan, Golam Rasul, Abdelsalam Abugharara, Mohammad Azizur Rahman, Yahui Zhang and Stephen Butt. The MEng candidate was involved with the planning and conduction of the experiments, the data analysis, and the writing of the paper.

Abstract

In this study, the mechanical property and ultrasonic velocity of granite, representing high strength of natural isotropic rock, and rock like material (RLM), representing high strength synthetic isotropic rock were determined in the laboratory. Empirical equations have been developed between the unconfined compressive strength (UCS), Brazilian tensile strength (BTS) and point load index (PLI), between BTS and PLI, between P-wave and UCS, Young's modulus and Poisson's ratio. The student t-test was performed to check the sensitivity of the empirical relations. Additionally, a novel strength testing method named mono UCS-PLI test, which may avoid the necessity for time consuming and tedious laboratory testing, was proposed in this study to reduce limitations and strictness of the conventional standard strength tests. Two types of splitting failure modes were observed,

including two blocks and three blocks. These results perform a relatively stable range between mono UCS-PLI testing values and conventional standard testing values which depict the research potential for the future study.

3.4.1 Introduction

In the process of analyzing rock mechanical properties, it is of great importance to get a good knowledge of relationships among unconfined compressive strength (UCS), indirect tensile strength (ITS), and point load index (PLI). These three strengths of rocks play an indispensable role in rock characterizations. Construction projects such as water conservancy and hydropower, transportation, mining, industrial and civil buildings, all involve rock works (Armaghani et al., 2015). Correct and timely evaluation of the stability of the rock mass involved in rock engineering construction is a prerequisite for rock excavation, reinforcement, and support to ensure construction safety, engineering economy, and building safety.

The UCS and ITS of rocks are the basic measures in mechanical properties. For a long time, the unconfined compressive strength of rocks has been widely used as the basis of rock classification and used to evaluate rock quality and stability (Chan et al., 2012). The Brazilian tensile strength test is a laboratory test for indirect measurement of tensile strength. Due to its simplicity and efficiency, it is the most widely used laboratory testing method in geotechnical investigation of brittle materials, including concrete, rock, rock-like materials, and cemented materials. PLI can quickly determine the strength of rocks on site and has been widely used worldwide (Chau & Wong, 1996). It can also be used to evaluate the anisotropy of rock strength and predict other related strengths such as UCS and ITS. Since the 1970s, many scholars have done a lot of research on the correlations among these three mechanical strengths. Wang et al. (2014) studied the relationship between the compressive and tensile strength of coal samples and the point load index and found that these three strengths are related. Verma et al. (2015) obtained formulas of PLI ($I_{s(50)}$), UCS and ITS of rocks with different lithology and weathering degree through experiments. Elizabeth et al. (2012) studied the relationship between the hardness of Hong Kong rock and the PLI and found that the UCS and PLI have a strong correlation. Sepahi et al. (2014) derived the conversion formula of andesite point load strength index and uniaxial compressive strength. However, because the point load index test calculation formula is not unified, and the above research on the point load strength mostly uses the point load strength index, the relationship between PLI ($I_{s(50)}$) and the uniaxial compressive strength is obtained (Garcia & Romo, 2009). It is feasible to use the point load strength of the rock to determine the standard value of the compressive strength of the rocks and can solve the problem that the broken core cannot provide the standard value of the unconfined compressive strength.

In addition, there are some limitations and strictness of conventional UCS, ITS, and PLI tests. UCS and PLI tests have been widely used in geotechnical, mining, and civil engineering, and its significance has been demonstrated by many researchers (Hoek, 1977; Barton et al., 1974). However, the limitations and strictness in standard methods for determining UCS and PLI make them tedious, time consuming, and expensive (Singh et al., 2012). Moreover, obtaining or coring standard samples is often impossible when the sample sizes are not on a big scale, the rocks have inside fractures that make the rocks fragile, or during oil or gas well drilling. Many indirect methods, such as Schmidt rebound number, impact strength and sound velocity test, are utilized to predict the strength of rocks. However, there are not any available big scale samples for conventional indirect testing methods especially during the drilling operations. The strict safety rules should be obeyed during the UCS tests because a high load is required by high strength rocks, which make the tests more complicated. In addition, the PLI method has strict valid fracture requirement for the rock breaking because it utilizes two conical platens which make the placement of samples inconvenient.

In this paper, two types of rocks were investigated, including granite, representing high strength of natural isotropic rock, and rock like material (RLM), representing high strength synthetic isotropic rock. The RLM was composed of Portland cement and fined-grained aggregate, whose isotropic properties have been confirmed (Abugharara et al., 2016). The strength of all rocks was determined through a comprehensive set of strength tests that included standard strength tests: unconfined compressive strength (UCS), indirect tensile strength (ITS), and point load index (PLI). Strength tests were conducted using the same calibrated geomechanics loading frame and applying the corresponding loading rate. Empirical equations have been developed among the unconfined compressive strength (UCS), Brazilian tensile strength (BTS), point load index (PLI), P-wave, Young's modulus and Poisson's ratio. The student t-test was performed to check the sensitivity of the empirical relations. The strength tests also involved an innovative strength test, named mono UCS-ITS test proposed in this study to reduce limitations and strictness of the conventional standard strength tests, which may avoid the necessity for time consuming and tedious laboratory testing procedure.

3.4.2 Materials, Equipment and Methods

3.4.2.1 Samples preparation

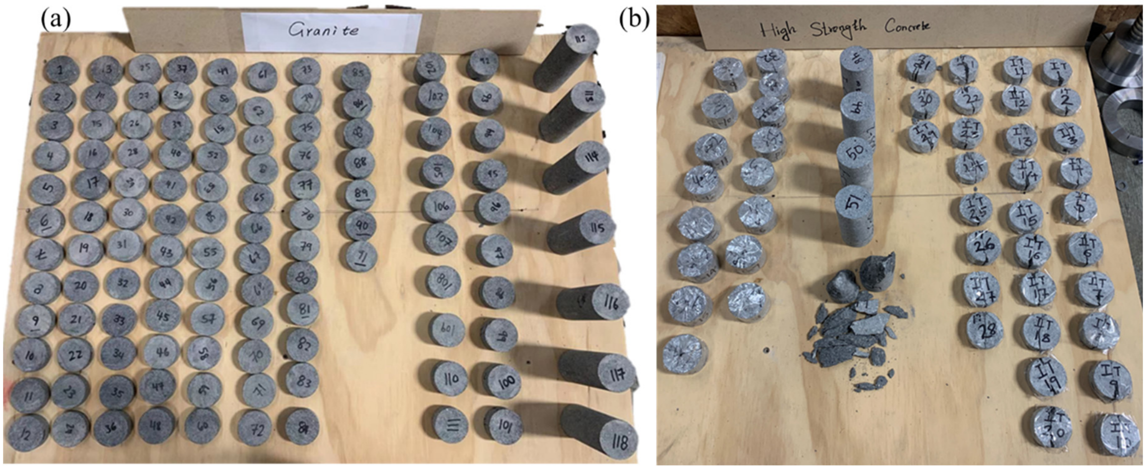

Figure 3.4 (a) Granite and (b) RLM samples for characterization

Two types of rocks have been investigated in this study, including granite, representing high strength of natural and isotropic rocks, and rock-like materials (RLM) high strength concrete, representing high strength synthetic isotropic rocks. The tested samples were cored from big rock blocks by small drilling simulator (SDS) in Drilling Technology Laboratory with the approximate diameter 47.17 mm coring samples. Then, the coring samples were cut into small samples with different thicknesses and lengths for UCS, ITS, and PLI tests by an electrical saw. The obtained rock samples were demonstrated in Figure 3.4 and the dimensions of rock samples are based on ASTM D7012, ASTM D3967, and

ASTM D5731. The water contents of the samples varied from 0.02% to 0.45%, which suggests the effect of water content on the rock properties can be neglected.

3.4.2.2 Methods

Data collection

This study focused on the behavior of granite and rock-like materials (RLM) high strength concrete. The properties of interest are bulk density, compressive and tensile strengths, point load index, compressive modulus, and ultrasonic velocities of the granite and RLM rocks. The density study focused on the statistical distribution and the range of variation using 91 data on granite and 50 data on RLM. The number of data collected based on the properties of the rock was also a clear indicator of the interest in rock behavior around the world.

Unconfined compressive strength (UCS) test

The strength of rocks can be estimated by determining its UCS. Before conducting UCS tests on the specimens, the ends of each specimen were trimmed off by an electric saw to ensure the surfaces of the specimens were flat and parallel, and the specimens had the average heights of 100 mm and diameters of 47 mm. A grinder is usually used to grind concrete specimens, natural stones, tiles, block pavers, ceramic materials, etc., and provided the final step in preparing test specimens. The sample sizes and testing procedure are based on ASTM D7012 and the UCS can be estimated by Eq. [2]:

$$\mathrm{UCS\ (MPa)} = \frac{\mathrm{P}}{\mathrm{A}} \qquad [2]$$

where P=failure load, N; A=cross-sectional area, mm^2.

Tensile strength test

The Brazilian test is a laboratory test for indirect measurement of tensile strength. In this test, the thickness to diameter ratio was 0.2 to 0.4 for the granite and RLM samples. The specimens were placed between the machine plates, as shown in Figure 3.5, with a loading configuration of flat loading platens. The load was continuously increased at a constant rate within the range of 0.05 to 0.35 MPa/min (500 to 3000 psi/min) splitting tensile stress until failure of the specimens occurred. Usually, the indirect tensile strength is determined based on the assumption that failure occurs at the highest tensile stress point, that is, at the middle of the disc. At the failure point, the tensile strength of the specimen can be calculated as Eq. [3] (ASTM D3967-08):

$$\sigma_t = \frac{2P}{\pi Dt} = 0.636\frac{P}{Dt} \qquad [3]$$

where P is maximum applied load by the testing machine (N), D is the diameter of the test specimen (mm), and t is the thickness of the test specimen, measured at the center (mm).

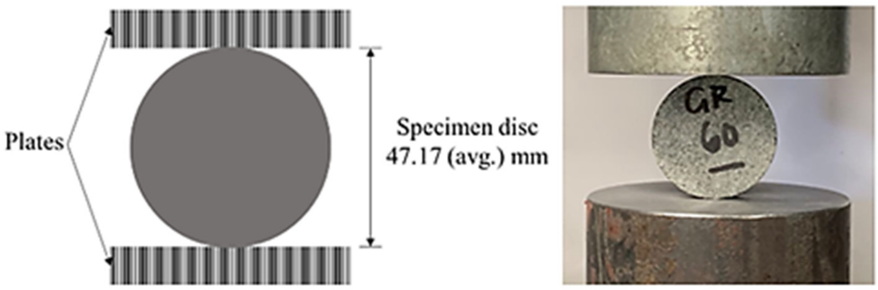

Figure 3.5 Brazilian tensile strength test

Point load index (PLI) test

The point load index (PLI) is the indirect way of estimating UCS when the sample is not in regular shape or it is hard to core. This test was conducted following ASTM D5731−16. Figure 3.6 demonstrates one test on one RLM core sample which was put between the two conical platens. According to the standard, core length was no less than 0.5 times of core diameter. The load was steadily increased within 10 to 60 s and the failure pressure was recorded. In this study, axial point load tests were conducted for all PLI samples with length/diameter ratio of 0.38 to 0.59 because of the laboratory equipment setup.

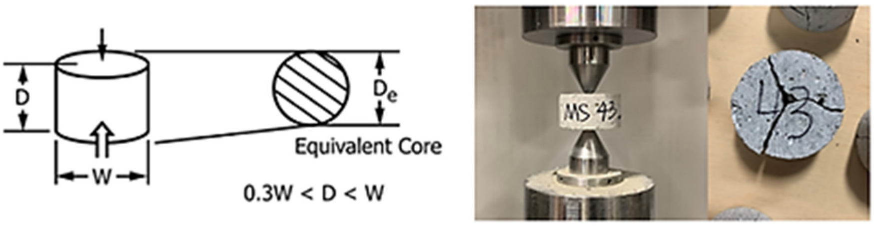

Figure 3.6 Demonstration of PLI test and failure on specimen

According to the failure load, PLI can be estimated from the Eq. [3-5]:

$$I_{S(50)} = F \cdot I_S \qquad [4]$$

$$I_s = P/D_e^2 \qquad [5]$$

where P = failure load, N; D_e = equivalent core diameter, mm, F is correction factor and is given by:

$$F = (D_e/50)^{0.45} \qquad [6]$$

where D_e^2= 4WD/π for axial, block, and lump tests, mm^2.

Acoustic elastic properties test

Dynamic elastic constants were calculated from density and P- or S- wave velocities following ASTM D2845-08. The test apparatus was demonstrated in Figure 3.7. Pulse was initiated and transmitted through one rock core by one S-wave transducer and received by the other S-wave transducer. The pulse and received wave were displayed in one oscilloscope. S-wave transducers were used due to that it obtained both P- and S-waves. P-wave was recognized by the first arrival of received waves due to higher magnitude of P-wave velocity than S-wave velocity. S-wave was recognized by rotating one of the transducers on the purpose of changing the polarization angle between two transducers. In this way, the amplitude of S-wave changed with the rotation of transducer. The first arrival of S-wave lay the position behind P-wave.

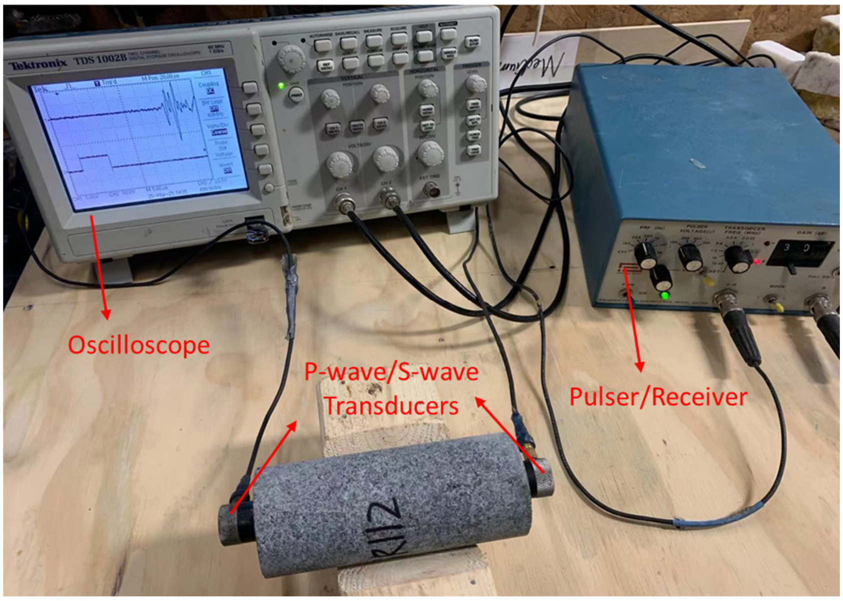

Figure 3.7 Demonstration of ultrasonic test for rock samples

P-wave and S-wave velocities V_P and V_S, respectively:

$$V_p = L/T_p \qquad [7]$$

$$V_s = L/T_s \qquad [8]$$

where L = Pulse propagation distance, m; T_P = P-wave travel time, s; T_S = S-wave travel time, s.

Acoustic elastic constants were calculated based on density and acoustic travel times:

$$E = \left[\rho V_s^2\left(3V_p^2 - 4V_s^2\right)\right]/(V_p^2 - V_s^2) \qquad [9]$$

$$\mu = (V_p^2 - 2V_s^2)/[2\left(V_p^2 - V_s^2\right)] \qquad [10]$$

where E = Young's modulus, Pa; μ = Poisson's ratio.

Novel mono UCS-PLI test

In mining and geotechnical engineering, determination of mechanical properties of the rocks plays a significant role in the analysis of geotechnical problems. Determination of various mechanical properties of rocks is expensive and time consuming, and sometimes it is difficult to get cores to perform direct tests in restricted sampling conditions. In this study, a novel strength testing method named mono UCS-PLI tests is proposed. The novel mono UCS-PLI test utilizes the bottom flat platen from UCS test and the top conical platen from PLI test (shown in Figure 3.8). The bottom flat platen makes the testing samples easier to be placed than conventional PLI test, which can shorten the preparation time. And the top conical platen makes the testing samples easier to break, which needs less energy than conventional UCS test. Four types of rocks, granite, sandstone, RLM-high strength concrete and RLM-medium strength concrete, were prepared for the mono UCS-PLI test. All the samples were in the diameter of 47 mm and length of approximate 50 mm.

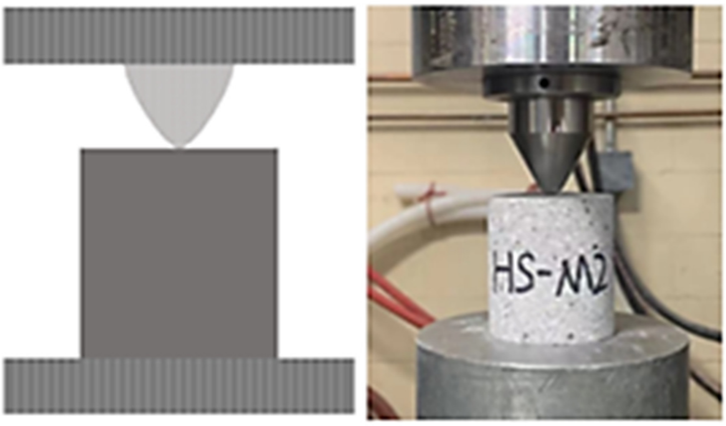

Figure 3.8 Demonstration of novel mono UCS-PLI test

3.4.3 Results and Analysis

3.4.3.1 Bulk density

The bulk density of a rock was obtained from the weight of dried specimen divided by the total volume of the specimen, including the pore space. Based on the 91 and 50 data for granite and RLM respectively, the average bulk densities were 2.88 g/cm^3 and 2.31 g/cm^3. In this study, the statistical details of densities and the histograms were developed for each type of rock bulk density data sets to identify the distribution as shown in Figure 3.9. The histograms show the relationship between the class of data and the frequency distribution of the data.

According to 91 data for granite samples, the bulk density varied from 2.74 g/cm^3 to 3.06 g/cm^3 with the standard deviation of 0.048 g/cm^3 and coefficient of variation (COV) of

1.65%. Approximately 80% of granite samples were distributed between 2.88 g/cm^3 to 2.91 g/cm^3. The largest extreme value distribution for granite bulk density was found using the Anderson-Darling statistic (AD) and P-value (hypothesis testing).

Based on 50 data for RLM samples, the bulk density varied from 2.26 g/cm^3 to 2.39 g/cm^3 with the standard deviation of 0.048 g/cm^3 and coefficient of variation (COV) of 1%. Approximate 76% of RLM samples were distributed between 2.29 g/cm^3 to 2.33 g/cm^3. Different distribution analysis, the Anderson-Darling statistic (AD) and P-value (hypothesis testing), for the densities of RLM were performed to find the largest extreme value distribution.

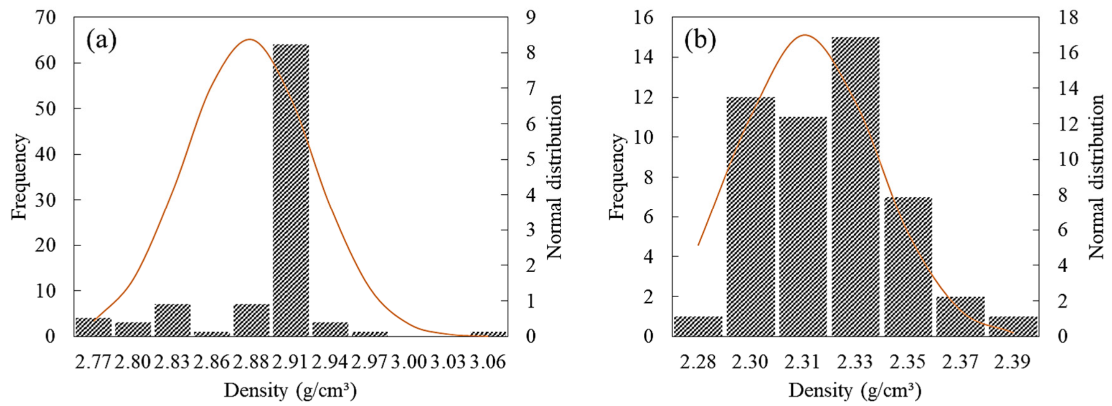

Figure 3.9 Largest extreme value distribution of density for (a) granite and (b) RLM

3.4.3.2 Mechanical properties

Unconfined compressive strength (UCS)

Based on the limited granite and RLM rock samples for UCS tests, the compressive strength value for granite varied from 111.9 MPa to 139.9 MPa with an average of 126.1 MPa, a standard deviation of 13.9 MPa and coefficient of variation (COV) of 11.1%. The compressive value for RLM varied from 81.9 MPa to 109.6 MPa with an average of 98.6 MPa, the standard deviation of 10.3 MPa and coefficient of variation (COV) of 10.4%. The results of UCS tests of different rocks are given in Table 3.2.

Brazilian tensile strength (BTS)

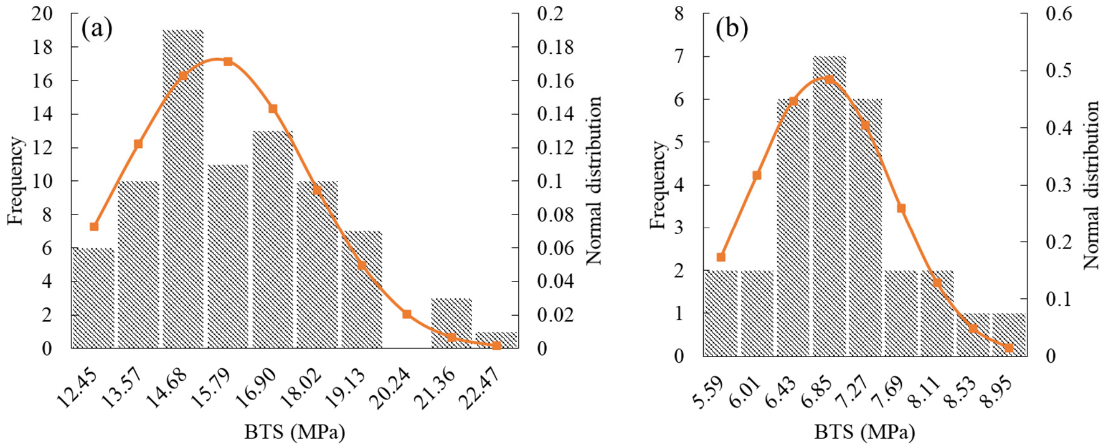

Figure 3.10 Largest extreme value distribution of BTS for (a) granite and (b) RLM

Tensile strength is also an essential parameter. The Brazilian tensile tests were carried out as part of this analysis and showed suitable results. With 79 data of the granite samples, the tensile strength data for granite varied from 11.3 MPa to 22.5 MPa with an average of 15.5 MPa, a standard deviation of 2.3 MPa and coefficient of variation (COV) of 14.9%. Based on the 30 tensile strength data for RLM, it varied from 5.2 MPa to 8.9 MPa with an average of 6.8 MPa, standard deviation of 0.82 MPa and coefficient of variation (COV) of 12.1%. The results of BTS tests of different rocks are given in Table 3.2. It can be seen from Figure 3.10 that the tensile strengths of granite and RLM are basically normally distributed. The granite BTS has higher frequency distributed from 14.68 MPa to 15.79 MPa and the RLM

BTS has higher frequency distributed between 6.43 MPa to 7.27 MPa, indicating that the BTS values of these rock samples are widely distributed in the corresponding intervals.

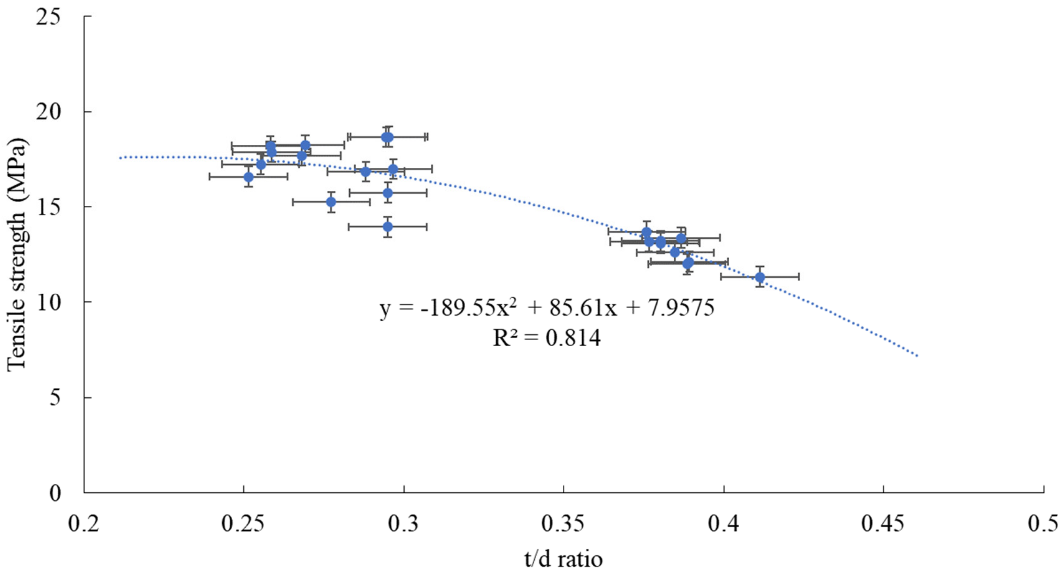

Figure 3.11 BTS versus t/d ratio of granite

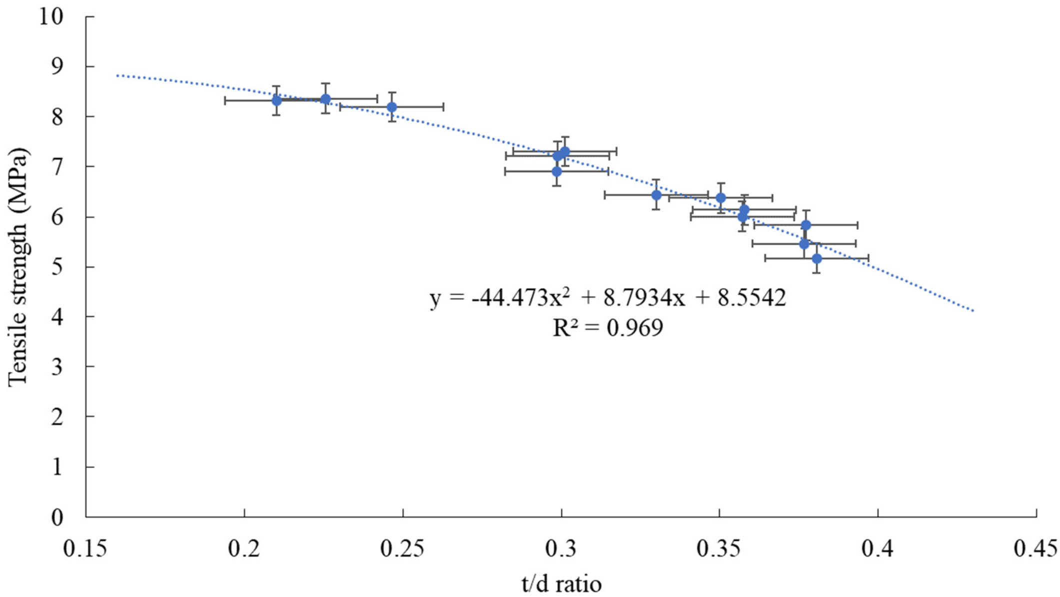

Figure 3.12 BTS versus t/d ratio of RLM

The average tensile tests results of each thickness to diameter ratio (t/d) are plotted in Figure 3.11 and Figure 3.12. In this study, the average diameter of the granite samples is 47.73 mm. Figure 3.11 shows that the tensile strengths of the granite disc samples increase with the decreasing thickness to diameter ratio. Furthermore, when the t/d ratio is greater than 0.27, the corresponding tensile strengths obviously decreases with the increase of the t/d ratio, while as the t/d ratio approaches or is less than 0.27, the tensile strength increases slowly and gradually tends to be stable. The fitting curve performs a high R square value (0.814) relationship. The granite tensile strength behaviour is consistent with the rock splitting tensile strength performance reported by Deng (2012). When the ratio of thickness to diameter is less than 0.3, the distribution of tensile stress on the central axis of the disk specimens tends to become uniform gradually, which also explains the reason why the tensile strength tends to be stable when the thickness to diameter ratio is less than 0.3. As for the testing of the RLM disc samples, it also shows that the tensile strength is decreasing with the increasing of t/d ratio in Figure 3.12. The R square value of this RLM reaches 0.969 which means the equation can give an accurate prediction of tensile strength tests when t/d ratio is given. RLM is a type of high strength synthetic isotropic rock which is prepared by several materials. The greater the thickness of the sample, the greater the possibility of defects in the sample, and the lower the tensile strength.

The significance of R square values can be determined by the student t-test, assuming that both variables are normally distributed and the observations are chosen randomly. The student t-test compares the computed t value with the tabulated t value using the null hypothesis. In this test, the alpha level was set at 0.05 (95% confidence level). If the calculated t value is larger than the tabulated t value, the null hypothesis is rejected which mean the R square value is significant. The granite and RLM rock samples have different data numbers, the corresponding degree of freedom and critical t value were calculated and obtained from the related tables. As shown in Table , all the calculated t values of the relationships between BTS and t/d ratio of granite and RLM are larger than the tabulated t values which indicate that the BTS has a strong relationship with t/d ratio.

Point load index (PLI)

The point load index (PLI) test is widely utilized because of the simplicity of testing and sample preparation (Kahraman & Gunaydin, 2009). The point load strength index was corrected to those with a specimen diameter of 50 mm ($I_{s(50)}$) according to the method proposed by ASTM D5731−16. In this study, the point load index data for granite varied from 12.77 MPa to 15.25 MPa with an average of 14.17 MPa, the standard deviation of 0.69 MPa and coefficient of variation (COV) of 4.9% analyzing 20 data of the granite samples. Based on the 15 PLI data for RLM, it varied from 5.05 MPa to 6.62 MPa with an average of 6.06 MPa, standard deviation of 0.45 MPa and coefficient of variation (COV) of 7.4%. The results of PLI tests of different rocks are given in Table 3.2. The histograms are shown in Figure 3.13, indicating that the PLI of granite and RLM rock samples are basically normally distributed.

The average PLI results of each D/W ratio are plotted in Figure 3.14 and Figure 3.15, exhibiting linear relationships between these two parameters. With the increasing of the D/W ratio, the PLI will increase correspondingly. In order to verify the significance of R value, the student t-test was used to compare the computed t value with the tabulated t value.

In this test, the confidence level was set at 95%. As indicated in Table , all the calculated t values of the relationships between PLI and D/W ratio of granite and RLM are larger than the tabulated t values, the null hypothesis is rejected which mean the BTS has a strong relationship with t/d ratio.

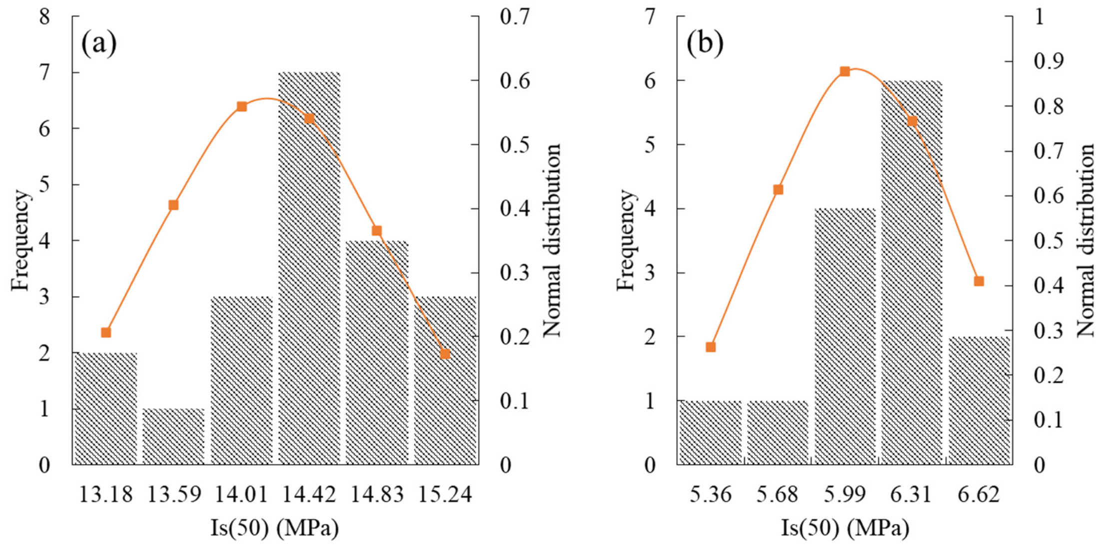

Figure 3.13 Largest extreme value distribution of PLI for (a) granite and (b) RLM

Table 3.1 Student t-test values

Correlations	t test (α=0.05)	
	Calculated value	Tabulated value
BTS and t/d ratio of granite	27.85	2.08
BTS and t/d ratio of RLM	20.52	2.18
PLI and W/D ratio of granite	88.08	2.09
PLI and W/D ratio of RLM	50.74	2.14

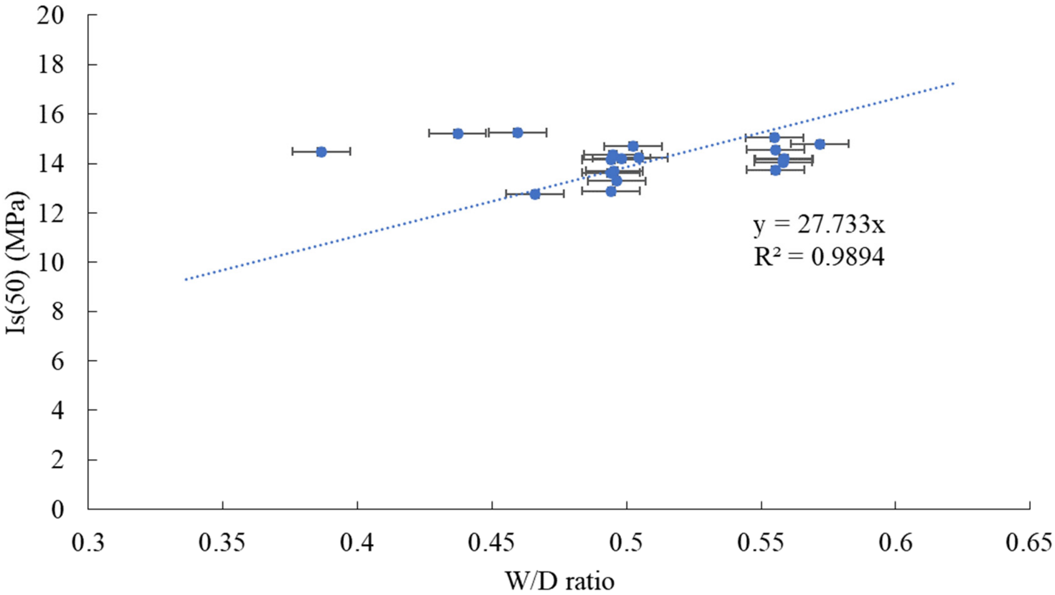

Figure 3.14 PLI versus D/W ratio of granite

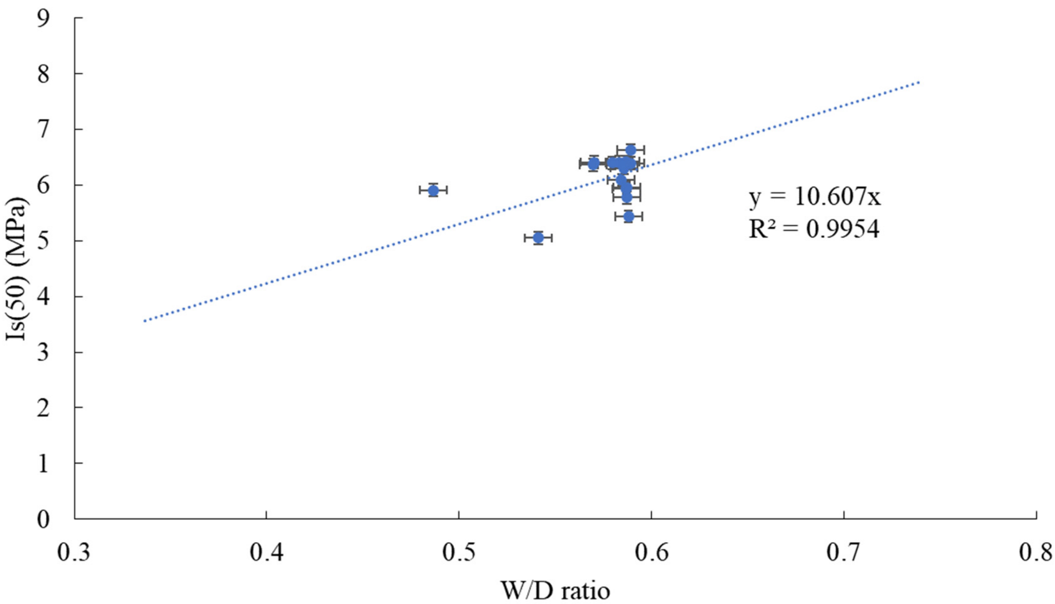

Figure 3.15 PLI versus D/W ratio of RLM

Table 3.2 Statistical parameters of rock properties

	Statistical parameters	Density (g/cm³)	UCS (MPa)	Young's modulus (GPa)	BTS (MPa)	PLI (MPa)	Ultrasonic velocities (km/s)		Elastic constants	
							P-wave	S-wave	E'	Poisson's ratio
Granite	Range	2.73-3.06	111.9-139.9	8.1-13.17	11.34-22.47	12.77-15.25	5328.72-5628.83	3348.48-3480.80	79.49-82.51	0.13-0.21
	Average	2.88	126.1	10.87	15.49	14.17	5480.91	3433.19	81.14	0.18
	Standard Deviation	0.047	13.9	2.57	2.31	0.69	109.34	53.97	1.41	0.033
	COV (%)	1.65	11.1	23.6	14.9	4.89	1.99	1.57	1.74	19.15
RLM	Range	2.26-2.39	81.9-109.6	5.71-10.07	5.17-8.94	5.05-6.02	4936.59-5008.83	2903.67-2976.47	49.01-50.35	0.21-0.25
	Average	2.32	98.6	7.89	6.77	6.1	4977.54	2932.31	49.65	0.23
	Standard Deviation	0.023	10.3	3.08	0.82	0.43	33.59	34.04	0.64	0.014
	COV (%)	1.01	10.4	39.07	12.09	7.05	0.67	1.16	1.29	5.92

3.4.3.3 Ultrasonic velocities

The velocity of ultrasonic pulses travelling in a solid material depends on the density and elastic properties of the material. To determine comparable P-wave and S-wave velocities of different rocks, the samples were cored to provide NX cylinders. The velocities were determined using a Portable Ultrasonic Non-destructive Digital Indicating Tester (PUNDIT) from Tektronix (TDS 1002B). The elastic constants are calculated according to Eq. [8-9] and the results are given in Table 3.2.

3.4.3.4 Property correlations

The relationship between UCS and BTS

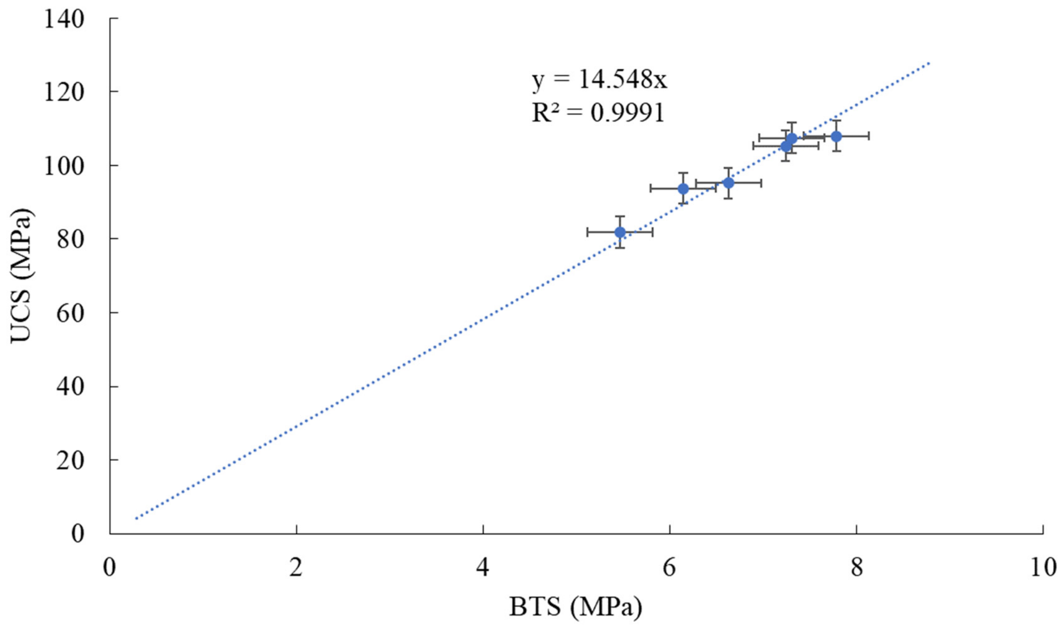

Figure 3.16 Relationship between UCS and BTS of RLM

Figure 3.16 exhibits the obtained UCS versus the BTS of RLM from laboratory tests. As it is shown in this figure, a strong linear correlation (R^2=0.9991) is found between UCS and BTS for RLM. The proposed correlation for prediction of UCS of RLM is given as UCS (MPa)=14.548*BTS. The proposed relationship between UCS and BTS exhibits higher conversion factor than the suggested ratio of compressive strength to tensile strength given by Kahraman et al., (2012). The scattering of our limited data still gives a conversion factor with high confidence which means the new correlation has the advantage of being developed for specific type of rock that is RLM-high strength concrete with a relatively high coefficient of determination.

The relationship between UCS and BTS of RLM

Based on the statistical analysis of the UCS and PLI values of RLM, the selected experimental results were plotted. As shown in Figure 3.17, the best fitted relationship between these two parameters of RLM was found to be represented by linear regression curve (R^2=0.9984) by regression analysis of the scattered points. The proposed correlation for prediction of UCS of RLM is given as UCS (MPa)=16.654*$I_{s(50)}$. The proposed relationship between UCS and PLI is close to suggested ratio of compressive strength to tensile strength given by Forster (1983) and Ghosh et al. (1991). The generalized index to strength conversion factor (K) for NX (47 mm) core is 21 to 23 (ASTM D5631-16). The strength conversion factor of the RLM in this study is 16.654, which is lower than the suggested value, while the accuracy is approximate 72.4% to 79.3% which basically meets the needs of field tests.

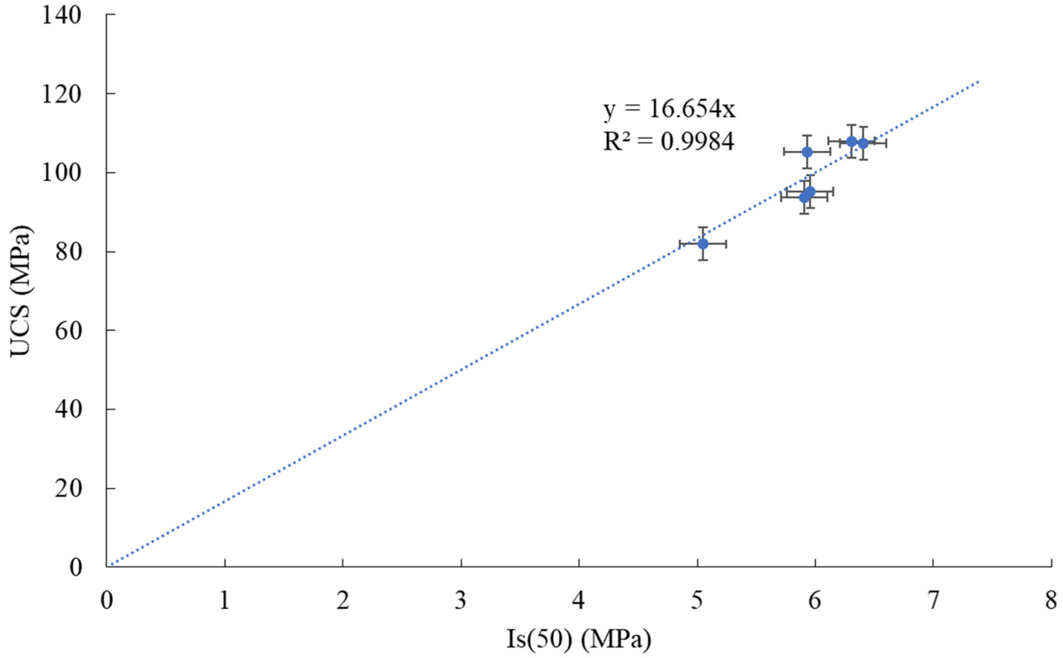

Figure 3.17 Relationship between UCS and PLI of RLM

The relationship between BTS and PLI

The relationships between Brazilian tensile strength (BTS) and point load index (PLI) for tested samples of the granite and RLM are presented in Figure 3.18 and Figure 3.19. The plots indicate a significant correlation between these two parameters and the linear relationships are shown in the regression curve plots. The BTS data was divided into different groups for the regression analysis due to different data number of PLI. Based on these testing results, the average conversion factors between the BTS and $I_{s(50)}$ of granite and RLM are 1.0763 and 1.1053, respectively.

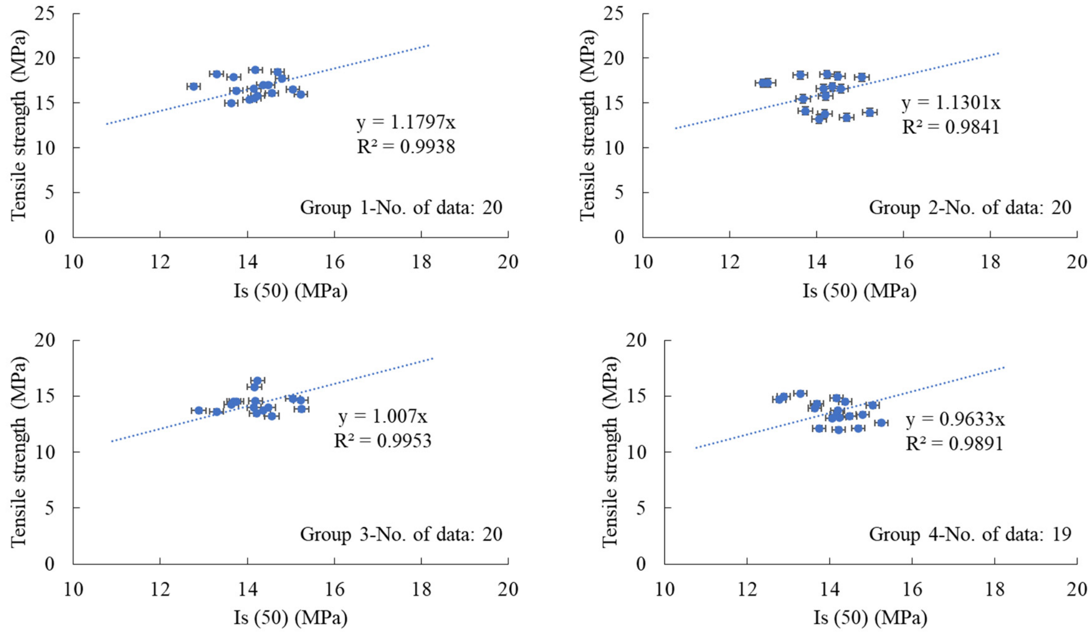

Figure 3.18 Relationship between BTS and PLI of granite

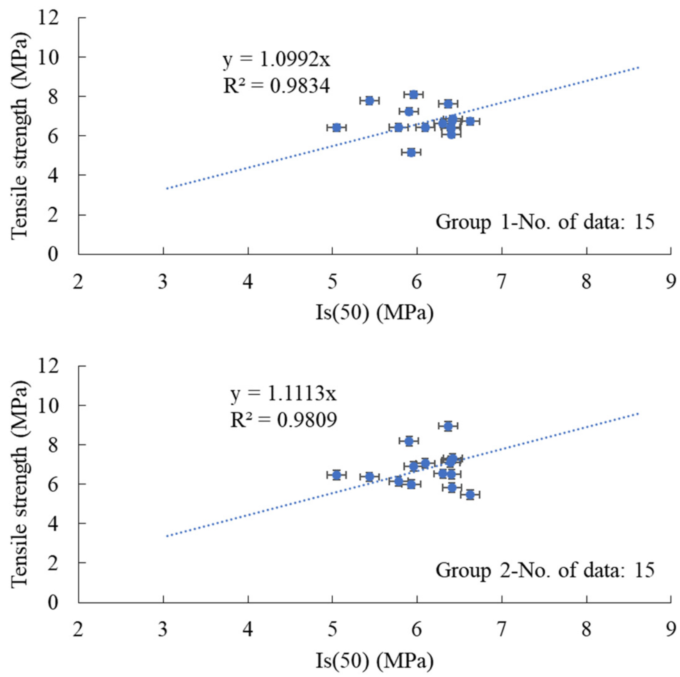

Figure 3.19 Relationship between BTS and PLI of RLM

The relationship between ultrasonic velocities and other properties

To describe the relationship between P-wave velocity and other properties, such as UCS, Young's modulus and Poisson's ratio of the two tested types of rocks, regression analyses were made. The equation of the best fit line and the correlation coefficient (R^2) were determined for each test result. As shown in Table 3.3, in each case, the best fitted relations were found to be represented by linear regression for correlations between P-wave velocity and UCS, Young's modulus, and exponential regression for the correlation between P-wave with Poisson's ratio.

Table 3.3 Relation between P-wave and other properties

Rock type	Parameters to be related	Regression euqations	R^2
Granite	UCS	$V_p = 0.1361*UCS - 614.37$	0.961
	Young's modulus	$V_p = 0.0255*E - 127.59$	0.995
	Poisson's ratio	$V_p = 4E\text{-}07e^{0.0024\mu}$	0.976
RLM	UCS	$V_p = 0.0559*UCS - 170.16$	0.951
	Young's modulus	$V_p = 0.0923*E - 452.01$	0.951
	Poisson's ratio	$V_p = 3E\text{-}09e^{0.0037\mu}$	0.939

3.4.3.5 Mono UCS-PLI test results

Mono UCS-PLI test is a novel method proposed in this study to reduce the limitations and strictness for conventional rock strength prediction methods. Four types of rocks (granite, sandstone, RLM-high strength concrete and RLM-medium strength concrete) specimens were tested. RLM materials were prepared by the different compositions of Portland cement and fine-grained aggregate to obtain different strengths. High strength RLM has the average UCS of 98.6 MPa and medium strength RLM has the average UCS of 69.3 MPa. As it is shown in Figure 3.20, two types of splitting failure modes were observed, including two blocks and three blocks. This performance is consistent with the PLI test valid failure modes because of the top conical platen. The Eq. 2 and Eq. 4 were used to calculate the mono-UCS and mono-PLI values. The obtained average results are shown in Table 3.4. Generally, the size of tested specimens has effect on its mechanical properties. This performance is highly related to the non-homogeneous nature of rock materials. The bigger the size of the specimen, the greater probability of a weaker plane or a fracture affecting the behaviour of material. For sandstone and RLM specimens, the mono-UCS values account for 10.93%-13.01% of standard UCS values and the mono-PLI obtained 10.38%-11.15% higher strength than the standard PLI. These results perform a relatively stable range between mono UCS-PLI testing values and standard testing values which depict the research potential for the future study.

Figure 3.20 Failure mode of mono UCS-PLI tests

Table 3.4 Mono UCS-PLI results of four types of rocks

Rock type	Std. UCS (MPa)	Mono UCS (MPa)	Percentage (%)
Granite	126.09	30.57	24.24
Sandstone	61.43	7.99	13.01
RLM-HS	98.60	10.78	10.93
RLM-MS	78.98	9.00	11.39
Rock type	Std. PLI (MPa)	Mono PLI (MPa)	Difference (%)
Granite	14.17	18.77	32.46
Sandstone	4.32	4.80	11.14
RLM-HS	6.10	6.78	11.15
RLM-MS	5.01	5.53	10.38

3.4.4 Conclusions

In this study, unconfined compressive strength (UCS) tests, Brazilian tensile strength (BTS) tests, point load index (PLI) tests and novel mono UCS-PLI tests have been conducted on hundreds of rock specimens. The testing data was analyzed comprehensively. Based on the current study, the following conclusions can be made:

1) The largest extreme value distribution for granite and RLM densities was determined using the Anderson-Darling statistic (AD) and P-value (hypothesis testing). The densities of both tested rocks are normally distributed.
2) The tensile strengths of granite and RLM are basically normally distributed. The tensile strengths of the granite disc samples increase with the decreasing thickness to diameter (t/d) ratio. When the t/d ratio is greater than 0.27, the corresponding tensile strengths obviously decreases with the increase of the t/d ratio, while as the t/d ratio approaches or is less than 0.27, the tensile strength increases slowly and gradually tends to be stable. As for RLM disc samples, it also shows that the tensile strength is decreasing with the increasing of t/d ratio.

3) The average PLI results of each length to diameter (D/W) ratio exhibit strong linear relationships between these two parameters. With the increasing of the D/W ratio, the PLI will increase correspondingly. The student t-test was used to verify the significance of R square value. All the calculated t values of the relationships between PLI and D/W ratio of granite and RLM are larger than the tabulated t values, which mean the BTS has a strong relationship with t/d ratio.
4) The UCS exhibits strong linear correlations with BTS and PLI. The data gives a conversion factor with a relatively high coefficient of determination which means the new correlation has the advantage of being developed for specific type of rock (RLM-high strength concrete). Significant linear correlations exist between the BTS and PLI of the studied rocks. The results of the sound velocity test show strong linear correlation with UCS and Young's modulus, and exponential correlation with Poisson's ratio.
5) A novel strength testing method named mono UCS-PLI test is proposed in this study. Mono UCS-PLI test utilizes the bottom flat platen from UCS test and the top conical platen from PLI test to reduce the limitations and strictness of conventional rock strength prediction methods. Two types of splitting failure modes were observed, i.e., two blocks and three blocks. These results perform a relatively stable range between mono UCS-PLI testing values and conventional standard testing values which depict the research potential for the future study. Further study is required to investigate how varying the rock type affects the correlations.

Chapter 4. Investigation of Drilling Performance using PDC and RC Drill Bits

4.1 Introduction

In petroleum drilling, improving the drilling process for optimal drilling performance and minimize costs is significant. The drilling rate known as rate of penetration (ROP) can be evaluated as main function of drilling performance. In the field of oil and gas exploration and development, achieving optimal ROP to produce safer and more efficient drilling performance is a key requirement (Zhang et al., 2013; Jain et al., 2017). Various factors have certain effects on ROP, including weight on bit (WOB), rotary speed (rpm), bit hydraulics, drill bit type, cutter wear, etc. In this study, sandstone is used as the testing rock, representing a tight and low permeability isotropic formation. The UCS test, ITS test, and PLI test are adopted to determine the strengths. A fully instrumented laboratory scale large drilling simulator (LDS) is utilized for conducting drilling experiments. The specimens of sandstone are tested through rotary drilling by different types of RC and PDC bits. Various WOBs and rpms are applied during drilling experiments under the same condition of water flow rate. The applied WOB and operational rpm are recorded to analyze the rate of penetration (ROP). The purpose of this study is to evaluate the drilling performance based on drilling parameters and drill bit type, which have a certain guiding significance for on-site drilling operations.

4.2 Tensile and Shear Fracture Examination for Optimal Drilling Performance Evaluation[1] (Paper #2)

Weizhou Quan[1], Golam Rasul[1], Abdelsalam Abugharara[1], Mohammad Azizur Rahman[2], Yahui Zhang[1] & Stephen Butt[1]

[1]Department of Process Engineering – University of Newfoundland, St. John's, NL, Canada

[2]Department of Petroleum Engineering – Texas A&M University at Qatar, Doha, Qatar

This section is a paper accepted in the 74th Canadian Geotechnical Conference and authored by Weizhou Quan, Golam Rasul, Abdelsalam Abugharara, Mohammad Azizur Rahman, Yahui Zhang and Stephen Butt. The MEng candidate was involved with the planning and conduction of the experiments, the data analysis, and the writing of the paper.

Abstract

In oil and gas drilling, it is essential to maximize the drilling process for optimal drilling performance and minimize costs. In this paper, the drilling rate of penetration (ROP) as main function of drilling performance was evaluated through two different drill bit types, including roller cone (RC) bit and polycrystalline diamond compact (PDC) bit. Sandstone was used as the testing rock, representing a tight and low permeability isotropic formation. The strength of sandstone was determined through the tests of unconfined compressive strength (UCS), indirect tensile strength (ITS), and point load index (PLI). Sandstone specimens were tested through rotary drilled in the laboratory by both drill bits. Several

[1] Title appears as *Tensile and Shear Fracture Examination for Optimal Drilling Performance Evaluation: Part II* in GeoNiagara Conference 2021. Part I was authored by Golam Rasul and it is not included in this thesis.

sets of weight on bit (WOB) and rotary speed (rpm) under the same condition of water flow rate (FR) were applied. A fully instrumented laboratory scale drilling simulator was used for drilling experiments. The applied load on bits for WOB and operational rpm were recorded, rate of penetration (ROP) and depth of cut (DOC) were calculated in all tests. A comparative study was conducted, and drilling performance was evaluated based on drilling parameters and drill bit type.

4.2.1 Introduction

As an essential part of drilling operations, the drilling bit rotates at high speed under a mechanical drive to complete the exploitation of rocks. At the same time, the bit drills downward to complete the drilling of oil and gas wells. Currently, two kinds of bits are widely used in the petroleum industry: the roller cone (RC) bit and the polycrystalline diamond compact (PDC) bit. Under different mining environment conditions, there are some differences in the shape and specification of the bits selected. The selection of bits is not only related to the drilling efficiency and quality, but also has a great impact on the drilling operations. Therefore, it is necessary for the oil and gas industry to select bits properly, ensure drilling efficiency, and reduce drilling costs.

Both analytical and empirical ROP prediction models have been studied for many years. Maurer et al. (1962) established an empirical correlation for predicting roller cone bits penetration rate (ROP). In this study, it was assumed that the cutting cleaning efficiency of the drilling fluid circulation was perfect. The influence of WOB, rock strength, rpm and bit size were incorporated in this model. An analytical model was created that used WOB, rpm, and bit type to determine ROP (Galle & Woods, 1963). The created model introduces a new way of computing ROP, although it ignores formation rock attributes. ROP computation was refined by considering formation tightness, depth, and mud hydrostatics (Mechem et al., 1965). Alum and Egbon (2011) discovered that pressure losses have a significant impact on ROP. However, the empirically based parameters used in their models are incapable of adapting to a variety of drilling conditions. Hedge (2017) developed data-driven models rather than physical experiment, which provides different insights on ROP prediction. The data pool for their model, however, is still restricted.

Since the 1980s, PDC bit, a new type of bit based on polycrystalline diamond, can significantly improve drilling efficiency and has been widely used. The PDC bit is a kind of cutting bit, which has the characteristics of low weight on bit (WOB), low pump pressure and high rate of penetration (ROP) (Offenbacher, 1983; Glowka, 1984). In the process of drilling, PDC bit's cutting teeth intrude into the formations under the action of WOB. The WOB is one of the most important factors affecting the ROP of the PDC bit because WOB affects the penetration depth of PDC bit. Some studies (Williams, 1987; Johnson, 2008) have shown that the ROP of PDC bit is very sensitive to WOB. Under the perfect-cleaning condition of hole bottom, the relationship between WOB and ROP is almost linear, but the change rate of ROP with WOB is different with different rock strengths. In fact, with the gradual increasing of WOB, the cuttings cannot be eliminated over time, and the ROP will decrease. The relationship between ROP and WOB can be expressed as $R \propto W\alpha$ (α is WOB index) (Peng, 2004). The reasons why the ROP of PDC bit increases with the increase of WOB are as follows: in the case of perfect-cleaning condition of hole bottom, with the increase of WOB, the depth of cut of PDC bit increases, and the cuttings are developed increasingly per unit time, thus increasing the ROP; with the increase of WOB, the lithology of bottom hole rock changes from brittleness to pseudoplasticity because of the unique rock breaking mode of PDC bit, which is conducive to cutting. From numerous laboratory experiments and field tests, it can be demonstrated that when WOB is low, ROP increases with the increase of rotation speed (rpm), but when WOB is high, the increasing of ROP gradually slows down with the increase of rpm, which is mainly caused by the accumulation of cuttings.

In the gas and oil industry, the roller cone (RC) bit is also one of the main rock breaking tools, which can adapt to drilling in various formations. The movement states and stress states of RC bit are very complex when it is working at the bottom of well. There are three kinds of crushing action of RC bit on rocks: crushing, impacting, and shearing. The crushing is to break rocks by the action of WOB applied on the bit. Its effect mainly depends on the WOB and the strength of the rocks. The impacting occurs when the teeth alternately act on the rocks when the roller is rolling, which makes the roller shaft vibrate up and down. The impacting is related to the number of teeth, rpm and WOB. The impacting force is inversely proportional to the number of teeth and is directly proportional to the rpm and WOB. The shearing happens when the roller is rolling on the rocks, the gear still slips, resulting in shearing and broken rocks. Applying on the different WOB, the broken rocks will show different characteristics, such as surface fracture (abrasive fracture), fatigue fracture and volume fracture. The rpm of the roller bit is related to the speed of the teeth contacting the rock and the impacting on the rocks, which has a great influence on the drilling efficiency. When the rpm increases, the impacting speed of the teeth on the rock also increases, and the impacting energy will increase, which can effectively improve the drilling efficiency. If the rpm exceeds the rated rotation speed of the bit, the bearing, seal and locking device of the bit will be accelerated to wear and fail early. If the rpm is low, the drilling efficiency will be affected.

All drill bits perform in similar manners. The cutting structure indents the rock to some depth as WOB is applied, and then the rock to the right of the buried cutting structure is destroyed when the drill bit is rotated. The indentation depth in a given rock is calculated by the applied WOB and the used rpm determines the rotating sliding distance per minute.

The rock strength and bit aggressiveness will influence the drill rate when working efficiently, but major variations in drill rate are typically because of inefficiency or dysfunction in the process of rock cutting. Something interferes with the indentation depth if the increase in ROP is not proportionate to the increase in WOB or rpm. Bit founder point is referred to as the undesired results of WOB. Bits tend to be inefficient at very low loads, since weight is initially added. As the weight is increasing, the productivity will increase. The method of evaluating the WOB founder is to repeat the drilling experiment at different rotary speeds.

In this study, sandstone was used as the testing rock, representing a tight and low permeability isotropic formation. The unconfined compressive strength (UCS) test, indirect tensile strength (ITS) test, and point load index (PLI) test were conducted to determine the strengths of rocks by geomechanics loading frame. Then, a fully instrumented laboratory scale large drilling simulator (LDS) was utilized for conducting drilling experiments. The specimens of sandstone were tested through rotary drilling by different types of RC and

PDC bits. Different weight on bit (WOB) and rotary speed (rpm) were applied during drilling experiments under the same condition of water flow rate (FR). The applied WOB and operational rpm were recorded, and the experimental data were statistically analyzed by using mathematical statistics method to calculate rate of penetration (ROP). The corresponding cuttings were analyzed by X-ray diffraction (XRD) analysis. Drilling performance was evaluated based on drilling parameters and drill bit type. In this paper, the optimal drilling mechanical parameters for drilling sandstone were obtained through laboratory simulation drilling experiments, which have a certain guiding significance for on-site drilling operations.

4.2.2 Equipment and Materials

4.2.2.1 Sandstone specimen preparation

In this study, sandstone, representing a tight and low permeability isotropic formation, was chosen for the drilling performance tests. The sandstone samples were cored from big natural rock blocks by small drilling simulator (SDS) in Drilling Technology Laboratory as per the ASTM standard for mechanical strength and ultrasonic velocity tests with the diameter of 47.17 mm. The cores were drilled using NQ core barrel at vertical direction. Then, the cores were cut into small samples for unconfined compressive strength (UCS), indirect tensile strength (ITS), and point load index PLI tests by an electrical saw. The samples for drilling experiments were cored with the bigger diameter of 152.4 mm (6 in) and the length of 304.8 mm (12 in).

The mineral composition of sandstone was analyzed by X-ray diffraction (XRD). The sandstone mainly consists of quartz (81%), albite (14.3%), clinochlore (3%) and kaolinite (0.6%) as shown in Figure 4.1.

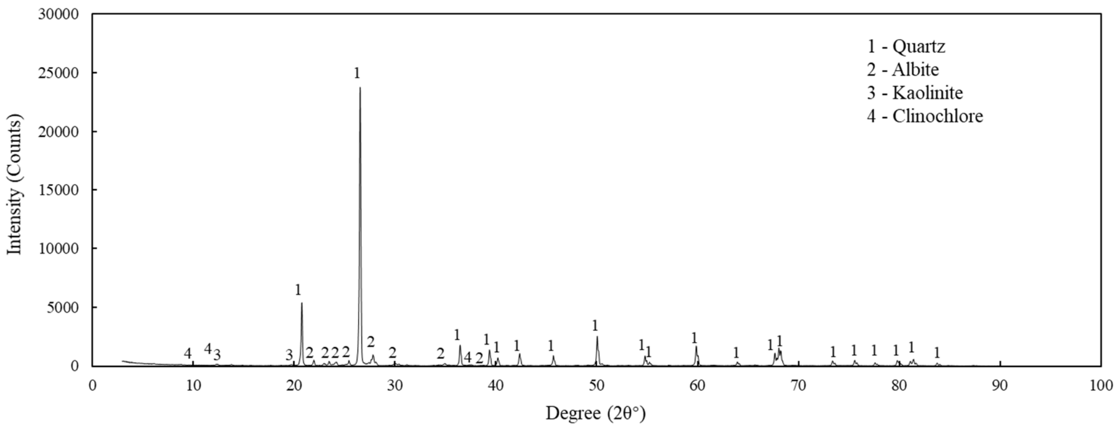

Figure 4.1 XRD pattern for sandstone

4.2.2.2 Drill bits

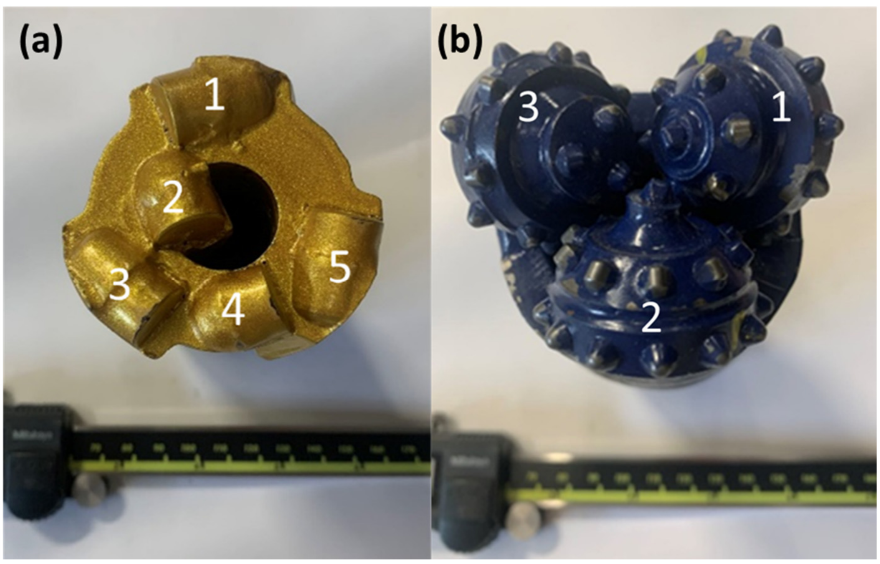

Figure 4.2 (a) Five cutters PDC bit; (b) Tri-cone RC bit

A PDC bit and a RC bit with the diameter of 57.15 mm (2.25 in) were used to drill the sandstone specimens. The PDC bit has five cutters with cutter lengths of 19.77 mm, 15.50 mm, 19.95 mm, 16.07 mm and 20.01 mm for 1-5 (Figure 4.2 (a)) respectively, and with the approximately cutter diameter of 13.61 mm. The RC bit (Figure 4.2 (b)) has three rotating cones (Tri-cone bit). All three cones have the same shape and different number of cutters on the inner, middle, and outside rows. Cone 3 has three cutters on the inner row and seven cutters on middle and outside rows. Cones 1 and 2 both have only one cutter on the inner row, 6 and 10 cutters on the middle row, and 11 and 13 cutters on outside rows, respectively.

4.2.2.3 Drilling apparatus setup

The Laboratory drilling experiments were conducted utilizing a large drilling simulator (LDS) in the Drilling Technology Laboratory as shown in Figure 4.3. The drilling parameters were controlled and recorded by many sensors connected to a DAQ system. The data acquisition system gathers the necessary information from all sources, sensor and processes the data to prepare it for the LabVIEW software. The sensors include a draw wire linear position transducer (LPT), which measures axial displacement between the motor head and the drill pipe used to calculate the ROP, and a laser triangulation sensor (LTS). The LabVIEW software shows various information, including observed WOB, pneumatic applied WOB, hydraulic WOB, rpm, drilling condition, air pressure reading, hydraulic servo valve reading, applied torque, and LVDT (Linear Variable Differential Transformer) vertical displacement. The DAQ-Sys uses LabVIEW software that records at a sampling rate of 100 Hz for these tests. The LVDT sensor provides the resolution of 1×10^{-6} mm.

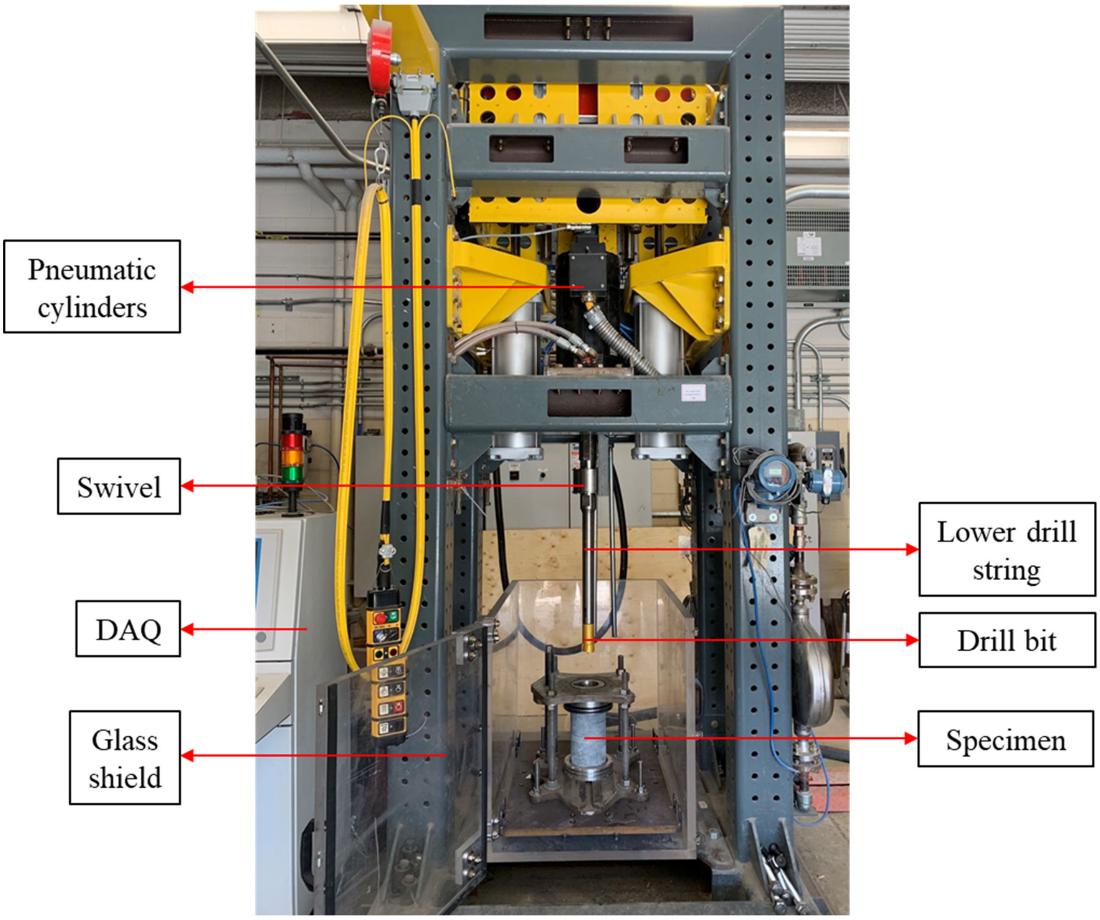

Figure 4.3 Large drilling simulator (LDS) in Drilling Technology Laboratory at Memorial University

4.2.2.4 Geomechanics loading frame

The geomechanics loading frame in Drilling technology Laboratory was utilized for the mechanical strength tests of sandstone. The loading frame is equipped with a Data Acquisition System (DAQ-Sys) that records the main parameters needed to construct the stress-strain relationship, including the load in kN and displacement in mm. The DAQ-Sys uses LabVIEW software that records at a sampling rate of 100 Hz for these tests.

4.2.3 Experimental Details

4.2.3.1 Mechanical strength measurement

The unconfined compressive strength (UCS) of sandstone was determined in accordance with the ASTM D7012. The ends of each specimen were trimmed off to ensure the surfaces of each specimen were flat and parallel, and the specimens had the average heights of 100 mm and diameters of 47 mm. The Brazilian indirect tensile strength (ITS) test is a laboratory test for indirect measurement of tensile strength. According to this test, the thickness to diameter ratio of all tested disc specimens was 0.24 to 0.33. The specimens were placed between two flat platens. The ITS is determined based on the assumption that failure occurs at the highest tensile stress point, that is, at the middle of the disc (ASTM D3967). The point load index (PLI) was conducted following ASTM D5731. According to the standard, core length was no less than 0.5 times of core diameter. The load was steadily increased within 10 to 60 s and the failure pressure was recorded. In this study, axial point load tests were conducted for all PLI samples with length/diameter ratio of 0.48 to 0.51. The average results of each strength testing were calculated and summarized in Table 4.1. The UCS and ITS correlation has been utilized to report sandstone isotropy and can be found (Abugharara et al., 2019).

4.2.3.2 Ultrasonic velocity measurement

Dynamic elastic constants were calculated from density and P-wave or S- wave velocities following ASTM D2845. Pulse was initiated and transmitted through one rock core by one S-wave transducer and received by the other S-wave transducer. S-wave transducers were used due to that it obtained both P-wave and S-wave. The velocities were determined using a Portable Ultrasonic Non-destructive Digital Indicating Tester (PUNDIT) from Tektronix (TDS 1002B). The elastic constants are calculated and given in Table 4.1. The circular ultrasonic wave velocity measurement approach has been adopted to investigate the sandstone rock anisotropy (Abugharara et al., 2017).

The specific experimental details and correlations of sandstone characterization can be found in Part I (Golam et al., 2021).

Table 4.1 Summary of sandstone properties

Rock type	Density (g/cm^3)	E (GPa)	P-wave (m/s)	S-wave (m/s)
Sandstone	2.27	6.03	3366.68	2271.08
E' (GPa)	μ	UCS (MPa)	ITS (MPa)	PLI (MPa)
25.38	0.08	59.72	6.11	4.32

(E is static Young's modulus; E' is dynamic Young's modulus.)

4.2.3.3 Drilling experiments

A fully instrumented laboratory scale large drilling simulator (LDS) was used for the drilling experiments. The sandstone rock samples were tested through rotary drilling by five-cutter PDC bit (57.15 mm) and tri-cone RC bit (57.15 mm). The experiments can be divided into three groups. First, the rpm was set at 10, while the WOB increased from 2 kN to 6 kN to investigate the ROP performance under low rpm. The second group had a constant WOB (4 kN) and the rpm varied from 20 to 50 to study the effect of rpm on ROP. The last group was set at a high rpm rate (50) and the WOB increased from 5 kN to 10 kN. Three groups of experiments were conducted by PDC and RC bits separately as the testing matrix shown in Table 4.2.

The drilling experiments were conducted under atmospheric pressure. A constant water flow rate of 27.91 L/min was adopted to keep the drill hole clean and remove the cuttings to the cuttings collection system. The 75-micron and 100-micron sieves were used during drilling to collect the cuttings samples of sandstone. The measured drilling parameters were recorded by the sensors connected to a data acquisition (DAQ) system. Drilling performance was evaluated based on the relationships between WOB, rpm, ROP, and depth of cut (DOC). Figure 4.4 demonstrates the cross-section surfaces of drilled holes by two types of bits. Due to the shearing drilling mechanism, it is found that the surface of drilled hole by PDC bit is smoother than the drilled hole by RC bit.

Figure 4.4 Cross section of sandstone samples after drilling

4.2.4 Results and Discussions

4.2.4.1 Theory of ROP prediction model

Maurer (1962) affirmed that the ROP is directly proportional to the ratio between rotary speed times the square of the difference between the WOB and threshold WOB before cratering is initiated, and the square of the drill bit diameter times the square of the rock strength. According to the Maurer model, the ROP is proportional to rpm and proportional to the square of the difference between the actual WOB and the threshold WOB, as presented in Eq. [11]. If the actual WOB is far higher than the threshold WOB, then the threshold WOB can be neglected in the model, which is given as Eq. [12].

$$\mathrm{ROP} = \mathrm{k} \times \left(\frac{\mathrm{N}-(\mathrm{W}-\mathrm{W}_0)^2}{60\mathrm{D}^2\mathrm{S}^2}\right) \quad [11]$$

$$\mathrm{ROP} = \mathrm{k} \times \left(\frac{\mathrm{N}-\mathrm{W}^2}{60\mathrm{D}^2\mathrm{S}^2}\right) \text{ for } \mathrm{W} \gg \mathrm{W}_0 \quad [12]$$

where, ROP is the rate of penetration (m/h); k is the drillability constant; N is rpm; W is WOB (kN); W_0 is threshold WOB (kN); D is bit diameter (mm) and S is rock strength (MPa).

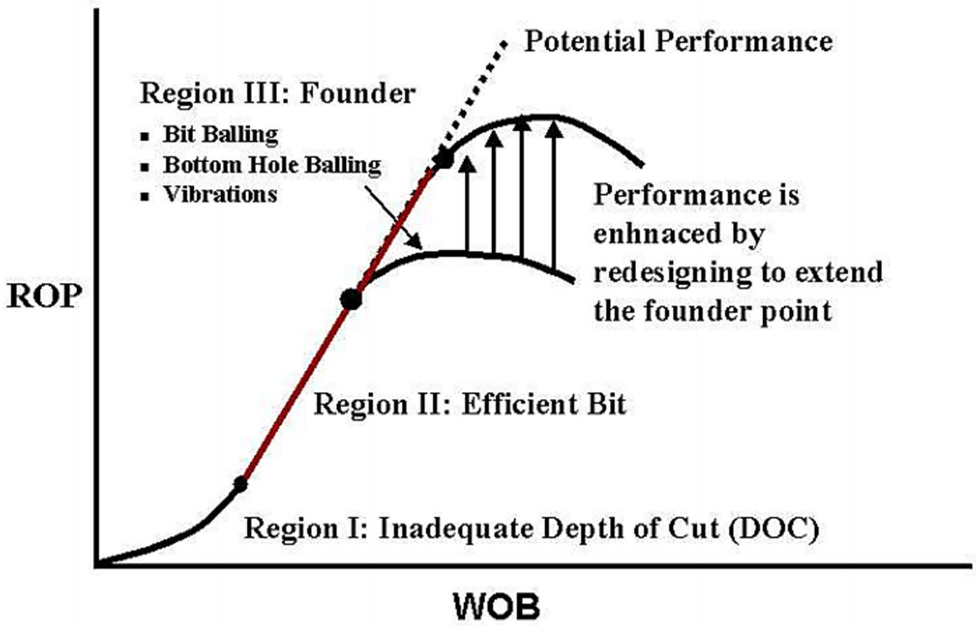

Figure 4.5 Three regions in the ROP-WOB relationship (Dupriest & Koederitz, 2005)

ROP is regarded as a function of WOB and rpm by many ROP prediction models. The typical output is to plot ROP against WOB at constant rpm on a Cartesian graph (Ahmed et al, 2020). Three regions are identified when ROP is plotted against ROP: i) inadequate

Table 4.2 Drilling parameters of rpm, WOB, ROP and DOC

Bit type	Rock type	Variable	rpm	WOB (kN)	Avg. ROP (m/hr)	DOC (mm/rev)
PDC (2.25")	Sandstone	WOB	10	2	0.040	0.067
				3	0.054	0.089
				4	0.059	0.098
				5	0.087	0.145
				6	0.116	0.193
		rpm	20	4	0.131	0.109
			30		0.161	0.090
			40		0.227	0.094
			50		0.423	0.141
		WOB	50	5	0.345	0.115
				6	0.393	0.131
				7	0.632	0.211
				8	0.518	0.173
				9	0.583	0.194
				10	0.920	0.307
RC (2.25")	Sandstone	WOB	10	2	0.021	0.035
				3	0.023	0.039
				4	0.030	0.050
				5	0.042	0.071
				6	0.055	0.092
		rpm	20	4	0.051	0.043
			30		0.058	0.032
			40		0.087	0.036
			50		0.095	0.032
		WOB	50	5	0.132	0.044
				6	0.135	0.045
				7	0.176	0.059
				8	0.195	0.065
				9	0.191	0.064
				10	0.176	0.059

depth of cut (DOC); ii) efficient drilling; as well as iii) inefficient drilling (Figure 4.5). Region I is identified, when the DOC is too small and the rock breaking process has not fully start, due to the low WOB. Following that, at certain WOB and so on, then depth of cut, and ROP increase more rapidly. This productive drilling region is designated as Region II. Region III is defined as the point of origin from which the increase rate of ROP with WOB tends to decrease as WOB increases. In this section, the drilling efficiency decreases due to inefficient hole cleaning, bit balling, excessive vibrations and insufficient torque.

4.2.4.2 Analysis of testing results

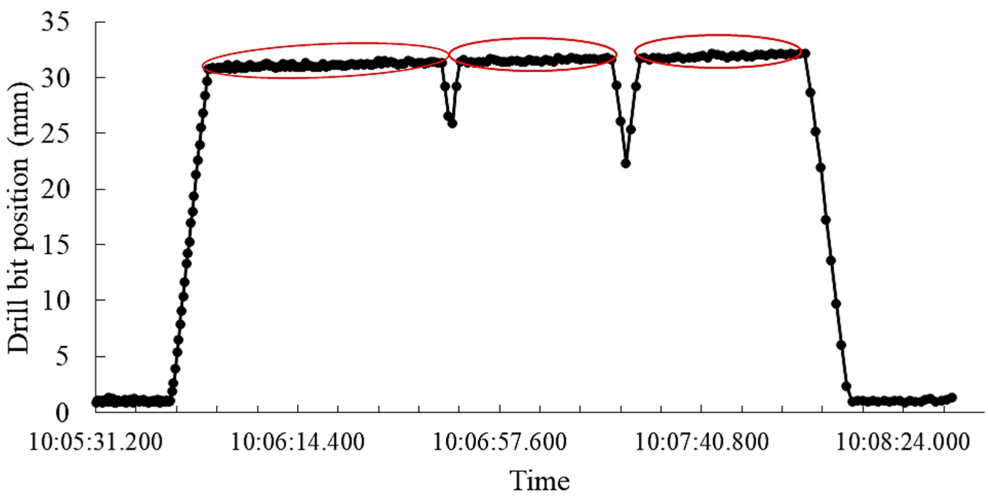

Figure 4.6 Sample position data versus time of drilling test

For each drilling test, the drill bit penetrated the rock sample with controlled rpm and WOB for each test, with certain bit type and rock type. During the drilling process, the bit was stopped and tripped up in some tests. The tripping interval was not counted in the drilling performance evaluation. As shown in the Figure 4.6, which is one example among these tests, the drilling sections in the red mark were considered in the drilling performance calculation, while the tripping sections were ignored. In Figure 4.6, the position data of drill bit and time recorded by DAQ system were plotted. The average slope of the drilling section was calculated as the ROP. Then the DOC was calculated from the ROP accordingly. The ROP and DOC for tests with different configurations were stated in Table 4.2.

4.2.4.3 Effect of applied drilling WOB and ROP

In practical drilling process, the cutters of bits drill into the rock by the action of WOB. Meanwhile, the WOB has the most significant effect on ROP, which determines the depth of cutter and the size of rock cuttings volume. In order to investigate the relationship between ROP and WOB, several sets of WOB and two values of rpm were applied on the laboratory drilling experiments under the constant water flow rate. The corresponding ROPs and DOCs are calculated and summarized in Table 4.2. Then, regression analysis was performed on the test data.

Figure 4.7 indicates the regression analysis when a low rpm was adopted at 10. Note that the regression relationships between WOB and ROP of both PDC and RC bits are non-linear and the ROP increases with the increase of WOB. The influence of WOB tends to increase with the increasing of WOB itself. From the regression analysis, the best fitted relationships are exponential for both bits. The coefficients of determination of each regression equation are 0.9734 and 0.9743 of PDC bit and RC bit respectively, indicating the high fitting degree and the reliability of trend lines. Therefore, the quantitative relationship between WOB (W) and ROP (R) can be established and given in Table 4.3.

Figure 4.8 and Figure 4.9 show the regression analysis when a high rpm was adopted at 50. It is observed that two types of drill bits perform the different drilling performance on the same rock sandstone. The regression relationship between WOB and ROP of PDC bit is plotted in Figure 4.8. A strong exponential relationship, which is consistent with the performance under rpm at 10, exists between the ROP and WOB with a high determination coefficient of 0.9196. When drilled with a RC bit, the ROP increases with the increasing WOB. When WOB is at 8 kN, the ROP reaches its highest value. Then, the ROP starts to decrease when the WOB is still increasing. Figure 4.9 shows the relationship between WOB and ROP for bit balling, which forms the founder point. Initially, the RC bit is inefficient at the low applied WOBs. With the increase of WOB, the efficiency is improved. In Figure 4.9, the RC bit reaches its peak efficiency at Point A, then a proportional response is observed between Point A and Point B. Increasing WOB is the only action needed to increase the drilling efficiency under this linear condition. When it reaches Point B, the bit balling is about to occur. Because the cuttings stick to the spaces between cutters on a RC bit, the penetration depth is reduced. The nozzle is partially blocked, then the flushing water flow rate is reduced around the bit which causes the accumulation of cuttings. In addition, an individual cone may stop rotating during the drilling process, resulting in excessive shear and cutter wear. The bit becomes less inefficient even if additional WOB is applied. Point B is referred as the founder point, indicating that the WOB should be selected close to the founder point to achieve the peak drilling performance.

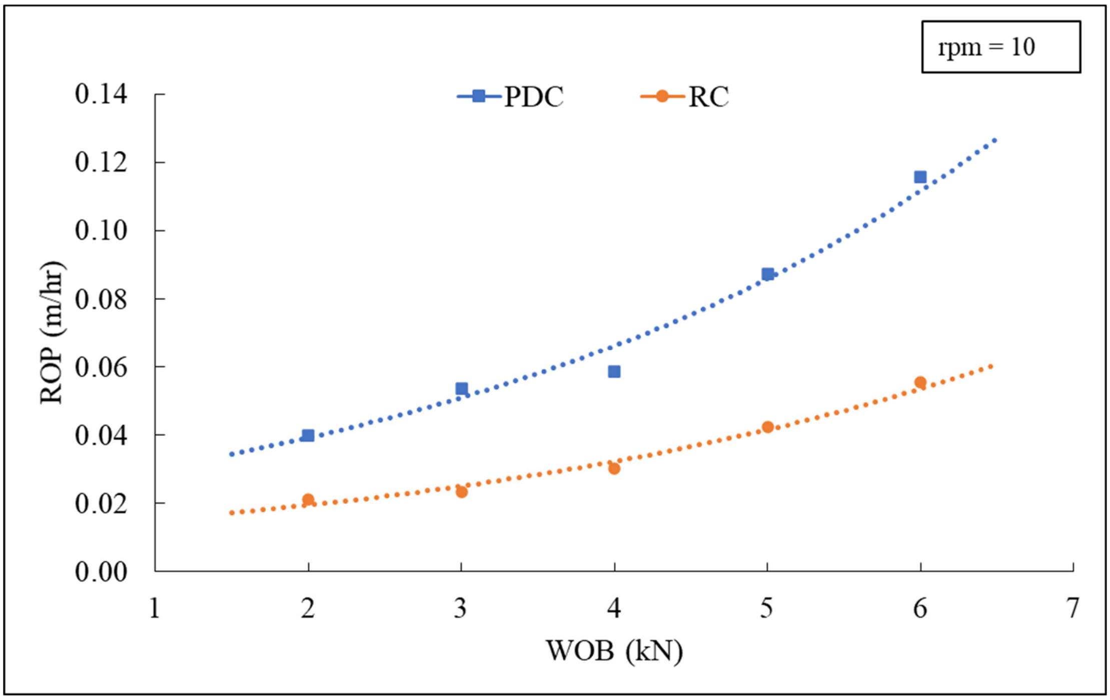

Figure 4.7 The regression relationship between WOB and ROP (rpm=10)

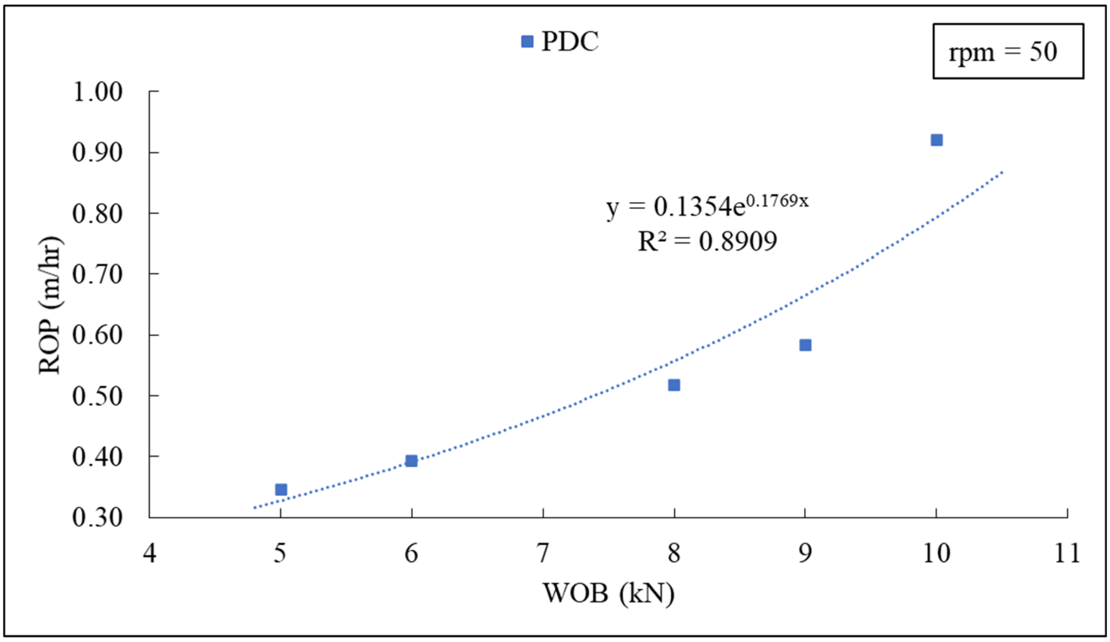

Figure 4.8 The regression relationship between WOB and ROP of PDC bit (rpm=50)

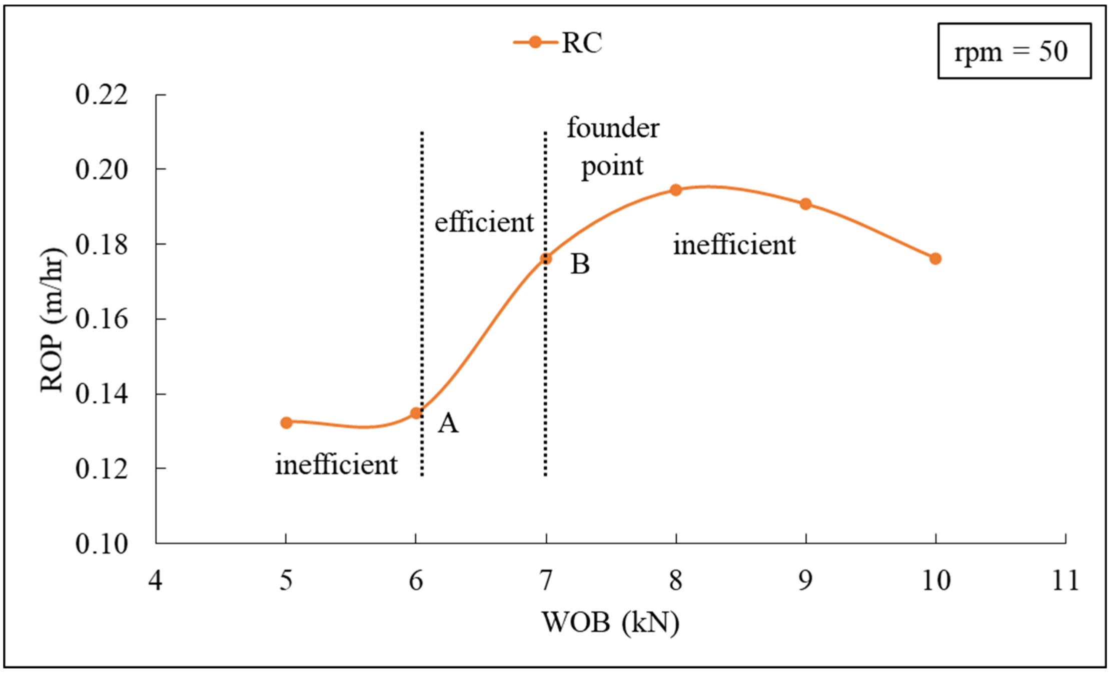

Figure 4.9 The regression relationship between WOB and ROP of RC bit (rpm=50)

4.2.4.4 Effect of applied drilling rpm on ROP

Under a certain applied WOB, the penetration depth will be relatively constant, and high rpm will improve the ROP. However, with the increasing of rpm, the contact time between the bit cutters and rock becomes shorter, which leads to the decreasing of penetration depth, especially for hard formations. To analyze the relationship between ROP and rpm, the WOB was set at 4 kN while the rpm varied from 20 to 50 to monitor the development of corresponding ROP. The ROPs and DOCs are calculated and summarized in Table 4.2. Then, regression analysis was performed on the test data as shown in Figure 4.10. The regression analysis revealed that the relationships between ROP and rpm of both PDC and RC bits are non-linear and the ROP increases with the increase of rpm. Particularly, the effect of rpm becomes larger with the increasing of rpm itself when drilled with a PDC bit. However, the influence of rpm on the RC bit is much lower, which means the rpm has a stronger influence on the PDC bit. From the regression analysis, the best fitted relationships are exponential for both bits. The quantitative relationship between WOB (W) and rpm (r) can be established and are given in Table 4.3.

Table 4.3 The regression analysis results

Relationships	Bit type	Regression model	Regression equation	R^2
ROP-WOB	PDC	Exponential	$R = 0.0233e^{0.2611W}$	0.9734
	RC	Exponential	$R = 0.0118e^{0.2527W}$	0.9743
ROP-rpm	PDC	Exponential	$R = 0.0551e^{0.0385r}$	0.9442
	RC	Exponential	$R = 0.0319e^{0.0226r}$	0.9354

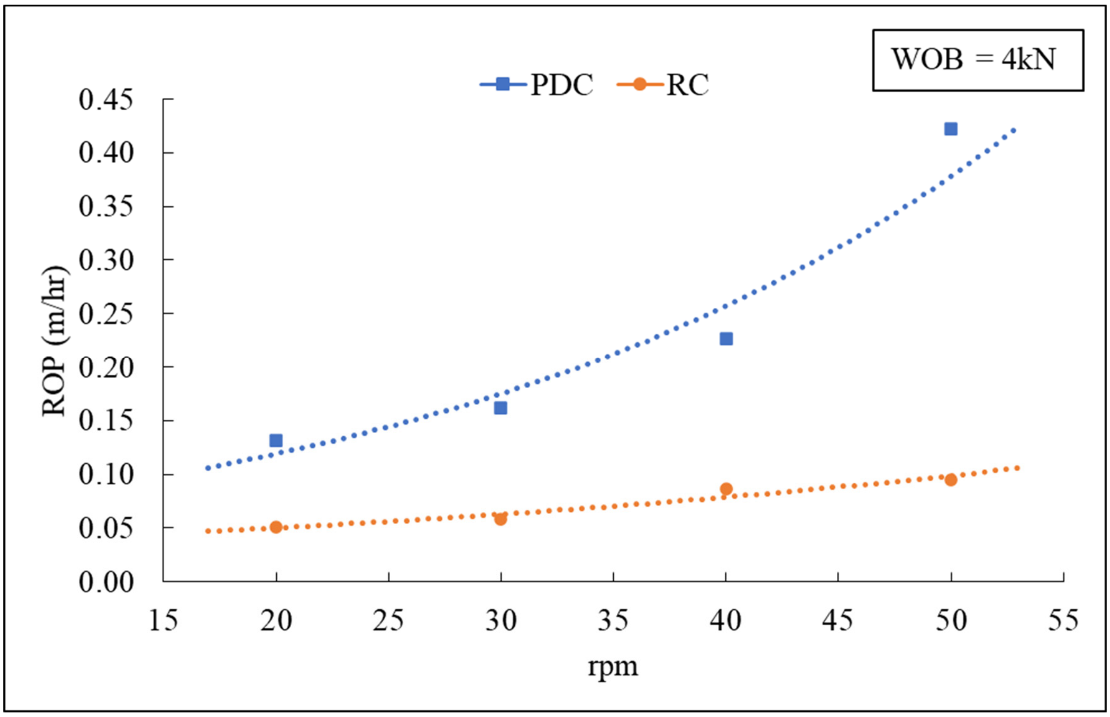

Figure 4.10 The regression relationship between rpm and ROP (WOB=4 kN)

4.2.4.5 Effect of drill bit type on ROP

A drill bit is considered to be mechanically efficient if it requires less WOB to perform a shearing rock removal process for a given rock hardness. As a result of this trait, substantially greater ROPs are achieved. As observed in Figure 4.7, the PDC bit always performs higher ROPs than the RC bit with the increasing of WOB for a given rpm. Although ROPs of both bits show a rising tendency, the WOB has greater influence on the PDC bit. This performance has also been demonstrated under the effect of rpm as shown in Figure 4.10. The PDC bit exhibits a sharp increment with the increasing of rpm when comparing to the small slope of RC bit. In medium-hard and non-abrasive formations, PDC bit tends to have better performance than RC bit.

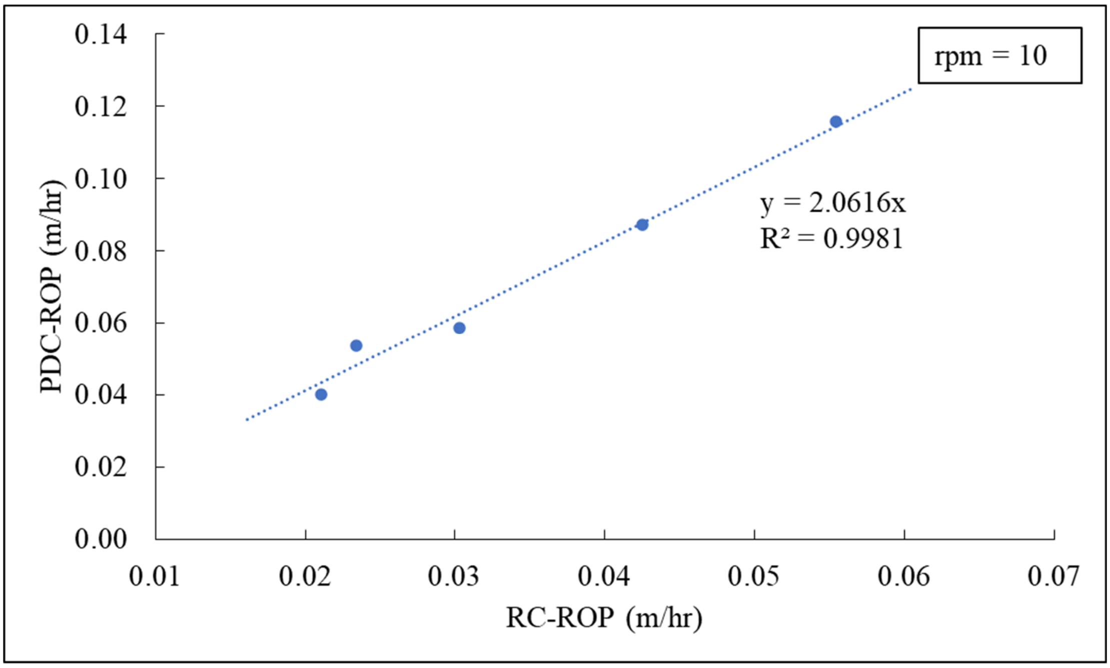

Figure 4.11 Correlation of ROPs of PDC and RC bits (rpm=10)

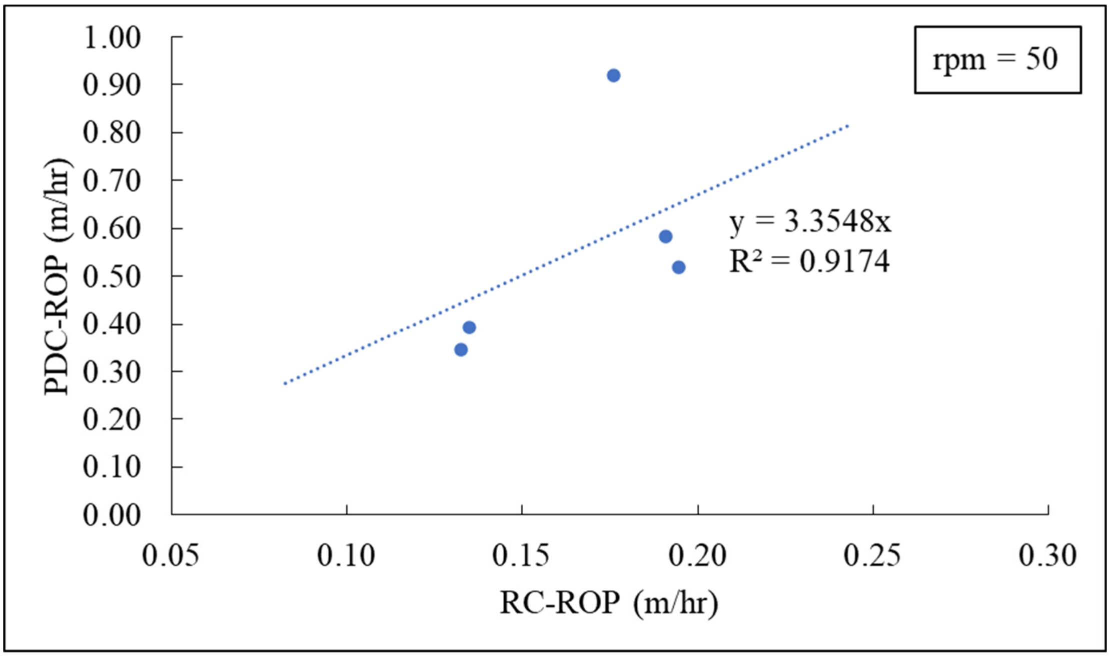

Figure 4.12 Correlation of ROPs of PDC and RC bits (rpm=50)

Mensa-Wilmot et al. (2002) stated that PDC bits usually drill twice as fast as RC bits in shale. As for sandstone, the ROP relationships between PDC bit and RC bit are plotted in Figure 4.11 and Figure 4.12 under two different rpms (10 and 50). The ROP of PDC bit is approximately two to three times of RC bit and the correlation ratio exhibits a slow rising trend with the increasing of rpm. Both correlations perform strong linear relationships and have the coefficients of determination over 0.9, which indicates the high fitting degree and means the new correlation has the advantage of being developed for specific type of rock (sandstone). The primary results depict the research potential for future studies. Further study is required to study how varying the rock type, drilling parameters affect the ROP correlations of PDC and RC bits.

4.2.5 Conclusions

In this study, drilling experiments under various WOBs, rpms and same water flow rate have been conducted on sandstone specimens. The mechanical strengths of sandstone have also been determined through strength tests. The testing data was analyzed comprehensively. Based on the current study, the following conclusions can be made:

1) The drilling rate of penetration (ROP) was found to be primarily dependent on the rotary speed (rpm), weight on bit (WOB) and type of bit.
2) The regression analysis shows exponential relationships between WOB and ROP of both PDC and RC bits and the ROP increases with the increase of WOB when a low rpm is adopted at 10. The influence of WOB tends to increase with the increasing of WOB itself.
3) The regression analysis exhibits different relationships between WOB and ROP when a high rpm is adopted at 50. As for PDC bit, the corresponding ROP increases first with A strong exponential relationship, which is consistent with the performance under rpm at 10. When drilled with a RC bit, the RC bit is inefficient at the low initial applied WOBs. With the increase of WOB, the ROP performs proportional response until reaching the founder point due to the bit balling. After that, the ROP starts to decline as additional WOB is applied.
4) The exponential relationships were found between ROP and rpm of both PDC and RC bits are non-linear and the ROP increases with the increment of rpm. In particular, the effect of rpm becomes larger with the increasing of rpm itself when

drilled with a PDC bit. However, the influence of rpm on the RC bit is much lower, which means the rpm has a stronger influence on the PDC bit.

5) As for sandstone, a strong linear relationship of ROP was found between PDC bit and RC bit. The ROP of PDC bit is approximately two to three times of RC bit, which indicates the high fitting degree and means the new correlation has the advantage of being developed for specific type of rock (sandstone).

Chapter 5. Optimization of Cemented Tailings Backfill (CTB) and First Field Backfill System Design

5.1 Introduction

Backfilling is a post mining process which can support the ground, provide working floor for personnel and machinery, and dispose the mining tailings properly. The technology of cemented tailings backfill (CTB) is implemented in many modern mines around the world, especially in Canada (Grice, 1998). The standard components of a cemented tailings backfill mixture, including the tailings, binder, and water, must be mixed thoroughly to produce a homogeneous mixture (Benzaazoua et al., 2004; Yilmaz et al., 2004).

For the initial experiments of CTB in SMD project, the backfill was prepared by three different binder proportions (6%, 8% and 10%) and two different binder compositions (one was only PC and another one was PC with FA) to investigate the unconfined compressive strength of the backfill during the curing time on 7 days, 14 days, and 28 days (Someehneshin et al., 2020). From the results, it was found that the UCS and the stiffness of backfill increased with the increasing binder proportions. When the binder Portland cement mixed with fly ash, the backfill performed a notable increase in the UCS and stiffness. And for the curing time, the UCS values of all studied backfill materials increased with curing time. There is no typical recipe for backfill materials. Each type of backfill material is based on laboratory optimization. From the initial study, the recommended CTB recipe for SMD project is 20 wt.% water (by total mass) and 80 wt.% solids (by total mass), which contains 6 wt.% (by solids mass) binder proportion and the binder is mixed by Portland cement and fly ash with a ratio of 4:1.

However, due to the relatively high cost of Portland cement, investigations of the use of lower binder proportions and optimization of backfill strength development are carried out. In this optimization investigation, the effects of lower binder proportions (2 wt.% and 4 wt.% by solids mass), and internal vibration on the designed CTB density, unconfined compressive strength (UCS), tensile strength, and the amount of tailings usage are evaluated.

5.2 Effects of low binder proportions and internal vibration on early age behaviour of cured cemented tailings backfill for mining by drilling applications (Paper #3)

Weizhou Quan, Javad Someehneshsin, Abdelsalam Abugharara, Yahui Zhang and Stephen Butt

Memorial University of Newfoundland, St. John’s, Newfoundland and Labrador, Canada

This section is a paper accepted in the 74th Canadian Geotechnical Conference and authored by Weizhou Quan, Javad Someehneshsin, Abdelsalam Abugharara, Yahui Zhang and Stephen Butt, and was published on OnePetro numbered 1735. The MEng candidate was involved with the planning and conduction of the experiments, the data analysis, and the writing of the paper.

Abstract

Cemented tailings backfill is generally prepared by mixing waste mining tailings, water, and cement to give designed outcomes. The CTB preparation recipe with 20 wt.% water (by total mass) and 80 wt.% solids (by total mass), which contains 6 wt.% (by solids mass)

binder proportion (Portland cement : fly ash 4:1), was recommended for the Sustainable Mining by Drilling (SMD) Project. However, due to the relatively high cost of Portland cement, investigations of the use of lower binder proportions and optimization of backfill strength development were carried out. In this paper, the effects of (i) lower binder proportions (2 wt.% and 4 wt.% by solids mass), and (ii) internal vibration on the designed CTB density, unconfined compressive strength (UCS), tensile strength, and the amount of tailings usage were evaluated. The results showed that the 4 wt.% binder backfill specimens obtained 1.035 (avg.) MPa compressive strength after 28 days curing time, which reached the designed target compressive strength of CTB. The results also showed that the fully vibrated CTB specimens possessed 14.7% higher density and 57.1% higher compressive strength than the specimens without vibration, which means that an extra 10.9% tailings can be placed into extracted wellbore when the CTB is fully vibrated. This behaviour allows more tailings to be securely placed underground and further reduces the surface tailings impoundment requirements and the costs of tailings disposal for the mining industry.

5.2.1 Introduction

Mining industry produces extracted voids in varying shapes, including stopes, tunnels, goafs, and gob voids. The extracted voids create instability risks for the excavation of adjacent pillars holding minerals, along with a subsidence danger for on-the-ground personnel and machinery during mining activities or after a mine has been decommissioned. Collapse of the created voids is one of the main factors in rock burst and potential land subsidence (Helm et al., 2013; Wang et al., 2013). Over the last few decades, the volume of tailings being generated increased dramatically due to the increase in the demand for minerals and metals and the mining of many low-grade ores. Mining industry faces the daunting challenge of environmental issues associated with the management of tailings.

The disposal of mining tailings in an economical and environmentally safe way has entailed the development of backfilling methods, which has a history of nearly 60 years. Some of the methods of backfilling which are widely used due to safety and economic factors, such as ground support and control, provision of a working floor and waste disposal, are rock backfill, hydraulic backfill, and paste backfill. Cemented tailings backfill (CTB) technology has been recognized and applied in many mines due to its excellent performance and low operating costs. CTB refers to an engineered wet fine process mixture, hydraulic binder and mixing water used in setting the density of the paste solids at the consistency desired. The solids proportion is between 70%~85% (by total mass), water is either clean water or mine processed water, and a hydraulic binder, usually from 3%~7% (by total mass), is added to the designed backfill (Kesimal et al. 2005). Binders used within the backfill are for providing mechanical strengthening. The various components used in CTB each play a fundamental role in strength and stability.

The mechanical behaviour of cured CTB is affected by binder types and contents. For instance, the unconfined compressive strength (UCS) of the CTB sample, increases significantly with the reduction of water-to-cement ratio, which increases binder content, regardless of the tailings sample or the type of binder (Qi & Fourie, 2019). According to the study done by Fall et al. (2005), decreasing the number of materials in making CTB has the corresponding change of reducing the CTB's strength. Similarly, the type of binder, as well as dosage, has a significant influence on the short and long term mechanical performance of CTB. An increase of binder dosage has a substantial increase in the long-term performance of CTB (Liu et al., 2019). This increased long-term performance of CTB is attributed to hydraulic reactions resulting from the pozzolanic reaction between calcium hydroxide formed during the process of hydration and mineral admixtures in CTB (Nasir & Fall, 2010). Also, according to Yilmaz et al. (2009), the provision of more binding capacity produces a proactive alumina coat rich phases, due to the C-S-H (CaO-SiO2-H2O) formed, which participates in ettringite formation. Moreover, the CTB microstructure is improved by the extra C-S-H, resulting from decreasing permeability and perhaps pyrite oxidation; hence the CTB vulnerability to attack by sulfite is reduced (Ercikdi et al., 2009; Thompson et al., 2012). Despite the associated potential benefit of binder dosage, increasing the binder content will increase CTB's operating cost.

In the preparation of concrete, when concrete is not effectively consolidated, it contains voids (air pockets), which reduce its strength. Vibrating consolidates voids and ensures that the concrete is strong and stable enough (Maryoto, 2018). This method can also be applied in the preparation of CTB. During CTB making, internal vibration is achieved in various ways, such as vibration using an electric, a pneumatic, or a hydraulic vibrator (Kanema et al., 2016). Vibrators also achieve consolidation in freshly placed CTB by helping the air trapped in the concrete to escape. As the CTB subsides, large air voids form between the coarse aggregate and particles filling with smaller particles. Increased vibration drives out more air trapped in the voids. Therefore, when the vibrators are appropriately operated, the consolidation enhances the appearance and performance.

The main purpose of this study was to evaluate the influence of lower binder proportions (2 wt.% and 4 wt.% mixture of Portland cement and fly ash) and internal vibration on the early age behaviour (i.e., wet properties, mechanical strength) of the cemented tailings backfill (CTB). Four different vibrating conditions were adopted using an electronic vibrator to give contrast analysis. The tests, including specimen casting, particle size distribution analysis (PSD), UCS test and the Brazilian tensile strength test, were conducted to measure the different parameters which were based on the American Society for Testing and Materials (ASTM) international standards.

5.2.2 Materials and Equipment

5.2.2.1 Tailings

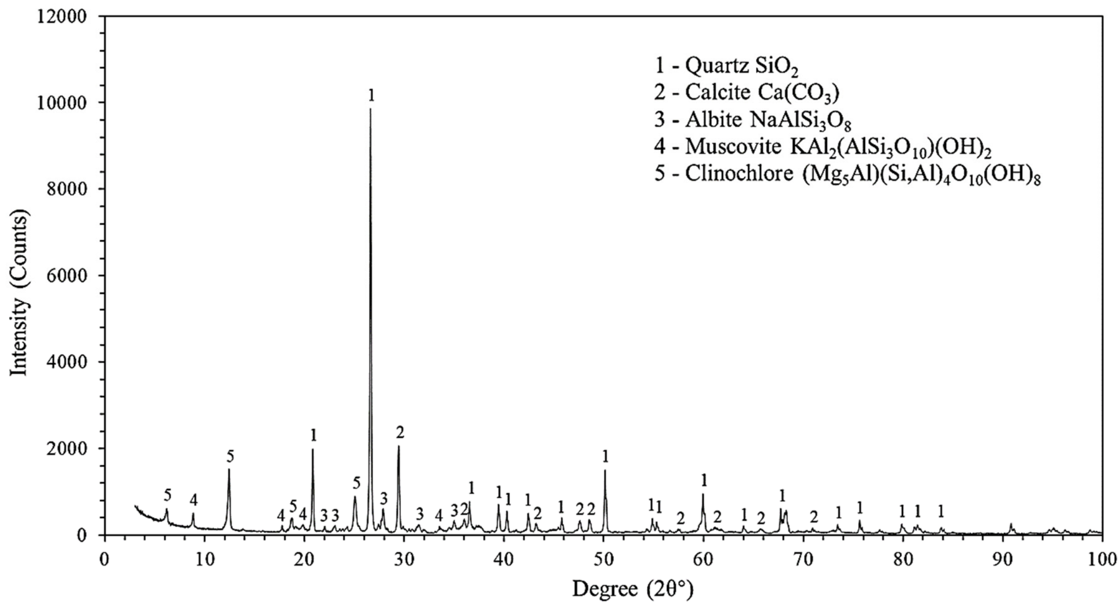

Figure 5.1 XRD pattern for tailing samples used in this study

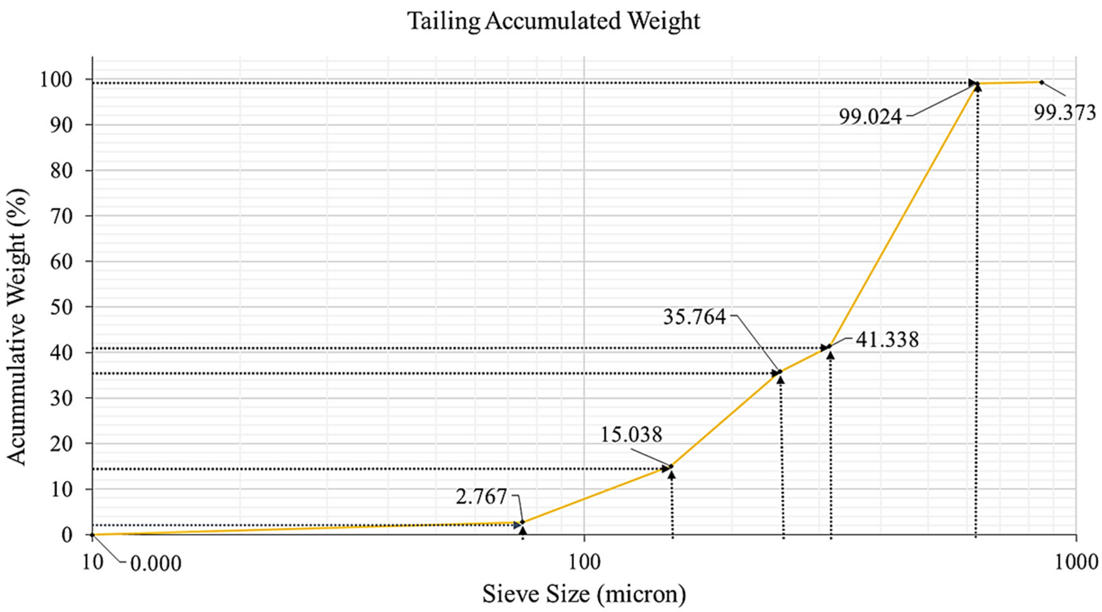

Figure 5.2 Grain size distribution of the studied tailings

The chemical composition of the tailings provided by a collaborated gold mine was analyzed by X-ray diffraction (XRD). The results indicated that quartz is the most abundant component contained in the tailings. Calcite, albite, muscovite and clinochlore are present as main minor contents (Figure 5.1). The silica and calcium contents are 31% and 5.5%, respectively. The tailings grain size distribution analysis, which has a great influence on the backfill rheology and mechanical performance, was conducted by sieve analysis based on ASTM D6913.

According to the previous work, the tailings were classified by an electric shaker containing 2000 μm, 630 μm, 315 μm, 250 μm, 150 μm, and 75 μm meshes. Figure 5.2 shows the grain size distribution of tailings used in this experimental study. The tailings are wellgraded, as 90% of the tailings less than 560 μm, 50% of the tailings less than 350 μm, and 10% of the tailings less than 130 μm (Someehneshin et al., 2020). The water content of the tailings stored in the laboratory is 7.4%.

5.2.2.2 Portland cement and fly ash

Regular type GU or type II Portland cement (PC) and type C fly ash (FA) were used as binders in the CTB mixture with a ratio of 4:1. The unique rheological properties of backfill highly depend on the particle size distribution and especially, the proportion of fines (less than 20 μm). CTB made of fine tailings usually generates lower strength (Fall et al., 2004). Additionally, CTB must contain at least 15% by mass of particles less than 20 μm in diameter (Landriault et al., 2001) in most cases. As for the tailings used in this study, there were only 10% of tailings less than 130 μm. Therefore, the PC and FA were added to backfill to improve pumpability and strength of the mixture significantly, due to its finer size distribution than in the mine tailings. In comparison to PC, FA has certain hydraulic properties and the particles are mostly spherical, varying in diameter from less than 1 to 150 μm, the majority being less than 45 μm. FA was used to achieve advantages, such as lowering cement content to reduce the CTB costs, enhancing workability and rheological properties, and reaching the required strengths in the CTB.

5.2.2.3 Moulds

The moulds (kraft tubes) for 2 wt.%, 4 wt.% and 6 wt.% binder proportion specimens were obtained from the Uline Company, with the size 2” × 4” (50.8 × 101.6 mm), using kraft tubes that are easily split to simplify the specimen removal. The plastic moulds for compaction tests were the size of 6’’ × 12’’ (152.4 × 304.8 mm), obtained from Paragon

Products. The length to diameter ratio of the specimens is 2:1 in this study, which is based on ASTM C192/C192M-15 and ASTM C39/C39M-12.

5.2.2.4 Geomechanics loading frame

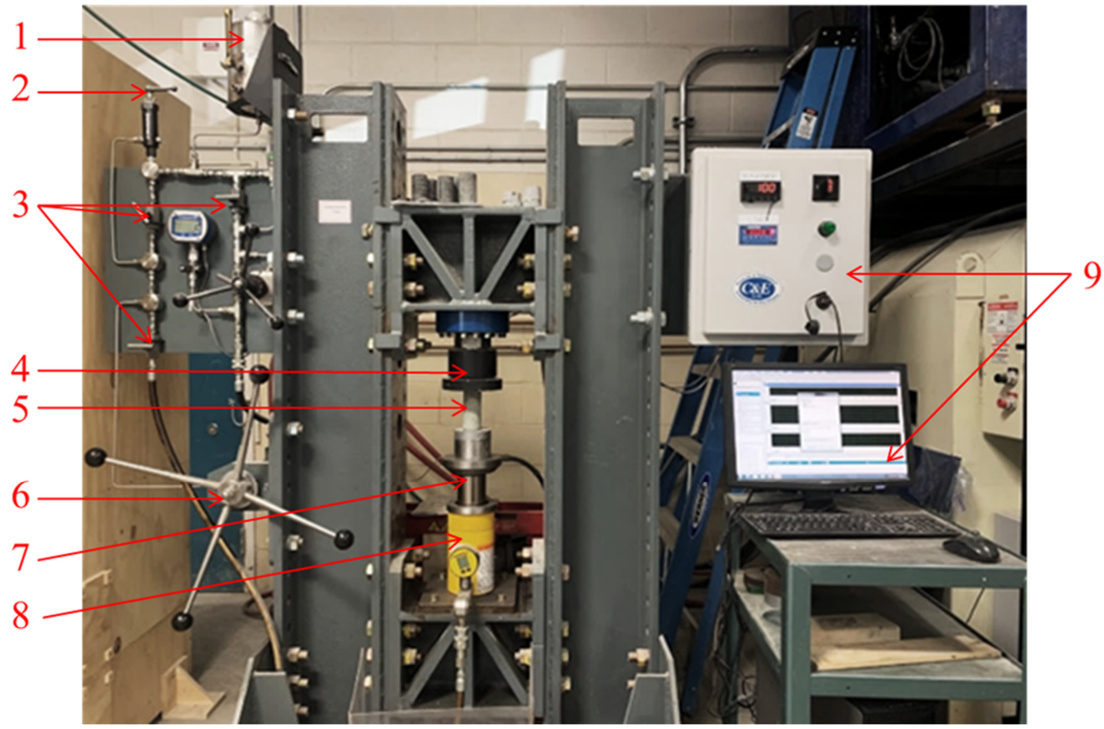

Figure 5.3 Geomechanics loading frame equipped with Data Acquisition System (DAQ-Sys)

[1-Hydraulic fluid reservoir, 2-Safety bypass valve, 3-Control valves, 4-Top fixed compression plate, 5-Test specimen, 6-Manual compression hydraulic pump, 7-Bottom compression plate, 8-Axial compression pressure piston, 9-Data Acquisition System (DAQ-Sys)]

Figure 5.3 displays the geomechanics loading frame utilized for the Unconfined Compressive Strength (UCS) tests and Brazilian tensile strength tests. The loading frame is equipped with a Data Acquisition System (DAQ-Sys) that records the main parameters needed to construct the stress-strain relationship, including the load in kN and displacement in mm. The DAQ-Sys uses LabVIEW software that records at a sampling rate of 100 Hz for these tests. The tests of the same sample types, percentage, parameters, and under the same conditions, are repeated at least nine times for 2 wt.%, 4 wt.% and 6 wt.% CTB specimens and three time for CTB specimens for vibration effect analysis.

5.2.2.5 Internal vibrator

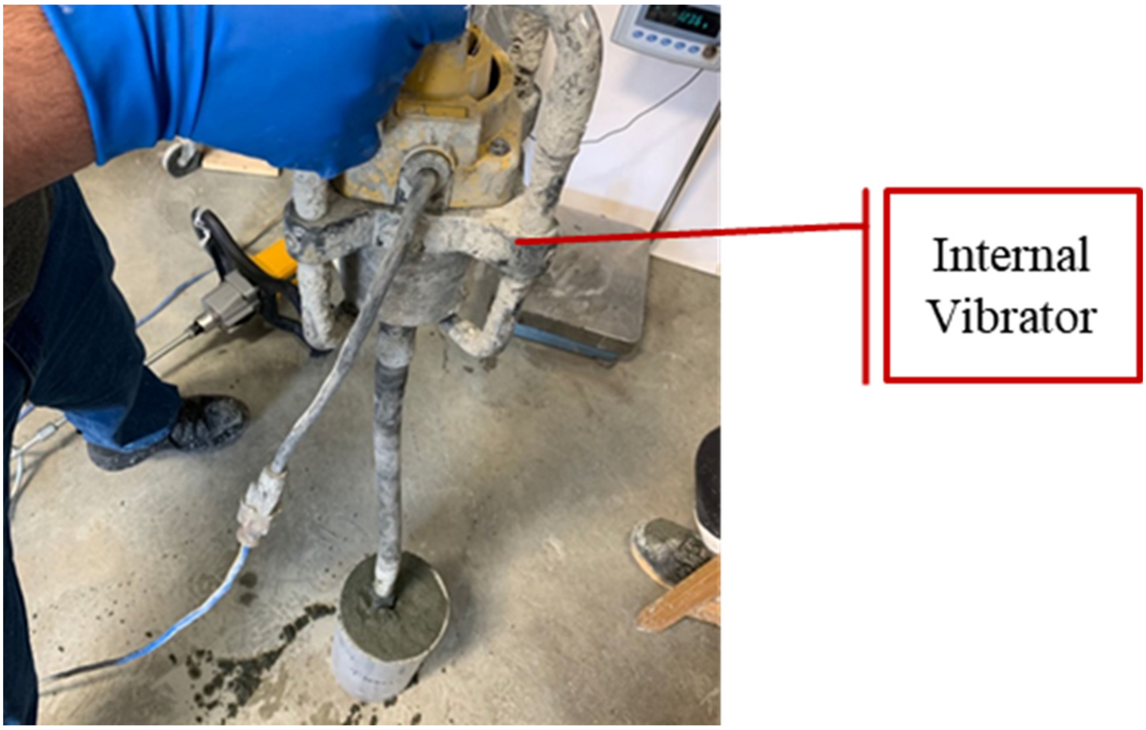

Figure 5.4 CPB specimen internal vibrating

When a vibrator is operating in fresh concrete, the vibration frequency should not be less than 9000 vibrations per minute and the vibrators should have a perimeter equivalent to the circumference of an appropriate round vibrator (ASTM C192). In this study, the 993-115V

WYCO concrete vibrator with a 1” diameter poker head (Figure 5.4) was utilized to consolidate the CTB specimens for internal vibration effect analysis. Typically, the vibrations of a vibrator are produced through a rotating eccentric. The frequency of a vibrator is determined by the rotating speed of the eccentric, while the eccentric moment determines the amplitude (Popovics, 1973). The rotation of the internal eccentric causes the vibrating head to run a simple harmonic oscillation.

5.2.3 Experimental Work

5.2.3.1 Backfill preparation and wet properties tests

The required mass of CTB ingredients, including tailings, Portland cement, fly ash and water, was prepared in the marked container. Table 5.1 shows the amount of each material based on both their percentage and mass for making specimens with 2 wt.%, 4 wt.%, and 6 wt.% binder proportions. The batch of specimens with 6 wt.% binder proportion was set as a contrast group. With 20% extra materials considered, based on ASTM Standards, 18 specimens of each binder proportion were casted. In order to ensure the homogeneity of the backfill, dry materials (tailings, PC and FA) were mixed thoroughly before the addition of water. After adding the water, the mixture was stirred by electronic mixer for 5 minutes. When pouring the mixture into the moulds, a tamping rod was used to reduce the air pockets inside the final specimens. After casting, the specimens, sealed with plastic covers, were kept at room temperature for 24 hours; then the specimens were extruded from the moulds and were kept in the moisture room to prepare them for the UCS tests after 14 days and 28 days curing time. The backfill preparation procedures were based on ASTM C192.

Table 5.1 Percentage of each required material

Materials	Binder dosage		
	2%	4%	6%
Mass of Tailings	78.4%	76.8%	75.2%
Mass of PC	1.3%	2.6%	3.8%
Mass of FA	0.3%	0.6%	1.0%
Mass of water	20.0%	20.0%	20.0%

During the backfill preparation process, the wet properties, such as wet density, pulp density and void ratio, of the prepared backfills were also measured and calculated.

When the mixture was ready to cast, a standard measuring cup was used. The wet density of the mixture can be calculated from Eq. [13]:

$$\text{Wet density}=\frac{\text{Mass of full cup of backfilling-mass of empty cup}}{\text{Volume of the cup}} \quad [13]$$

Hydraulic and paste backfills are often described in terms of their pulp densities. The pulp density can be defined as Eq. [14]:

$$\text{Pulp Density}=\frac{\text{Dry weight of aggregates+Binder}}{\text{Dry weight of all solids+Weight of all liquids}} \quad [14]$$

The void content was determined according to the ASTM C1688. The void content is defined as the total percentage of voids present by volume in a specimen. The void content of backfill can be calculated using Eq. [15]:

$$\text{Void content(\%)}=\frac{T-D}{T}\times 100\% \quad [15]$$

where,

$D = (M_c - M_m)/V_m$ (density of fresh concrete)

M_c = mass of measure filled with concrete

M_m = net mass of concrete by subtracting mass of measure

V_m = volume of measurement

$T = M_s/V_s$ (theoretical density)

M_s = total mass of materials batched

V_s = total absolute volume of materials

5.2.3.2 Internal vibration tests

In order to consolidate the CTB, an internal vibrator and 12 moulds (6” × 12”) were needed. The moulds were divided into four batches, Batch #1, Batch #2, Batch #3, and Batch #4. All required materials were weighted accurately, based on the 6 wt.% binder proportion recipe, and the materials were mixed for 3 minutes. When pouring the mixture into the mould, the mould was tapped at each 1/3 height of the mould, until it was full of mixture. Then, the weight of the mixture was measured. The internal vibrator was slowly inserted into the mould to compact the mixture. Generally, 7 seconds of vibration was adopted for each insertion to adequately consolidate the mixture. When the surface of the mixture became relatively smooth and large air bubbles ceased to break through the top surface, the proper consolidation (considered as 100%) of the mixture was achieved. After vibration, the vibrator was slowly withdrawn so that no large air pockets were left in the specimen. The decreased height of the mixture inside the mould was recorded for the calculations. A 100% vibration was conducted to fully vibrate Batch #1. The procedures were repeated on

Batch #2 and Batch #3 but with lower extent of vibration, 66.7% and 33.3%, respectively. The specimens in Batch #4 were set as s contrast group without vibration (0%). Then, the UCS tests of all specimens were conducted after they were kept in the moisture room for 28 days. All the UCS tests were carried out in triplicate and the average UCS values were presented in the results.

5.2.3.3 Uniaxial compressive strength (UCS) tests

The strength of backfill can be estimated by determining its UCS. Before conducting UCS tests on the specimens, the ends of each specimen were trimmed off by a grinder to ensure the surfaces of the specimens were flat and parallel, and the specimens had the average heights of 100 mm and diameters of 50 mm. A grinder was used to flatten both sides, and provided the final step in preparing test specimens.

Figure 5.5 Testing samples after failure

5.2.3.4 Tensile strength tests

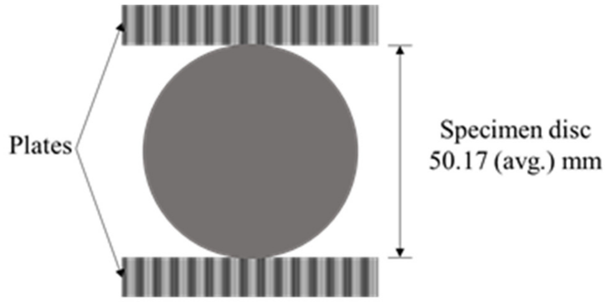

(a) Flat loading platens

(b) Placement of specimens and failure occurrence

Figure 5.6 Brazilian tensile strength test

The Brazilian test is a laboratory test for indirect measurement of tensile strength. In this test, the thickness to diameter ratio of the samples was 0.3 to 0.5. The specimens were placed between the machine plates, as shown in Figure 5.6, with a loading configuration of flat loading platens. The load was continuously increased at a constant rate within the range of 0.05 to 0.35 MPa/min (500 to 3000 psi/min) splitting tensile stress until failure of the specimens occurred. Usually, the indirect tensile strength is determined based on the assumption that failure occurs at the highest tensile stress point, that is, at the middle of the disc. At the failure point, the tensile strength of the specimen can be calculated as Eq. [16] (ASTM D3967-08):

$$\sigma_t = \frac{2P}{\pi Dt} = 0.636\frac{P}{Dt} \quad [16]$$

where P is maximum applied load by the testing machine (N), D is the diameter of the test specimen (mm), and t is the thickness of the test specimen, measured at the center (mm).

5.2.4 Results and Discussions

5.2.4.1 Wet properties of the designed backfill

Table 5.2 presents the wet properties of the prepared CTB with different binder proportions. Note that the wet density of the CTB increases with the increasing amount of binder, as well as the pulp density. McGeary (1961) reported that the backfill with a void ratio of 83% is considered to have a good density. However, the void ratios of three different binder proportion backfills in this study are from 50% ~ 60.52%. The reason for this phenomenon is that most of the contents of the used tailings have certain coarse particle size distribution, which gives more space between the particles. When the binder proportion is low, the coarse tailings particles will have higher void ratio. Meanwhile, the low proportion of binder is insufficient to fill the space between tailings particles. Then, the void ratio increases with the decreasing binder proportion. Thereby, the binders, PC and FA, are necessary for the void filling within the CTB mixture, fewer of them are available for coating particles and the cohesion is also decreased.

Table 5.2 Wet properties of prepared CTB

Binder proportion	Wet density (kg/m³)	Pulp density (kg/m³)	Void ratio (%)
2 wt.%	1826.43	798	60.52
4 wt.%	2049.79	800	53.78
6 wt.%	2055.97	800	50.95

5.2.4.2 Effect of lower binder proportions on UCS development of CTB

The binder proportion plays a significant role in the UCS development of CTB specimens. Figure 5.7 shows that the UCS values for the CTB specimens with 4 wt.% and 6 wt.% binder proportions increase with curing time. This performance is mainly because of the cement hydration increasing along with the curing time and because of the settlement of particles within the CTB specimens. Some studies (Taylor, 1997; Fall et al., 2008) demonstrated this time-dependent increase in cement hydration and the associated refinement of the pore pressure. Due to the existence of FA, the pozzolanic activity (the presence of calcium hydroxide in water) also contributed to the UCS development. Sakai et al. (2005) stated that the FA started to react and consume calcium hydroxide after 28 days curing time, which meant the consumption of calcium hydroxide was equal to zero at 28 days. The UCS development rate reduced as the content of calcium hydroxide decreased. Our previous work (Someehneshin et al., 2020) has shown the same performance in the UCS development of the CTB specimens with binder proportions 6 wt.%, 8 wt.%, and 10 wt.%.

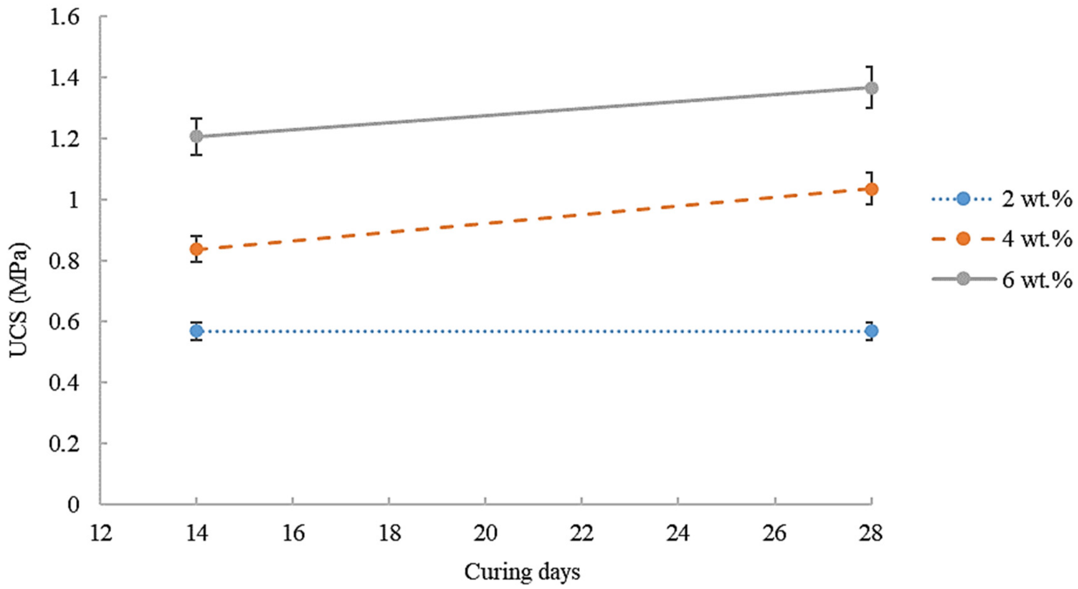

(a) Graph of UCS development trend

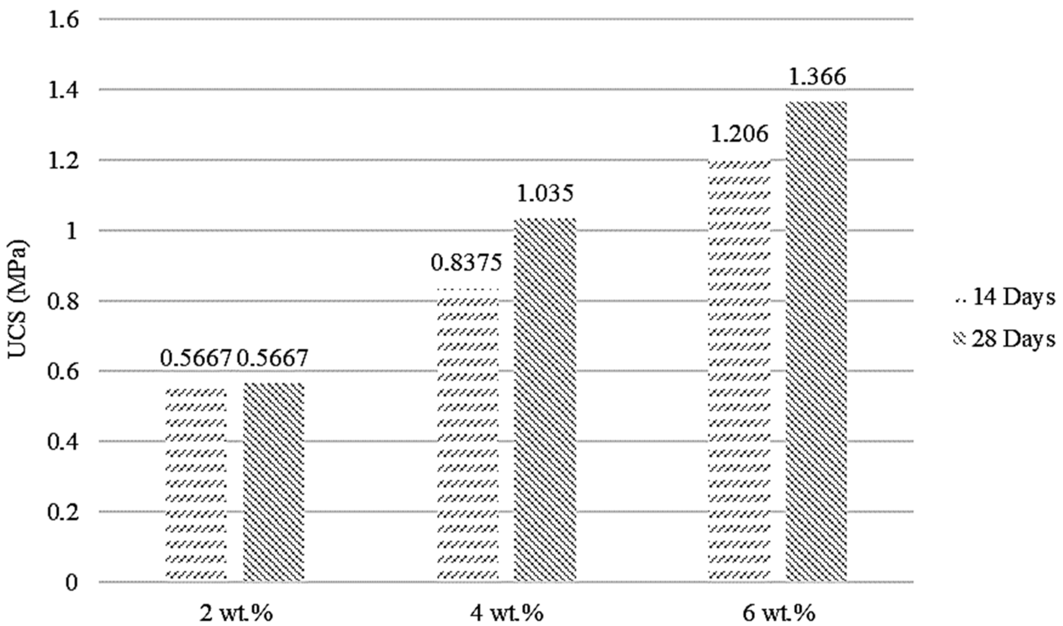

(b) Histogram of UCS development trend

Figure 5.7 UCS development of 2 wt.%, 4 wt.% and 6 wt.% binder proportion specimens

Table 5.3 Results of tensile tests of the CPB specimens

Sample #	Diameter (mm)	Thickness (mm)	t/d ratio	Peak load (N)	Tensile strength (MPa)	Compared to UCS (%)
4-2	50.19	16.35	0.326	642.114	0.498	48.1
4-4	50.17	15.29	0.305	574.442	0.478	46.1
4-5	50.00	17.29	0.346	574.442	0.423	40.9
4-9	50.15	20.80	0.415	506.771	0.309	29.8
4-11	50.17	19.87	0.396	574.442	0.367	35.4
6-1	50.17	16.37	0.326	912.798	0.707	51.7
6-6	50.17	16.96	0.338	777.456	0.582	42.6
6-7	50.17	18.10	0.361	642.114	0.450	32.9
6-11	50.17	15.61	0.311	980.469	0.797	58.3
6-12	50.17	18.16	0.362	642.114	0.449	32.8
6-13	50.15	17.11	0.341	709.785	0.527	38.6
6-15	50.18	20.20	0.403	642.114	0.450	32.9

For cyclical mining, both a short curing time and enough early strength will accelerate the mining operations. Regarding the Sustainable Mining by Drilling (SMD) Project (Lopez-Pacheco, A. 2019), the target designed CTB strength is 1 MPa (Someehneshin et al., 2020). It is found that the specimens of 6 wt.% binder proportion obtain almost the same UCS values as in previous tests, which can provide adequate strength. The specimens with 4 wt.%

binder proportion performed 1.035 MPa UCS after 28 days and reached the target backfill strength, which means the CTB of 4 wt.% binder proportion can provide enough strength as well. As for the specimens of 2 wt.% binder proportion, they even started to collapse while in the moisture room. The CTB of 2 wt.% binder proportion has a higher void ratio due to a large amount of tailings usage, which undermines the cohesion between the particles, requiring more binder for void filling.

5.2.4.3 Tensile strengths of the CTB with 4 wt.% and 6 wt.% binder proportions

Tensile strength is also an essential parameter. The Brazilian tensile tests were carried out as part of this analysis and showed suitable results. The tensile testing samples were paired with UCS testing of the same, or as similar as possible, samples to determine the ratio between tensile and UCS values. The tensile tests results are shown in Table 5.3 and plotted in Figure 5.8.

In this study, the average diameter of the samples is 50.17mm. Figure 5.8 shows that the tensile strengths of the CTB discs increase with the decreasing thickness to diameter ratio. Furthermore, when the t/d ratio is greater than 0.31, the corresponding tensile strengths obviously decreases with the increase of the t/d ratio, while as the t/d ratio approaches or is less than 0.31, the tensile strength increases slowly and gradually maintains a stable value. As for the testing of the CTB disc samples, the greater the thickness of the sample, the greater the possibility of defects in the sample, and the lower the tensile strength. The previous different tensile strength testing methods (Ming et al., 2001; Dou et al., 2004) showed that the tensile strengths obtained by Brazilian tensile are quite different from those obtained by the direct tensile method, using the recommended standard sample sizes. The

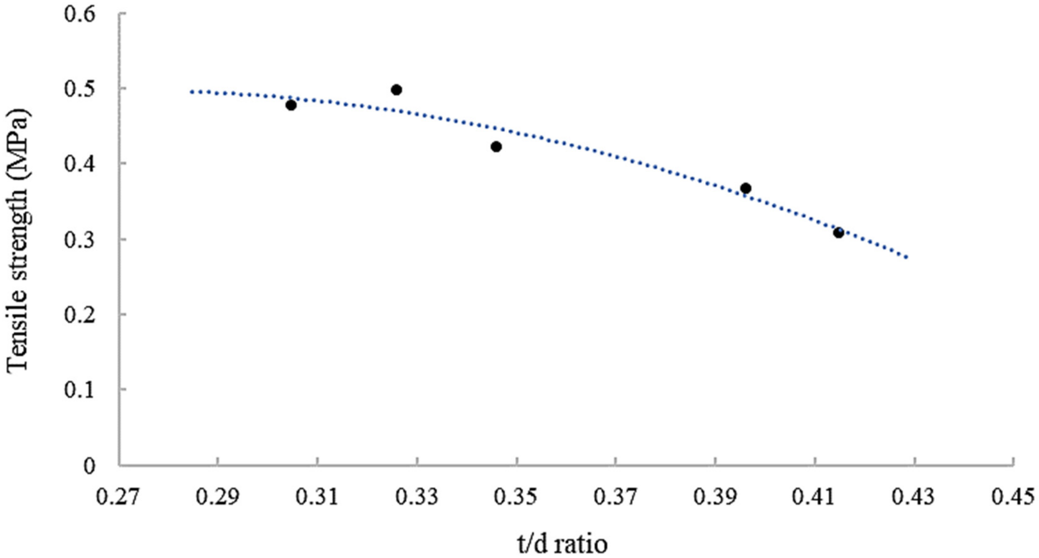

(a) Tensile strength of 4 wt.% specimens

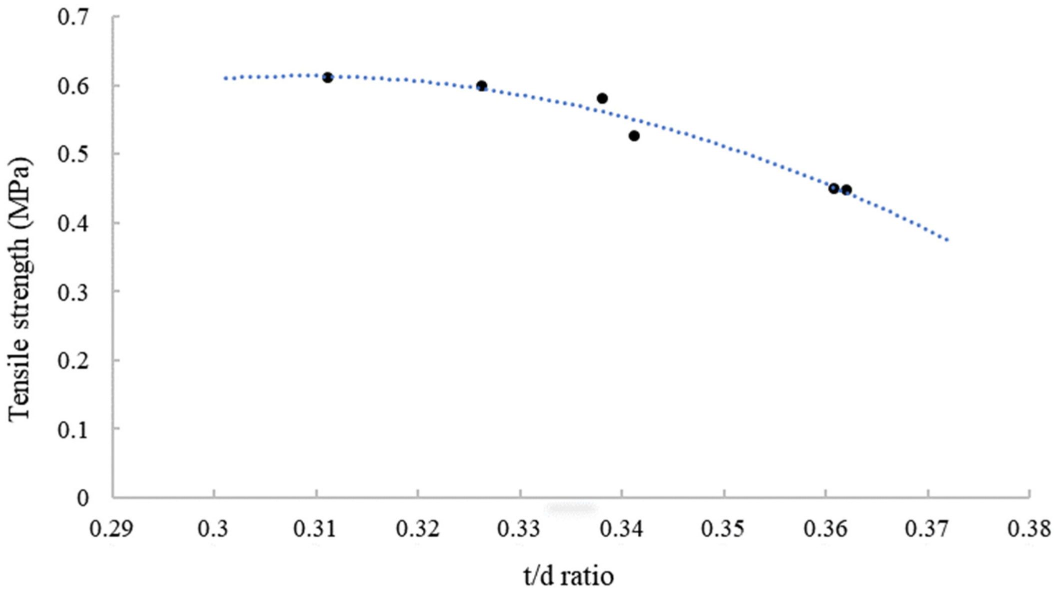

(b) Tensile strength of 6 wt.% specimens

Figure 5.8 Tensile strengths of (a) 4 wt.% and (b) 6 wt.% specimens prepared CTB tensile strength behaviour is similar to the rock splitting tensile strength, which has been reported by Deng (2012). When the ratio of thickness to diameter is less than 0.3, the distribution of tensile stress on the central axis of the disk specimens tends to become uniform gradually, which also explains the reason why the tensile strength tends to be stable when the thickness to diameter ratio is less than 0.3.

5.2.4.4 Effect of internal vibration on physical properties of CTB

After the backfill placement operation, the CTB contains as much as 20% entrapped air, which greatly reduces the density, strength, and stiffness. Internal vibration is commonly utilized for consolidating fresh concretes in field construction. In this study, internal vibration was applied during the consolidation of CTB to investigate the behaviour changes. The vibration operation has a two-part process. The first process is that the internal vibrator creates pressure waves to separate aggregate particles, reducing friction between them, and large air pockets disappear. Almost simultaneously, the second process starts to occur as entrapped air rises to the surface. The deaeration process continues until the surface of the specimen is smooth and the bubbles stop breaking at the surface. During the consolidation, the particles within the CTB specimen will rearrange. There may be a nesting effect, where smaller particles (PC and FA) occupy the void space between larger particles (tailings), implying that a single larger particle is surrounded by smaller ones (shown in Figure 5.9). Hence, the height, volume and porosity of the specimen will be reduced.

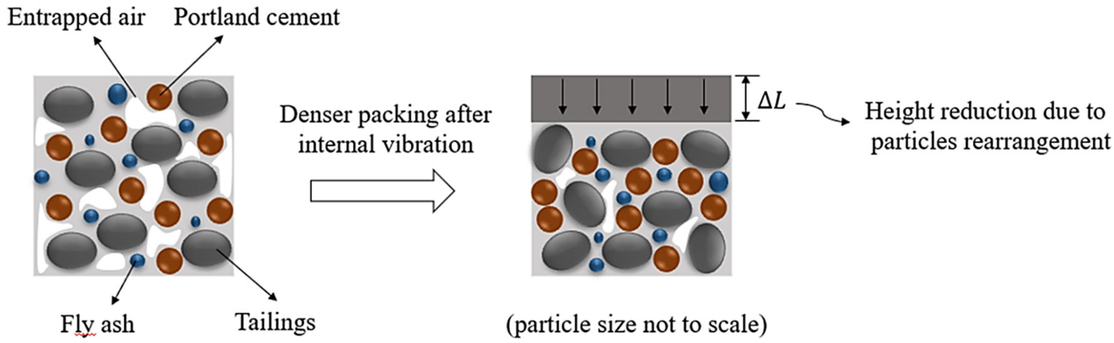

Figure 5.9 Schematic presentation of particles denser packing

The testing results of physical properties are shown in the Table 5.4. Note that the density increased with the increasing of the vibration times. Compared with the CTB density without vibration (Batch #1), the density of fully vibrated CTB (Batch #4) obtained an increase of approximately 14.6%. The fully vibrated CTB had about 14.37% reduction in volume and porosity, which means more space would be provided to place the backfill in the extracted stopes. In the studied mine, the diameter and depth of the extracted stope are 1 m and 300 m, respectively. When a 6 wt.% binder proportion recipe for the CTB preparation is adopted, each wellbore can be refilled with extra 33.86 m^3 fully vibrated backfill, which means extra 50,925 kg tailings can be sent underground for each extracted wellbore. The amount of surface tailings will be reduced about 10.9% and the surface tailings impoundment requirements will be further reduced.

Table 5.4 Physical properties of the CTB with different vibration degrees

Batch #	Vibration degree	Density of mixture (kg/m³)	Reduction volume (m³)
1	0%	1978.69	0
2	33.30%	2049.62	0.000306
3	66.70%	2096.6	0.000361
4	100%	2268.31	0.000798
Batch #	**Vibration degree**	**Reduction percentage (%)**	**UCS after 28 days (MPa)**
1	0%	0	0.38
2	33.30%	5.51	0.41
3	66.70%	6.49	0.45
4	100%	14.37	0.55

5.4.2.5 Effect of internal vibration on UCS development of CTB

Suprenant et al. (1988) reported that each percent of air in the concrete will decrease compressive strength by about 3% to 5% when the water-cement ratio is constant. From Table 5.4, it is observed that the CTB has the same behaviour as the concrete that the UCS increases with the increasing degree of vibration. Although it is not practical to remove all the entrapped air with standard vibrating equipment, the fully vibrated specimens have shown a 57.1% higher UCS than the specimens without vibration after 28 days curing time, owing to the denser packing of the particles within the CTB. Also, note that the UCS value of specimens of size 6” × 12” is lower than that of 2” × 4” specimens. The reason for this performance is that the small volume specimens provide a decreased number of micro-cracks and pores in the homogenous matrix, as compared with the larger specimen sizes (Yilmaz, 2015). The internal vibration increases the UCS of CTB, which can reduce the requirement of binder addition, thereby reducing the cost of the CTB plant in a mining industry.

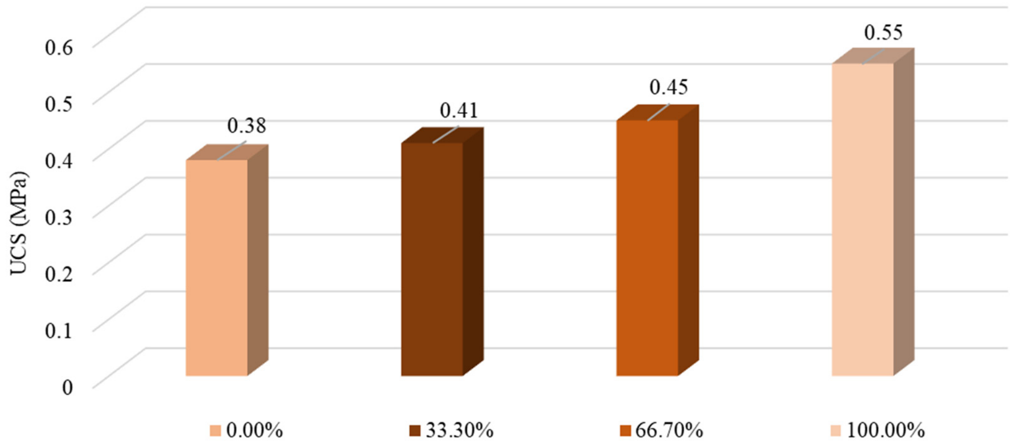

Figure 5.10 UCS development of CPB specimens with internal vibration after 28 days

5.2.7 Conclusions

Based on the results obtained from this study, the following conclusions can be made:

1) The CTB with 4 wt.% binder proportion can obtain sufficient UCS, which reaches the designed target UCS of CTB, after short-term 28 days curing time. The costs of backfill usually account for a large proportion in mining operations. However, the costs of a backfill plant in a mining industry will be reduced with less addition of Portland cement and partial substitution with fly ash. Additionally, the CTB with 2 wt.% has insufficient UCS for the backfill operation, due to the low cohesion between the particles inside CTB structure resulting from low binder addition.

2) The Brazilian tensile test was adopted to measure the tensile strength of 4 wt.% and 6 wt.% CTB disc samples. The tensile strengths of the CTB discs increase with the decreasing thickness to diameter ratio. Furthermore, when the t/d ratio is greater than 0.31, the corresponding tensile strength obviously decreases with the increase of the t/d ratio, while when the t/d ratio approaches or is less than 0.31, the tensile strength increases slowly and gradually maintains a stable value. This performance is consistent with the splitting tensile strength of rock.

3) Internal vibration not only has an influence on the fresh concrete, but also has positive effects on the CTB. Internal vibration (consolidation) involves expelling entrapped air and repositioning the aggregate particles in a denser state without causing segregation. In the process of compacting concrete and removing trapped air, the density increases while the mass remains constant and the volume of the CTB decreases, which allows an extra 10.9% tailings to be sent underground, further reducing the surface tailings pond. Internal vibration also increases the compressive strength of the CTB by 57.1%. When the internal vibration method is applied to the placement of CTB, the CTB can obtain the target UCS, with a lower requirement of added binder, which will further reduce the costs of the backfill plant.

5.3 Design of Primary Field Backfill Preparation System

Backfill system design has three main design components, including backfill preparation, backfill distribution and backfill displacement. In the design work, the characterization of backfill material has been identified as the central component. The physical, chemical, and mechanical properties of the tailings affect the ability of the backfill to meet the required target design criteria (Sveinson, 1999). The significant target design criteria include geomechanics properties, distribution and placement criteria, environment performance, and socio-economic performance. Cemented tailings backfill design criteria are based on the target properties determined from the required backfill functions. The design of first field backfilling operation for SMD project has borrowed many technical experiences from those successful operations (Belem & Benzaazoua, 2004; Cayouette, 2003; Cooke, 2006; Guo et al., 2017; Wang et al., 2009; Wu et al., 2015). According to the practical situation of the SMD wellbore, more optimizations will be made in the continuous design work.

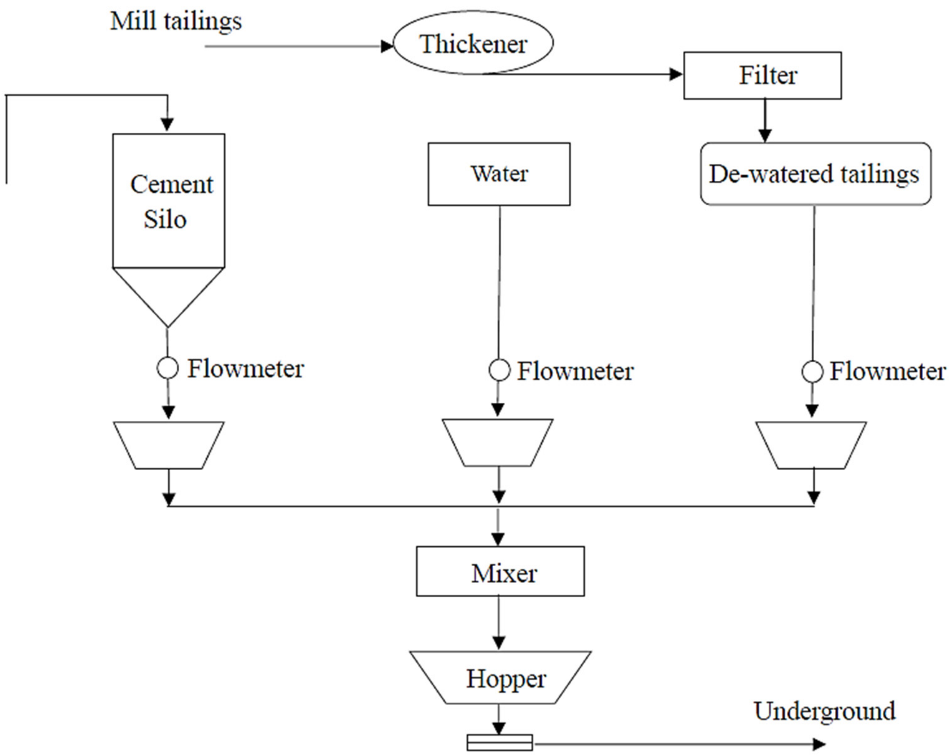

Figure 5.11 Design flowchart of backfill preparation system

The design of cemented tailings backfill preparation system is a batch system as the design flowchart shown in Figure 5.11. The dewatered tailings, binder and water are weighted and combined individually. The batch system can give a better control of backfill quality. The most widely used thickener or dewatering systems use flocculant-aided settling.

Figure 5.12 exhibits the design diagram of cemented tailings backfill preparation system. When the backfilling plant is working, the tailings first report to the hydrocyclones for desliming where a part of fine particles is eliminated at the overflow. Then, the tailings transfer to deep cone thickener. After thickening, the tailings report to holding tank. From the holding tank, the thickened tailings are fed by gravity to the disc filter. The tailings, which is 92% solid, is then discharged and weighted on a belt conveyer. In the backfill plant, Portland cement and fly ash are mixed with a ratio of 4:1 as used binder. Each binder feed system is comprised of a twin-screw conveyer with a variable speed drive followed by a belt feeder equipped with a scale. Dry Portland cement and fly ash stored in the silos will be strictly weighted by a powder scale feeder and transported to the mixing hopper. Then, the binders, tailings and water are reported to the hopper, which can provide a pre-mixing place for the materials. And the two-stage continuous mixing technique is used to give a through mixing.

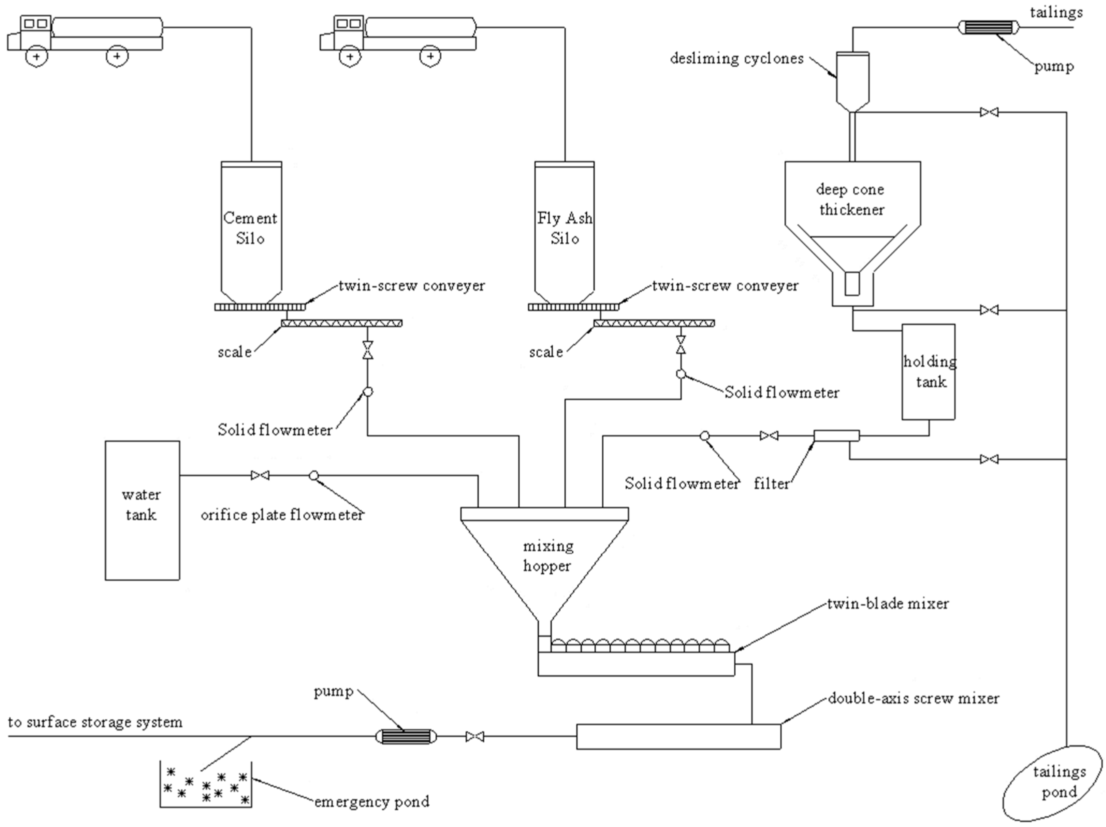

Figure 5.12 Diagram of backfill preparation system

Two techniques have been widely used for the tailings dewatering. One is two-stage dewatering system consisting of high efficiency thickener and vacuum filter. Another is one-stage thickening using a deep cone thickener (Wu et al., 2015). In this cemented tailings backfill system design, one-stage thickening technique is utilized. The two-stage dewatering system usually needs high costs and energy consumption. It is not reliable when dealing with large portion of fine tailings. The deep cone thickener can simplify the complex conventional dewatering procedures and perform a satisfactory underflow concentration.

In the backfill preparation system, the disc filters system is comprised of two water/air separators in series. The first one has two filtrate pumps and the second, located higher, serves as a backup. The filtrate water will return to the deep cone thickener and then to the recycled water pit. The disc filters are used to give required target a solids concentration of mill tailings before mixing.

Chapter 6. Investigation of Cemented Tailings Backfill (CTB) with Anti-washout Admixture

6.1 Introduction

Cemented tailings backfill (CTB) is an engineered mixture of processed tailings (75 –85% solids by weight), a hydraulic binder (3 – 7% by dry total paste weight) and mixing water to set the paste solids density of 70 –80% at the desired consistency. The binders are added into backfill to produce and enhance mechanical strength. Each component of CTB plays a significant role on its short- and long-term performance, such as strength and workability, and its transportation and placement to underground extracted boreholes (Yilmaz et al., 2003).

From the previous work, the CTB with 2 wt.%, 4 wt.%, 6wt.%, 8 wt.%, and 10 wt.% binder proportions after a short curing time (7 days, 14 days, and 28 days) have been investigated. The results showed that the UCS values for the CTB specimens increase with curing time and the increasing binder proportion. Regarding the Sustainable Mining by Drilling (SMD) Project, the target designed CTB strength is 1 MPa. It is found that the specimens with 4 wt.% or higher binder proportion can provide the adequate UCS values for the SMD project after 28 days curing time. As for the specimens of 2 wt.% binder proportion, they even started to collapse while in the moisture room. The CTB of 2 wt.% binder proportion has a higher void ratio due to a large amount of tailings usage, which undermines the cohesion between the particles, requiring more binder for void filling.

Considering the practical operation, the designed CTB will be placed into the wellbore filled with water. To reduce the influence of the water on CTB behaviour, underwater concrete method is a potential solution to be applied on the CTB to achieve this target. Underwater concrete is one special type of high-performance concrete used for constructions, with foundations in soil with high water levels, and almost all off- and on-shore structures (Mindess, 2019). The high-performance concrete is a type of concrete that performs well at many key aspects, especially strength, workability, and service life. Underwater concrete is a concrete that has high flowability which can place down to the borehole by its self-weight and the good compaction can be achieved without vibration and defects due to segregation. The anti-washout admixture (AWA) is the indispensable thing to achieve the benefits for underwater concrete method. AWA is added into the concrete to improve or enhance the stability of fresh cementitious mixtures. Neeley (1988) and Khayat et al. (1991) have stated that the anti-washout property and in-place property of underwater cast concrete are improved with the existence of AWAs. The concrete with AWAs performs higher viscosity and yield value compared with the concrete without AWAs. Usually, water reducer or superplasticizer is utilized with AWAs to enhance the performance of underwater concrete. Increasing the dosage of water reducer or superplasticizer with AWA will ensure flowable concrete of relatively low yield value and moderate-to-high plastic viscosity of high washout resistance (Khayat & Sonebi, 2001).

Based on the obtained previous conclusions, the main purpose of this study is to explore anti-washout admixtures in our designed backfill to investigate the property of anti-washout when placing into the water and performance of curing under water.

6.2 Tested Admixtures

In this study, total 7 anti-washout admixtures (AWA) were tested based on different percentages. And 1 high-range water reducing admixture (HRWR) was tested to improve the rheology. The admixtures V-MAR 3 and ADVA-140 M were provided by local company Concrete Product. V-MAR 3 is the AWA used for the underwater concrete placing and ADVA-140 M is the HRWR, which is usually used with VMAR-3. Both of them are liquid admixtures. The admixtures named Sika 100SC, Stabilizer Aquagel, VMA-1, VMA-2, VMA-3 and VMA-4 were AWAs provided by company Sika Canada in Montreal. All the AWAs are powder (solid) admixtures except Sika 100SC in liquid.

6.3 Investigation of Feasible Dosages for Anti-washout Admixture

Finding the feasible admixture dosages is the target of this study. No paper containing the general reference dosages for admixtures added in backfill was found from literature review because the different mining tailings have different properties. To figure out the suitable admixture dosages for our backfill is the priority investigation. A direct method is used to check the performance of backfill when it is pouring into the water, as shown in Figure 6.1 (target performance). A water tank and batch of transparent mason jars are utilized to provide the water condition. For each trial test, 0.6L backfill will be prepared and the admixture dosages will start from a certain number. The accurate mass of each constituent is calculated based on the typical dosages for the concrete industry and considering the higher water content in our backfill materials. The trial tests are continued until the target the backfill will be not disperse in water and perform self-settle down or self-consolidating is achieved. Otherwise, the admixture is proved to be not suitable for the designed backfill.

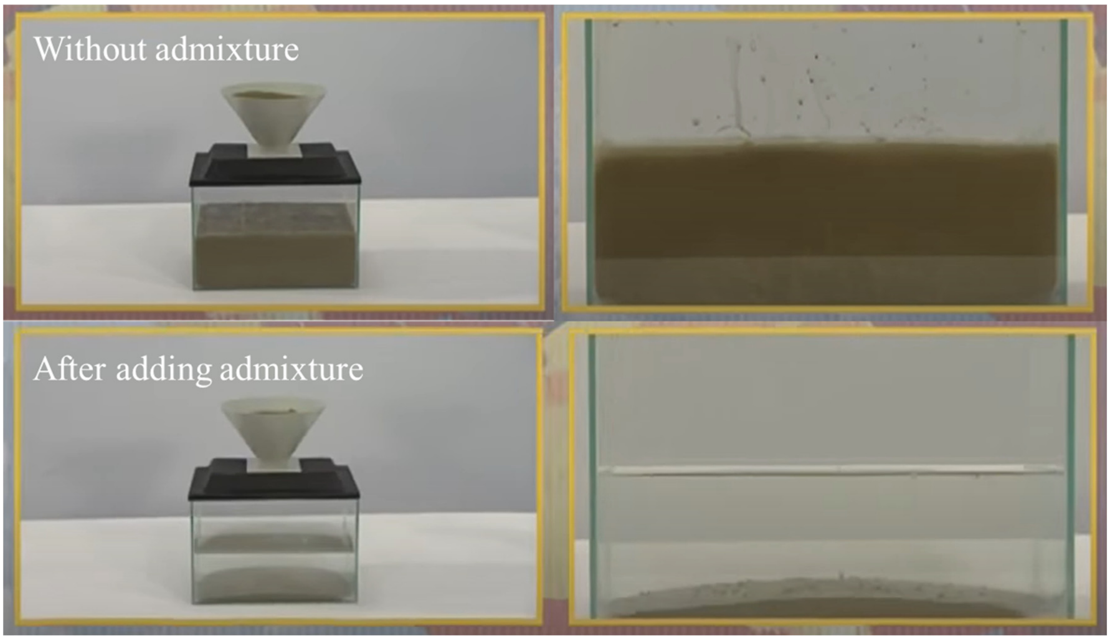

Figure 6.1 Target CTB performance when pouring into water (Sika, 2016)

6.3.1 Mixing procedure

For liquid admixture: Initially, all dry materials, including tailings, Portland cement and fly ash, were mixed for homogenisation. After dry mixing, 80% of the total water was added and mixed for 60s. Subsequently, the remaining water was added along with the admixtures and mixed for 2 minutes. Then 2-minute-rest was applied and followed by a final mixing of 2 minutes.

For solid admixture: Initially, all dry materials, including tailings, Portland cement and fly ash, were mixed for homogenisation. After dry mixing, total water was added and mixed for 60s. Subsequently, the admixture was added to the blended mixture and mixed for 2 minutes. Then 2-minute-rest was applied and followed by a final mixing of 2 minutes.

6.3.2 Testing matrix for different admixtures

Table 6.1 shows the amount of each material (tailings, Portland cement, fly ash, and water) based on both percentage and weight of them for making 720 mL backfill mixture with 6 wt.%, 8 wt.% and 10 wt.% binder compositions. 20% extra mass of backfill are considered based on ASTM Standards.

Table 6.1 Needed amount of each material for different binder proportions

Binder recipe	6 wt. %	8 wt.%	10 wt.%
Mass of tailings %	75.20%	73.60%	72.00%
Mass of cement %	3.84%	5.12%	6.40%
Mass of Fly Ash %	0.96%	1.28%	1.60%
Mass of water %	20.00%	20.00%	20.00%
Needed tailing (g)	692.7	682.2	671.4
Water content in the tailing (g)	35.8	35.3	34.7
Needed water (g)	138.9	140.5	142.1
Mass of cement (g)	33.5	45.0	56.6
Mass of Fly Ash (g)	8.4	11.3	14.1

Table 6.2 Testing matrix of V-MAR 3 and ADVA-140 M

Admixture	Recommended dosage	Trial 1	Trial 2	Trial 3	Trial 4	Trial 5	Trial 6	Trial 7
V-MAR 3	2	3	7	10	20	40	60	60
ADVA-140 M	0.5	1	3	5	5	5	5	5
Binder recipe			6 wt.%					10 wt.%
Typical water content: 166 - 190 kg/m³			Water content of our backfill: 424 kg/m³					Unit: mL

Table 6.3 Testing matrix of Sikament 100SC

Binder recipe	Test #	Sikament 100SC Dosage (mL)	Settlement time (min)					
			20	40	60	80	100	120
6 wt.%	Recommended	1.3	√	√	√	√	√	√
	Trial 1	3.34	√	√	√	√	√	√
	Trial 2	5.38	√	√	√	√	√	√
	Trial 3	7.4	√	√	√	√	√	√
	Trial 4	15	√	√	√	√	√	√
	Trial 5	15	√	√	√	√	√	√
Adding ratio: 630 mL/100 kg						water/cement: 0.4		

Table 6.4 Testing matrix of Stabilizer Aquagel

Binder recipe	Test #	Stabilizer Aquagel Dosage (g)	Settlement time (min)					
			20	40	60	80	100	120
6 wt.%	Trial 1	0.45 (0.8%)	√	√	√	√	√	√
	Trial 2	3 (8%)	√	√	√	√	√	√
	Trial 3	3.8 (10%)	√	√	√	√	√	√
8 wt.%	Trial 4	4.6 (12%)	√	√	√	√	√	√
	Trial 5	3.9 (7%)	√	√	√	√	√	√
	Trial 6	5.1 (9%)	√	√	√	√	√	√
10 wt.%	Trial 7	3.5 (5%)	√	√	√	√	√	√
	Trial 8	5 (7%)	√	√	√	√	√	√
	Trial 9	6.4 (9%)	√	√	√	√	√	√
Recommended adding ratio: 0.03%~0.25% of cementitious materials								

Table 6.5 Testing matrix of four types of VMAs

VMA-1						
Binder recipe	Test #	Dosage (g)	Settlement time (min)			
			30	60	90	120
10 wt.%	Trial 1	5 (7%)	√	√	√	√
	Trial 2	3.5 (5%)	√	√	√	√
	Trial 3	6.4 (9%)	√	√	√	√
VMA-2						
Binder recipe	Test #	Dosage (g)	Settlement time (min)			
			30	60	90	120
6 wt.%	Trial 1	4.2 (11%)	√	√	√	√
	Trial 2	5 (13%)	√	√	√	√
8 wt.%	Trial 3	5.1 (9%)	√	√	√	√
	Trial 4	6.2 (11%)	√	√	√	√
10 wt.%	Trial 5	5 (7%)	√	√	√	√
	Trial 6	3.5 (5%)	√	√	√	√
	Trial 7	6.4 (9%)	√	√	√	√
VMA-3						
Binder recipe	Test #	Dosage (g)	Settlement time (min)			
			30	60	90	120
10 wt.%	Trial 1	5 (7%)	√	√	√	√
	Trial 2	2.1 (3%)	√	√	√	√
	Trial 3	3.5 (5%)	√	√	√	√
8 wt.%	Trial 4	3.9 (7%)	√	√	√	√
6 wt.%	Trial 5	2.7 (7%)	√	√	√	√
VMA-4						
Binder recipe	Test #	Dosage (g)	Settlement time (min)			
			30	60	90	120
10 wt.%	Trial 1	5 (7%)	√	√	√	√
	Trial 2	3.5 (5%)	√	√	√	√
	Trial 3	6.4 (9%)	√	√	√	√

Table 6.2 to Table 6.5 provide the testing dosages for each anti-washout admixture. The dosage of V-MAR 3 is based on the mixture volume of 390 to 1550 mL/m^3 with the typical water content of 166 to 190 kg/m^3 for concrete industry. The tested dosages of V-MAR 3

were increased correspondingly as the water content is around 420 kg/m^3 for the recommended 6 wt.% recipe of the design CTB in SMD project. ADVA-140 M is a high-range water reducer that usually used with V-MAR 3 at rate of 130 mL/100 kg to 1300 mL/100 kg of cement. The dosage of Sikament 100SC is based on the water to cement ratio of 0.4. However, the higher tested dosages were applied due to the high water to cement ratio of the design CTB. The recommended adding rate for Stabilizer Aquagel is at 0.03% to 0.25% of cementitious materials (cement and fly ash). Because of the very low composition of cementitious materials in backfill mixture, the dosage of Stabilizer Aquagel was increased to 1%, 3%, 5%, 7% and 9% for the tests. Finally, the amount of VMA 1-4 is based on the mass of cementitious materials with the testing dosage at 3%, 5%, 7% and 9% based on the suggestions from Sika technician. The observance picture of settlement for Sikament 100SC and Stabilizer Aquagel was taken every 20 minutes until total 120 minutes. The observance picture of settlement for VMA 1-4 was taken every 30 minutes until total 120 minutes.

6.4 Testing Results of Anti-washout Property

6.4.1 Results of V-MAR 3 and ADVA-140 M

V-MAR 3 is a white liquid AWA with a high viscosity. It is more like a gel and cannot flow like a liquid. ADVA-140 M is a liquid brown high-range water reducing (HRWR) admixture that is usually used with V-MAR 3. Glass droppers were used to control the adding amount. The trial tests were conducted based on Table 6.2. For the CTB without admixture, the backfill had very low flowability. A shovel was needed to place the backfill into the water tank. And when the backfill was in the water, the particles would disperse in the water very quickly and the water became muddy.

The recommended dosage was calculated based on the concrete industry product sheet. Then the dosages were increased based on the performance. In this study, the first target is to achieve the washout property of backfill that is the backfill will not be affected by the water. The backfill can settle down without dispersing and the second target is to increase the rheology and workability of backfill. However, there was rare improvement when adopting recommended dosage due to the high water content of our CTB. In the subsequent trial tests, the dosages of admixtures were increased. When ADVA-140 M reached 5 mL (83 mL/kg) which was 6.4 times of recommended dosage (13 mL/kg), the CTB obtained a good flowability. But the anti-washout property was not achieved. Trial 6 and 7 adopted 6 wt.% and 10 wt.% recipe and the V-MAR 3 was increased to 60 mL which was 30 times of the recommended dosage to explore the performance. Unfortunately, the anti-washout performance was still bad. The particles would suspend in the water and was not cured at all even after 14 days. Consider the costs of high dosages and poor performance, these two admixtures are uneconomic.

6.4.2 Results of Sikament 100SC

Sikament 100SC is a brown liquid admixture and is formulated for use at a rate of approximately 2.58 L/m^3 (630 mL/100 kg)). Based on the tests performance, when the dosage was at recommended adding rate, the Portland cement and fly ash would still be washed out when placing into the water. There was a layer of Portland cement and fly ash settled down on the tailings after 24 hours. The specimen was weakly cured after 14 days, which cannot provide sufficient strength for the support. When the dosage of Sika 100SC was increase to 11.5 times of recommended dosage, the anti-washout property was still not improved, the high dosage of Sikament 100SC would suspend the cementitious particles in the water. The specimens were not cured after 14 days due to the suspension of cementitious materials. It is found that Sika 100SC is not suitable for the designed CTB.

6.4.3 Results of Stabilizer Aquagel

Stabilizer Aquagel anti-washout admixture is a ready-to-use, powdered admixture, especially for self-levelling concrete and concrete placed underwater. Concrete treated with Stabilizer Aquagel remains cohesive, homogeneous and workable with minimum loss of fines, including cement from freshly mixed concrete. Stabilizer Aquagel is recommended for use at 0.03% to 0.25% of cementitious materials (cement, fly ash, silica fume and slag). Because of the low proportions of cementitious materials containing in designed backfill, the dosages of Stabilizer Aquagel were set at 1%, 3%, 5%, 7% and 9% based on the mass of cementitious materials after consulting the technician in Sika Canada.

When the 6 wt.% binder recipe was adopted, the dosage of Stabilizer Aquagel was set at 0.8%, 8%, 10% and 12% respectively. The anti-washout properties of all four dosages were unexpected. After 21 days and 28 days, the specimens inside the jars were still soft and weakly cured. The specimens cannot provide sufficient strength after short term curing time.

When the 8 wt.% binder recipe was adopted, the dosage of Stabilizer Aquagel was set at 7% and 9% which were much higher than the recommended dosage. But the anti-washout property was undesirable, and the strength were insufficient after 21 days.

When the 10 wt.% binder recipe was adopted, the dosage of Stabilizer Aquagel was set at 5%, 7% and 9%. Although these dosages still didn't achieve good anti-washout property (Figure 6.2, Figure 6.3 and Figure 6.4), it was observed that the layer of washed out materials was much thinner than that of 6 wt.% binder recipe. The specimens were strongly cured after 28 days than the other two recipes. The Stabilizer Aquagel can be a promising potential admixture for the cemented tailings backfill when the 10 wt.% binder recipe is adopted.

Figure 6.2 Performance of Stabilizer Aquagel 5% (R 10 wt.%) after placing and 28 days

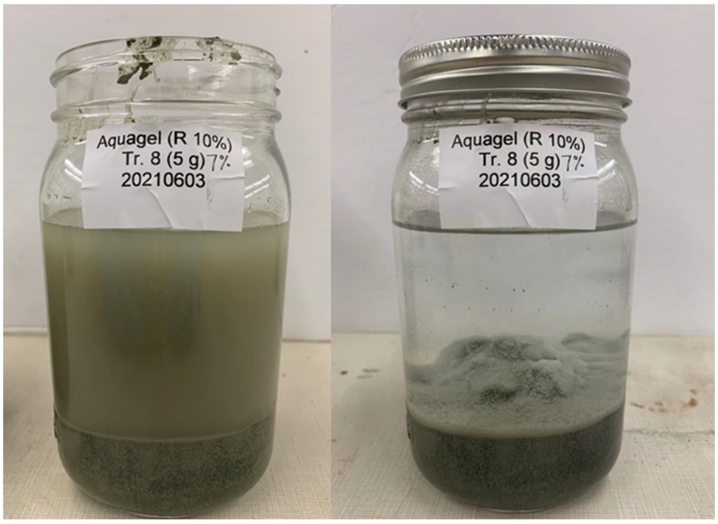

Figure 6.3 Performance of Stabilizer Aquagel 7% (R 10 wt.%) after placing and 28 days

Figure 6.4 Performance of Stabilizer Aquagel 9% (R 10 wt.%) after placing and 28 days

6.4.4 Results of four VMAs

VMA-1 is a white powder admixture. In this batch of tests, the 10 wt.% binder recipe was adopted, and the dosage of VMA-1 was set at 5%, 7% and 9% as per the mass of cementitious materials. After adding VMA-1, the CTB would become very dry which made the CTB had rare flowability. The anti-washout property was not achieved based on these dosages and the specimens were weakly cured after 10 days and 14 days curing time.

VMA-2 is a white powder admixture. In this batch of tests, the 6 wt.%, 8 wt.% and 10 wt.% binder recipes were adopted, and different dosages of VMA-2 were set for each binder recipe. After the addition of VMA-2, the CTB would be smooth and the particles of constituents were mixture thoroughly. Based on the 10 wt.% binder recipe, it is observed that the CTB performed the great anti-washout property when the dosage of VMA-2 was set at 7% and 9% of the cementitious materials (Figure 6.5 and Figure 6.6). The water remained clear when placing the CTB. But the performance of 5% was not as good as others, a small portion of cementitious materials was washed out. After 14 days curing time, these three specimens were strongly cured. However, the anti-washout property was not achieved using the 8 wt.% and 6 wt.% recipes and the specimens were weakly cured after 14 days.

Figure 6.5 Performance of VMA-2 7% (R 10 wt.%) after placing and 14 days

Figure 6.6 Performance of VMA-2 9% (R 10 wt.%) after placing and 14 days

VMA-3 is a yellow-brown powder admixture. In this batch of tests, the 6 wt.%, 8 wt.% and 10 wt.% binder recipes were adopted, and different dosages of VMA-2 were set for each binder recipe. The CTB would become smooth and very sticky after adding VMA-3, which made the CTB hard to flow. When the dosage was at 5%, the CTB obtained a good anti-washout property (Figure 6.7) at first. However, the particles started to go up with the air bubbles and suspended in the water. The water became muddy after about 30 minutes. The reason for this performance is mainly because of the air pockets inside the CTB mixture which was entrapped during the mixing procedure. After placing of CTB, the entrapped air bubbles started to move upward to the surface and bring the fine particles (cementitious materials) upward as well. When the dosage of VMA-3 was increased to 7%, the CTB floated on the water right after placing, performing a great anti-washout property (Figure 6.8). But in a few minutes, the floated backfill started to collapse. The particles moved downward to the bottom and the cementitious materials were separated from the tailings. The similar performance was also observed from the specimens of 6 wt.% and 8 wt.% recipes. Both exhibited good anti-washout property right after placing. Due to the air bubbles, the particles were separated from each other. After 10 days and 14 days curing time, all of the specimens treated with VMA-3 were not cured at all.

VMA-4 is a white powder admixture. The 10 wt.% binder recipe was adopted and the dosage of VMA-4 was set at 5%, 7% and 9% as per the mass of cementitious materials. After adding VMA-4, the CTB would become very dry and the CTB had rare flowability, which were similar with the performance of VMA-1. The anti-washout property was not achieved based on these dosages and the specimens were weakly cured after 10 days and 14 days curing time.

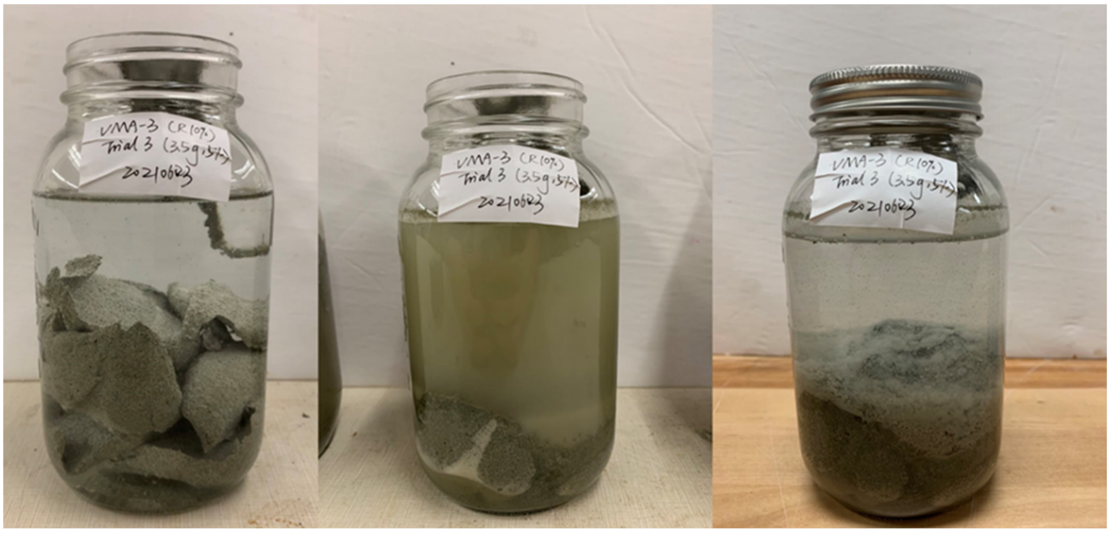

Figure 6.7 Performance of VMA-3 5% (R 10 wt.%) after placing, 30 minutes and 10 days

Figure 6.8 Performance of VMA-3 7% (R 10 wt.%) after placing, 30 minutes and 14 days

6.4.5 Summary

Total 7 different admixtures have been tested to investigate the anti-washout property for the design CTB. Based on the conducted experiments, we can conclude that VMA-2 is the most suitable anti-washout admixture for the designed cemented tailings backfill when the 10 wt.% binder recipe is adopted for backfill preparation and the dosage of VMA-2 is at least 5 wt.% of cementitious materials (Quan et al., 2021). Under this condition, the backfill can achieve anti-washout property and provide strong strength after short curing term 14 days. As for the Stabilizer Aquagel, it cannot give good anti-washout property as VMA-2, but the specimens can be strongly cured as well.

Chapter 7. Conclusions and Recommendations

For the evaluation of mechanical property and ultrasonic velocity for isotropic rocks, UCS tests, BTS tests, PLI tests, ultrasonic velocities and novel mono UCS-PLI tests have been conducted on hundreds of rock specimens. The densities and tensile strengths of granite and RLM are basically normally distributed. The tensile strengths of the granite and RLM disc samples increase with the decreasing thickness to diameter (t/d) ratio. The average PLI results of each length to diameter (D/W) ratio exhibit strong linear relationships between these two parameters. The UCS exhibits strong linear correlations with BTS and PLI, which mean the new correlations have the advantage of being developed for specific type of rock (RLM-high strength concrete). Significant linear correlations exist between the BTS and PLI of the studied rocks. In addition, the P-wave velocity shows strong linear correlations with UCS and Young's modulus, and exponential correlation with Poisson's ratio. The empirical correlations can give accurate predictions of studied rocks for future work. A novel strength testing method named mono UCS-PLI test is proposed. The results perform a relatively stable range between mono UCS-PLI testing values and conventional standard testing values which depict the research potential for the future study. The tests on different granite samples sizes should be conducted in the future work. Additionally, the obtained correlations are based on the experimental data for now and the mathematical models will be developed in the future study.

For the investigation of drilling performance using PDC and RC drill bits, drilling experiments under various WOBs, rpms and same water flow rate have been conducted on sandstone specimens. The ROP is found to be primarily dependent on the rpm, WOB and type of bit. Exponential relationships are found between WOB and ROP of both PDC and RC bits and the ROP increases with the increase of WOB when a low rpm is adopted. The rpm has a stronger effect on PDC bit than RC bit. In medium-hard and non-abrasive formations, the PDC bit tends to have better performance than the RC bit. As for sandstone, a strong linear relationship of ROP was found between PDC bit and RC bit. The ROP of PDC bit is approximately two to three times of RC bit, which indicates the high fitting degree and means the new correlation has the advantage of being developed for specific type of rock (sandstone). What's more, sandstone was the only rock that was analyzed in this study, the effect of different rock mechanical strengths on ROP needs more investigations in the future study.

For the optimization of cemented tailings backfill (CTB), the CTB with 4 wt.% binder proportion can obtain sufficient UCS after short-term 28 days curing time for SMD project. Additionally, the CTB with 2 wt.% has insufficient UCS for the backfill operation, due to the low cohesion between the particles inside CTB structure. The tensile strengths of the CTB discs increase with the decreasing thickness to diameter ratio. This performance is consistent with the splitting tensile strength of rock. Internal vibration has positive effects on the CTB. In the process of compacting concrete and removing trapped air, the density increases while the mass remains constant and the volume of the CTB decreases, which allows an extra 10.9% tailings to be sent underground, further reducing the surface tailings pond. Internal vibration also increases the compressive strength of the CTB by 57.1%. When the internal vibration method is applied to the placement of CTB, the CTB can obtain the target UCS, with a lower requirement of added binder, which will further reduce the costs of the backfill plant. In winter, backfilling operations needs to be carried out in frozen conditions. More investigations should be conducted to study the influence of water and admixtures phase change (from fluid to solid) on backfill strength development.

For the investigation of anti-washout property for CTB, it is found that the anti-washout admixtures (AWAs) can also provide anti-washout property for cemented backfill as it does for the underwater placement of concrete. The VMA-2 is found to be a promising anti-washout admixture when the CTB preparation recipe is adopted at 10 wt.% and the dosage of VMA-2 is at least 5 wt.% of cementitious materials in SMD project. Under this condition, the backfill can be placed into the water filled wellbore directly without flushing of cementitious materials. The achieved anti-washout property ensures the underwater curing and strength development of backfill after short curing time. After investigating the feasible anti-washout admixtures, the next step is to improve the flowability and workability of cemented tailings backfill. Some superplasticizers can be used to optimize the rheology of backfill. In addition, the mini-slump cone test should be conducted to monitor the workability loss in the future work.

References

Abugharara, A. N., Alwaar, A. M., Butt, S. D., & Hurich, C. A. (2016). Baseline Development of Rock Anisotropy Investigation Utilizing Empirical Relationships Between Oriented Physical and Mechanical Measurements and Drilling Performance. In International Conference on Offshore Mechanics and Arctic Engineering. American Society of Mechanical Engineers.

Abugharara, A. N., Hurich, C. A., Molgaard, J., & Butt, S. D. (2017). Implementation of circular wave measurements and multiple drilling parameter analysis in rock anisotropy evaluation. Proceedings of the International Conference on Offshore Mechanics and Arctic Engineering - OMAE.

Abugharara, A. N., Hurich, C. A., Molgaard, J., & Butt, S. D. (2019). Empirical Procedure Investigation for Sandstone Anisotropy Evaluation: Part I. Canadian Geotechnical Society / GEO ST. JOHN'S-2019.

Ahmed, D., Xiao, Y., de Moura, J., & Butt, S. D. (2020). Drilling Cutting Analysis to Assist Drilling Performance Evaluation in Hard Rock Hole Widening Operation. In ASME 2020 39th International Conference on Ocean, Offshore and Arctic Engineering. American Society of Mechanical Engineers Digital Collection.

Alum, M. A., & Egbon, F. (2011). Semi-analytical models on the effect of drilling fluid properties on rate of penetration (ROP). In Nigeria Annual International Conference and Exhibition. Society of Petroleum Engineers.

Armaghani, D. J., Mohamad, E. T., Momeni, E., Narayanasamy, M. S., and Amin, M. (2015). An adaptive neuro-fuzzy inference system for predicting unconfined compressive strength and young's modulus: a study on main range granite. Bulletin of Engineering Geology & the Environment, 74(4), 1301-1319.

ASTM C1688, "Standard Test Method for Density and Void Content of Freshly Mixed Pervious Concrete", American Society for Testing of Materials, Pennsylvania, PA, USA.

ASTM C192/C192M-15, "Standard Practice for Making and Curing Concrete Test Specimens in the Laboratory", American Society for Testing of Materials, Pennsylvania, PA, USA.

ASTM C39/C39M-12a, "Standard Test Method for Compressive Strength of Cylindrical Concrete Specimens", American Society for Testing of Materials, Pennsylvania, PA, USA.

ASTM D2845, "Standard Test Method for Laboratory Determination of Pulse Velocities and Ultrasonic Elastic Constants of Rock", American Society for Testing of Materials, Pennsylvania, PA, USA.

ASTM D3967, "Standard Test Method for Splitting Tensile Strength of Intact Rock Core Specimens", American Society for Testing of Materials, Pennsylvania, PA, USA.

ASTM D5731, "Standard Test Method for Determination of the Point Load Strength Index of Rock and Application to Rock Strength Classifications", American Society for Testing of Materials, Pennsylvania, PA, USA.

ASTM D6913, "Standard Test Methods for Particle-Size Distribution (Gradation) of Soils Using Sieve Analysis", American Society for Testing of Materials, Pennsylvania, PA, USA.

ASTM D7012, "Standard Test Methods for Compressive Strength and Elastic Moduli of Intact Rock Core Specimens under Varying States of Stress and Temperatures", American Society for Testing of Materials, Pennsylvania, PA, USA.

Avar, E., & Zcan, N. T. (2021). A Preliminary Study on the Relationships between the Grain Contact Pattern and the Tensile Strength of a Rock Salt. International Congress of Engineering and Natural Sciences Studies.

Boadu, F.K. (2000). Predicting the transport properties of fractured rocks from seismic information: numerical experiments. J. App. Geophysics 44, 103–113.

Barton, N.R., Lien, R., & Lunde, J. (1974). Engineering classification of rock masses for the design of tunnel support. RockMech. 6(4),189–239.

Belem, T., & Benzaazoua, M. (2004). An overview on the use of paste backfill technology as a ground support method in cut-and-fill mines. In Proceedings of the 5th Int. Symp. on Ground support in Mining and Underground Construction. Villaescusa & Potvin (eds.) (pp. 28-30).

Benzaazoua, M., Fall, M., & Belem, T. (2004). A contribution to understanding the hardening process of cemented paste fill. Minerals Engineering 17 (2), 141–152.

Bilgesu, H. I., Tetrick, L. T., Altmis, U., Mohaghegh, S., & Ameri, S. (1997). A new approach for the prediction of rate of penetration (ROP) values. In SPE Eastern Regional Meeting. Society of Petroleum Engineers.

Cayouette, J. (2003). Optimization of the paste backfill plant at Louvicourt mine. CIM bulletin, 96(1075), 51-57.

Chan, CheeMing, Kikuchi, Yoshiaki, & Mizutani, Takaaki. (2012). Correlation between unconfined compressive strength and mixing quality of solidified clay. International Journal of Civil & Structural Engineering.

Chau, K. T., & Wong, R. (1996). Uniaxial compressive strength and point load strength of rocks. International Journal of Rock Mechanics & Mining Sciences & Geomechanics Abstracts, 33(2), 183-188.

Coates, D. F. (1981). Rock mechanics principles.

Cooke, R. (2006). Thickened and paste tailings pipeline systems: design procedure. Australian Centre for Geomechanics, 129-140.

D. Landriault. (2001). Backfill in underground mining, in: W.A. Hustrulid (Ed.), Underground Mining Methods Engineering Fundamentals and International Case Studies, SME, USA, pp. 608–609.

Deng, H., Li, J., Zhu, M., Wang, R., Yan, X., & Luo, Q. (2012). Research on effect of disc thickness-to-diameter ratio on splitting tensile strength of rock. Chinese Journal of Rock Mechanics and Engineering, 4.

Dupriest, F. E., & Koederitz, W. L. (2005). Maximizing drill rates with real-time surveillance of mechanical specific energy. In SPE/IADC drilling conference. Society of Petroleum Engineers.

E. M. Galle, & H. B. Woods. (1963). Best Constant Weight and Rotary Speed for Rotary Rock Bits, API Drilling and Production Practice, 1 January, New York, API-63-048.

Elizabeth, S., Petrie, Tamara, N., & Jeppson. (2012). Predicting rock strength variability across stratigraphic interfaces in caprock lithologies at depth: correlation between outcrop and subsurface. Environmental Geosciences.

Ercikdi, B., Cihangir, F., Kesimal, A., Deveci, H., & Alp, İ. (2009). Utilization of industrial waste products as pozzolanic material in cemented tailings backfill of high sulphide mill tailings. Journal of hazardous materials, 168(2-3), 848-856.

Fall, M., & Samb, S. (2008). Pore structure of cemented tailings materials under natural or accidental thermal loads. Materials Characterization, 59(5), 598-605.

Fall, M., Benzaazoua, M., & Ouellet, S. (2004). Effect of tailings properties on paste backfill performance. 8th International Symposia on Mining with Backfill, Beijing, China,193-202.

Fall, M., Benzaazoua, M., & Ouellet, S. (2005). Experimental characterization of the influence of tailings fineness and density on the quality of cemented tailings backfill. Minerals engineering, 18(1), 41-44.

Forster IR. (1983). The influence of core sample geometry on the axial point-load test. Int J Rock Mech Min Sci 20:291–295.

Garcia, S. R., & Romo, M. P. (2009). Rockfill strength evaluation using cascade correlation networks. Geotechnical & Geological Engineering, 27(3), 289-304.

Gaviglio P. (1989). Longitudinal wave propagation in a limestone: the relationship between velocity and density. Rock Mech Rock Eng 22:299–306.

Ghosh DK, & Srivastava M. (1991). Point-load strength: an index for classification of rock material. Bull Int Assoc Eng Geol 44: 27–33.

Glowka, D. A. (1984). Thermal limitations on the use of PDC bits in geothermal drilling (No. SAND-84-0757C; CONF-840809-2). Sandia National Labs., Albuquerque, NM (USA).

Grice, T. (1998). Underground mining with backfill. 2nd Annual Summit œ Mine Tailings Disposal Systems, Brisbane, Nov, 24-25.

Guo, L., Wang, H., Sun, X., Zhou, J., & Liang, X. (2017). Design and construction of a combined underground paste backfilling and surface paste storage system in Baiyinchagan Polymetallic Mine. In Proceedings of the 20th International Seminar on Paste and Thickened Tailings (pp. 346-357). University of Science and Technology Beijing.

Habibi, A., Riazi, M., & Malayeri, M. R. (2021). Experimental and simulation study of the tensile strength of wet carbonate rocks using the brazilian test - sciencedirect. Journal of Petroleum Science and Engineering.

Haftani, M., Bohloli, B., Moosavi, M., Nouri, A., Moradi, M., & Javan, M. R. M. (2013). A new method for correlating rock strength to indentation tests. Journal of Petroleum Science and Engineering, 112, 24-31.

Hahri, A. A., Asheghi, R., & Zak, M. K. (2021). A hybridized intelligence model to improve the predictability level of strength index parameters of rocks. Neural Computing and Applications, 33(3), 1-14.

Hama, Y., Mimori, T., & Kamada, E. (1997). Strength development of concrete containing antifreezing admixtures. Concrete Reseach and Technology, 8(1), 161-170.

Helm, P., Davie, C., & Glendinning, S. (2013). Numerical modelling of shallow abandoned mine working subsidence affecting transport infrastructure. Engineering Geology, 154, 6-19.

Heniegal, A. M. (2016a). Developing underwater concrete properties with and without anti-washout admixtures. International Journal of Scientific and Engineering Research, 7(3), 97-106.

Heniegal, A., Abd, A., Maaty, E. S., & Agwa, I. S. (2016b). Influence of anti washout admixtures and coarse aggregate types on self-flowing underwater concrete properties. Journal of Civil & Structural Engineering, 6(3), 245-262.

Hoek, E. (1977). Rock mechanics laboratory testing in the context of a consulting engineering organization. Int. J Rock Mech. Min. Sci. Geomech. 14, 93–101.

Hsieh, S. C. (2021). Prediction of compressive strength of concrete and rock using an elementary instance-based learning algorithm. Advances in Civil Engineering, 2021(7), 1-10.

IADC Drilling Manual, 12th edition. (2014). ISBN: 978-8-9915095-0-8.

Imam, M. A. (2004). Evaluation of antiwashout admixtures for use in underwater concrete. Journal of Engineering and Applied Science, 51(1), 67-83.

Inoue, M., Ohomi M. (1981). Relation between uniaxial compressive strength and elastic wave velocity of soft rock, Proceedings of the Int. Symp. Weak Rock, Tokyo, 9–13.

Jain, J. R., Ricks, G., Ledgerwood, L. W., & Phillips, A. (2017). Mitigating Drilling Dysfunctions and Enhancing Performance with Self-Adjusting Bit Technology: Analytical and Experimental Case Studies. In SPE/IADC Drilling Conference and Exhibition. Society of Petroleum Engineers.

Johnson, S. C. (2008). A new method of producing laterally stable PDC drill bits. SPE Drilling & Completion, 23(03), 314-324.

Kahraman, S. (2001). A correlation between P-wave velocity, number of joints and Schmidt hammer rebound number. Int. J. Rock Mech. Min Sci 38, 729–733.

Kahraman, S., & Gunaydin, O. (2009). The effect of rock classes on the relation between uniaxial compressive strength and point load index. Bulletin of engineering geology and the environment, 68(3), 345-353.

Kahraman, S., Fener, M., & Kozman, E. (2012). Predicting the Compressive and Tensile Strength of Rocks from Indentation Hardness Index. Journal of the Southern African Institute of Mining and Metallurgy, 112(5), 331-339.

Kanema, J. M., Eid, J., & Taibi, S. (2016). Shrinkage of earth concrete amended with recycled aggregates and superplasticizer: Impact on mechanical properties and cracks. Materials & Design, 109, 378-389.

Kesimal A., Yilmaz E., Ercikdi B., Alp I., & Deveci H. (2005). Effect of properties of tailings and binder on the short-and long-term strength and stability of cemented tailings backfill. Mater Lett. 59:3703–3709.

KHANDELWAL, M., & RANJITH, P.G. (2010). Correlating index properties of rocks with P-wave measurements. Journal of Applied Geophysics. 71, 1–5.

Khayat, K. H., & Hester, W. T. (1991). Evaluation of concrete mixtures for underwater pile repairs. Cement, concrete and aggregates, 13(1), 32-41.00

Khayat, K. H., & Sonebi, M. (2001). Effect of mixture composition on washout resistance of highly flowable underwater concrete. Materials Journal, 98(4), 289-295.

Kolapo, P. (2021). Investigating the Effects of Mechanical Properties of Rocks on Specific Energy and Penetration Rate of Borehole Drilling. Geotechnical and Geological Engineering, 39(2), 1715-1726.

Kralik, M., & Biffis, A. (2001). Catalysis by metal nanoparticles supported on functional organic polymers. Journal of Molecular Catalysis A: Chemical, 177(1), 113-138.

Khandelwal, M., Singh, T.N. (2009), Correlating static properties of coal measures rocks with P-wave velocity. International Journal of Coal Geology. 79, 55–60.

Liu, L., Yang, P., Qi, C., Zhang, B., Guo, L., & Song, K. I. (2019). An experimental study on the early-age hydration kinetics of cemented tailings backfill. Construction and Building Materials, 212, 283-294.

Lopez-Pacheco, A. (2019). The golden key, CIM Magazine. Vol. 14, No. 5.

Mardoukhi, A., Mardoukhi, Y., Hokka, M., & Kuokkala, V. T. (2021). Effects of test temperature and low temperature thermal cycling on the dynamic tensile strength of granitic rocks. Rock Mechanics and Rock Engineering, 54(6).

Maryoto, A. (2018). Proposed concrete compaction method using an electrical internal vibrator: a review of compaction standard for concrete in laboratory according to SNI 2493: 2011. In MATEC Web of Conferences (Vol. 195, p. 01003). EDP Sciences.

Maurer, W.C. (1962). The "perfect-cleaning" theory of rotary drilling. In: 37th Annual Fall Meeting of SPE. California, Los Angeles.

McGeary, R. (1961). Mechanical packing of spherical particles. Journal of the American ceramic Society, 44(10), 513-522.

Mensa-Wilmot, G., & Fear, M. (2002). Innovative Technology Improves Penetration Rates of PDC Bits in Shales Drilled at Great Depth with Weighted Water Based Mud Systems. In IADC/SPE Drilling Conference. Society of Petroleum Engineers.

Mindess, S. (Ed.). (2019). Developments in the Formulation and Reinforcement of Concrete. Woodhead Publishing.

Nakhla, D. A., & Abou-Zeid, M. N. (2005). Performance of low-slump underwater concrete incorporating antiwashout admixtures. Transportation Research Record Journal of the Transportation Research Board, 1914(1), 61-70.

Nasir, O., & Fall, M. (2010). Coupling binder hydration, temperature and compressive strength development of underground cemented tailings backfill at early ages. Tunnelling and Underground Space Technology, 25(1), 9-20.

Nazir, R., Momeni, E., Armaghani, D. J., & Amin, M. (2013). Correlation between unconfined compressive strength and indirect tensile strength of limestone rock samples. Electronic Journal of Geotechnical Engineering, 18(18), 1737-1746.

Neeley, B. D. (1988). Evaluation of concrete mixtures for use in underwater repairs.

Niroshan, N., Sivakugan, N., & Veenstra, R. L. (2018). Flow characteristics of cemented paste backfill. Geotechnical and Geological Engineering.

Offenbacher, L. A., McDermaid, J. D., & Patterson, C. R. (1983). PDC bits find applications in Oklahoma drilling. In IADC/SPE Drilling Conference. Society of Petroleum Engineers.

Omar, M., Agawani, W., Abdelhamid, A., Al Ajmi, A., Al Rushoud, A., & Al Ghareeb, M. (2017). Multiple Deployments of Hybrid Drill Bits with Optimized Drilling Systems Prove Enhanced Efficiency in North Kuwait Development Wells. In SPE Middle East Oil & Gas Show and Conference. Society of Petroleum Engineers.

Ozkahraman, H.T., Selver, R., Isik, E.C. (2004). Determination of the thermal conductivity of rock from P-wave velocity. Int. J. Rock Mech. Min. Sci. 41, 703–708.

Paes, P., Aragao, A. F. L., Felicissimo, R. S., & Chen, D. C. (2005). Cost-effective drilling optimization technologies in Campos Basin. In SPE Latin American and Caribbean Petroleum Engineering Conference. Society of Petroleum Engineers.

Pak, M., Gumich, D., Zinnatullin, I., Mukkisa, S., Bits, S., & Gaynullin, I. (2017). Unique approach to bit design coupled with innovative rolling PDC cutter sets new performance benchmark drilling extremely abrasive sandstone formations, Usinsk Region Russia. In SPE Middle East Oil & Gas Show and Conference. Society of Petroleum Engineers.

Peng, Y., Hou, Q., Li, Bai., & Liu, Yi. (2004). Drilling parameter model with the "low rotation speed-high WOB" of PDC bits and its application. China Academic Journal Eletronic Publishing House.

Popovics, S. (1973). A review of the concrete consolidation by vibration. Matériaux et Construction, 6(6), 453-463.

Qi, C., & Fourie, A. (2019). Cemented tailings backfill for mineral tailings management: Review and future perspectives. Minerals Engineering, 144, 106025.

Qing-feng, D. O. U., Shun, Y. U. E., & Gao-fei, D. A. I. (2004). Experimental study on direct and indirect tension of rock. Underground Space, 24(2), 178-181.

Quan, W., Li, Z., & Butt, S. D. (2021, July). Qualitative analysis of cemented tailings backfill (CTB) with anti-washout admixture. Unpublished Q2-2021 technical report submitted to Novamera Inc.

Rasul, G., Quan, W., Abugharara, A., Zhang, Y., Rahman, A. M., & Butt, S. D. (2021). Tensile and shear fracture examination for optimal drilling performance evaluation: Part-I. GeoNiagara 2021, the 74th Canadian Geotechnical Conference.

Saito T, Mamoru ABE, & Kundri S. (1974). Study on weathering of igneous rocks. Rock Mech Jpn 2:28–30.

Sakai E, Miyahara S, Ohsawa S, Lee SH, & Daimon M. (2005). Hydration of fly ash cement. Cem Concr Res 35(6):1135–1140

Sepahi, A. A., Khanlari, Heidari, & Freidooni. (2014). Quantification of strength anisotropy of metamorphic rocks of the Hamedan Provine, Iran, as determined from cylindrical punch, point load and Brazilian tests. Engineering Geology.

Shaunik, D., & Singh, M. (2021). Applicability of critical state concept in determination of triaxial strength of non-persistent jointed rock. Geotechnical and Geological Engineering, 1-24.

Sharma, P. K., & Singh, T. N. (2008). A correlation between P-wave velocity, impact strength index, slake durability index and uniaxial compressive strength. Bulletin of Engineering Geology and the Environment, 67(1), 17-22.

Shcherban, E. M., Stelmakh, S. A., Sysoev, A., & Chernil'Nik, A. (2021). Studying the relationship between the strength and stress-related characteristics of concrete as a conglomerate and the properties of its components. Materials Science Forum, 1022, 71-79.

Shea, W. T., & Kronenberg, A. K. (1993). Strength and anisotropy of foliated rocks with varied mica contents. Journal of Structural Geology, 15(9-10), 1097-1121.

Sheshde, E. A., & Cheshomi, A. (2015). New method for estimating unconfined compressive strength (UCS) using small rock samples. Journal of Petroleum Science and Engineering, 133, 367-375.

Sika. (2016, August 29). Sika® Underwater Concrete. YouTube. https://www.youtube.com/watch?v=MjqaqdAUc4w.

Sikandar, M. A., Ahmad, W., & Khan, A. (2020). Effect of various anti-washout admixtures on the properties of non-dispersible underwater concrete. Construction and Building Materials, 245, 118469-.

Singh, T.N., Kainthola, A., & Venkatesh, A. (2012). Correlation between point load index and uniaxial compressive strength for different rock types. RockMech. Rock Eng. 45,259–264.

Someehneshin, J., Quan, W., Abugharara, A., & Butt, S. (2020). Assessment of Freestanding Vertical Face for the Backfill Using the Run of the Mine Tailings and Portland Cement. ARMA, 20(A), 1882nd ser.

Someehneshin, J., Quan, W., Abugharara, A., & Butt, S. (2020). Backfill analysis and parametric evaluation of the cement binder on cured strength and curing time. GeoCalgary.

Smorodinov, M.I., Motovilov, E.A., Volkov, V.A. (1970). Determinations of correlation relationships between strength and some physical characteristics of rocks. Proc. of the Second Congress of the Int. Society for Rock Mechanics, Vol. 2. Belgrade, 35–37.

Suprenant, B. A., & TAMPA, F. (1988). Concrete vibration. Concrete Construction, 563-568.

Tan, Z., Bernal, S. A., & Provis, J. L. (2017). Reproducible mini-slump test procedure for measuring the yield stress of cementitious pastes. Materials and Structures, 50(6), 1-12.

Taylor, H.F.W. (1997), Cement Chemistry, 2nd edition, Thomas Telford Ltd, London, UK.

Teymen, A. A. (2021). Statistical models for estimating the uniaxial compressive strength and elastic modulus of rocks from different hardness test methods. Heliyon, y(5), 1-15.

Thompson, B. D., Bawden, W. F., & Grabinsky, M. W. (2012). In situ measurements of cemented tailings backfill at the Cayeli Mine. Canadian Geotechnical Journal, 49(7), 755-772.

Verma, M., & Reddy, K. S. (2015). Quantification of anisotropy in quasi-static magnetohydrodynamic turbulence. 57th Annual Meeting of the APS Division of Plasma Physics. American Physical Society.

Wang, R. H., Jiang, Y. Z., Guo, J. L., & Tang, T. C. (2014). Study on the relation between uniaxial compressive strength and point load strength. Applied Mechanics & Materials, 501-504, 282-285.

Wang, X. M., Bin, Z. H. A. O., Zhang, C. S., & Zhang, Q. L. (2009). Paste-like self-flowing transportation backfilling technology based on coal gangue. Mining Science and Technology (China), 19(2), 137-143.

Wang, Y. M., Huang, M. Q., Wu, A. X., Yao, G. H., & Hu, K. J. (2013). Rock Backfill and Hazard Control of Abandoned Stopes: A Case Study. Applied Mechanics and Materials, 368, 1726-1731.

Williams, J. L., & Thompson, A. I. (1987). An analysis of the performance of PDC hybrid drill bits. In SPE/IADC drilling conference. Society of Petroleum Engineers.

Winters, W. J., Warren, T. M., & Onyia, E. C. (1987). Roller bit model with rock ductility and cone offset. In SPE Annual Technical Conference and Exhibition. Society of Petroleum Engineers.

Wu, A. X., Miao, X. X., Liu, X. H., Wang, Y. M., Wang, C. L., & Zhang, J. J. (2015). Paste backfill system design and commissioning at Chambishi Copper Mine. In Proceedings of the 18th International Seminar on Paste and Thickened Tailings (pp. 301-308). Australian Centre for Geomechanics.

Yahia, A., & Khayat, K. H. (2001). Experiment design to evaluate interaction of high-range water-reducer and antiwashout admixture in high-performance cement grout. Cement & Concrete Research, 31(5), 749-757.

Yasin, Abdi, Amin, Taheri, Garavand, & Reza, et al. (2018). Prediction of strength parameters of sedimentary rocks using artificial neural networks and regression analysis. Arabian Journal of Geosciences.

Yasar, E., Erdogan, Y. (2004). Correlating sound velocity with the density, compressive strength and Young's modulus of carbonate rocks. Int. J. Rock Mech. Min Sci 41, 871–875.

Yilmaz, E., Belem, T., & Benzaazoua, M. (2015). Specimen size effect on strength behaviour of cemented tailings backfills subjected to different placement conditions. Engineering Geology, 185, 52-62

Yilmaz, E., Benzaazoua, M., Belem, T., & Bussière, B. (2009). Effect of curing under pressure on compressive strength development of cemented tailings backfill. Minerals Engineering, 22(9-10), 772-785.

Yilmaz, E., Kesima, A., & Ercidi, B. (2004). Strength development of paste backfill simples at long term using different binders. In: Proceedings of 8th Symposium Mine Fill 04, China, pp. 281–285.

Yilmaz, E., Kesimal, A., & Ercikdi, B. (2003). Strength properties in varying cement dosages for paste backfill samples.

Yoshikawa, S., & Mogi, K. (1981). A new method for estimation of the crustal stress from cored rock samples: laboratory study in the case of uniaxial compression. Tectonophysics, 74(3-4), 323-339.

Youash Y. (1970). Dynamic physical properties of rocks: Part 2, experimental result. In: Proceedings of the second congress of the international society on rock mechanics, Belgrade, 1, 185–195.

Yu Lingzhu & Lu Jian. (2019). The Fundamental Principles and Applications of Scanning Electron Microscopy. Experiment Science and Technology, 17(5), 85-93.

Zhang, Y., Baker, R., Burhan, Y., Shi, J., Chen, C., Tammineni, S., & Segal, S. (2013). Innovative rolling PDC cutter increases drilling efficiency improving bit performance in challenging applications. In SPE/IADC Drilling Conference. Society of Petroleum Engineers.

Zhou, D., Ma, D., & Hou, J. (1987). The vertical interaction model of cone bit teeth-rock. Journal of Southwestern Petroleum Institute, 16 (3).